ISSN 1880-6503

Sustainable Humanosphere

BULLETIN OF
RESEARCH INSTITUTE FOR SUSTAINABLE HUMANOSPHERE
KYOTO UNIVERSITY

No. 3

August 2007

PUBLISHED BY
RESEARCH INSTITUTE FOR SUSTAINABLE HUMANOSPHERE
KYOTO UNIVERSITY
UJI, KYOTO 611-0011, JAPAN

'Sustainable Humanosphere' is a serial publication issued annually by the Research Institute for Sustainable Humanosphere (RISH) of Kyoto University, which aims to provide a report on the ongoing research at our Institute along with new research field of sustainable humanosphere. This journal is a continuation of 'Wood Research' published by Wood Research Institute of Kyoto University, which will be distributed free of charge and prefers to exchange similar articles with scientific institutions and libraries throughout the world. All communications concerning 'Sustainable Humanosphere' should be addressed to Research Institute for Sustainable Humanosphere (RISH), Kyoto University, Uji 611-0011, Japan. (Email: oubunshi@rish.kyoto-u.ac.jp)

CONTENTS

Wood Structure – macrostructure at time scale to ultrastructure at molecular scale

(Laboratory of Biomass Morphogenesis and Information, RISH, Kyoto University)

Junji Sugiyama and Kei'ichi Baba

Wood, the secondary xylem, is the most abundant terrestrial biotic product. From the Stone Age relationship between wood and man has always been intimate, and even unconsciously, wood surrounds us because of its versatility to make constructions, furniture, tools, fibers and paper. Therefore, wood is an important subject to be studied from many different aspects: paleobotany, ethnobotany, archeology, history in addition to the conventional view points such as biology, chemistry, physics and engineering.

The wood collection at xylarium, designated as KYOw, has been serving as basis for the exchange of knowledge and experiences in wood anatomy at national and international levels. Our activity linked to this xylarium are (1) research and education of wood anatomy and identification, (2) original collection of timbers from national cultural heritages, (3) indexing, exchange, home page publishing of wood collections, (4) rendering services on the identification of the taxon of wooden objects, and (5) promotion of cooperative research project.

In addition, wood identification project of whole parts of old construction equivalent of cultural heritage that we started recently, provides a valuable dataset to study the usage of timbers that differs by era or locality. Another new study includes dendroclimatological approach. Signals of climate recorded in the annual rings are to be analyzed by anatomical and chemical methods using precisely dated wood collection from our xylarium.

Apart from the xylarium, our laboratory is involved in many structural studies of plant polysaccharides and plant cell walls. One of the examples from the cellulose fields is *in vitro* cellulose synthesizing experiment in collaboration with a Swedish group at KTH. From higher plant suspension cultured cells as well as one of the cellulose synthesizing animals the system to synthesize cellulose *in vitro* is being established. Also novel systems to characterize *in vitro* product are under development.

Another example from cell wall fields is about the mechanism of tensile force generation in relation to the ultrastructure of gelatinous fibers in tension wood. Morphological and molecular approach has been unveiling the complicated role of the key molecule and a unique enzyme that regulate them to function together.

Finally, as a mission project, functional biocomposite materials are under development by mimicking biological process and ultrastructure. Polysaccharides-based biomedical materials are investigated in collaboration with biomaterial experts.

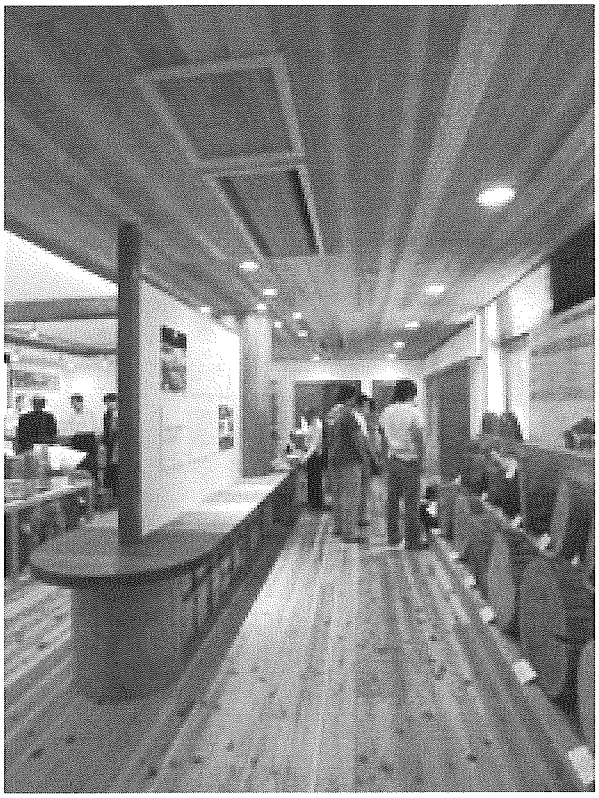

A snapshot of reformed Xylarium.

Unsaturated fatty acids in selective lignin degradation by the white-rot fungus, *Ceriporiopsis subvermispora*

(Laboratory of Biomass Conversion, RISH, Kyoto University)

Takahito Watanabe, Saeko Tsuda, Yoichi Honda and Takashi Watanabe

Unsaturated fatty acids (UFAs), such as linoleic acid (18:2n-6) and α-linolenic acid (18:3n-3), have crucial roles as structural components of biological membranes, cellular energy source, and cell signaling molecules. UFAs in phospholipids increase the membrane fluidity necessary to maintain the proper function of biological membranes. In the biosynthesis of UFAs, fatty acid desaturases are key enzymes that are responsible for the insertion of double bonds into alkyl chains, following the abstraction of two hydrogen atoms. These enzymes are almost universally found in microbial, plant, and animal cells, where they play important roles in a wide range of physiological processes.

It is well known that many poikilothermic organisms adapt to cold temperatures by increasing fatty acid desaturation to restore the fluidity of cold-rigidified membranes. Moreover, it have been gradually revealed that fatty acid desaturase genes are inducibly expressed by the ability of membrane-bounded proteins to sense a decrease in membrane fluidity generated either by a temperature downshift or by restricted availability of UFAs [1] [2].

In a budding yeast *Saccharomyces cerevisiae*, *OLE1*, encoding a Δ9-fatty acid desaturase to insert a double bond into the Δ9 position at stearic acid (18:0) and palmitic acid (16:0), is highly expressed during ethanol fermentation as well as under lower temperatures. The higher *OLE1* expression leads to increases in fatty acyl chain length and the proportion of UFA [3] [4]. These observations suggest that fatty acid deaturases may be inducibly expressed in the physical and chemical stress conditions, which drastically alter the membrane fluidity.

A selective lignin-degrading fungus, *Ceriporiopsis subvermispora*, can selectively degrade lignin without intensive damage of cellulose. We have demonstrated that extracellular lipid peroxidation by manganese-dependent peroxidase (MnP) occurred in the selective lignin degradation by *C. subvermispora*. At an incipient stage of cultivation on extractive-free wood meal cultures, this fungus produced MnP and large amounts of linoleic acid and palmitic acid, and MnP oxidized them to aldehydes. In prolonged cultivation period after 2-weeks, however, the amount of these fatty acids decreased with increasing organic hydroperoxide and the accumulation of lipid peroxidation products reacting with thiobarbituric acid (TBARS) in organic extracts from wood meal cultures. These observations suggest that UFAs might act as a precursor of lipid peroxidation that is a key reaction of the selective lignin degradation [5].

Because lipid peroxidation is the process whereby free radicals abstract electrons from the lipids, it is very likely to damage cell membranes of *C. subvermispora* even if lipid peroxidation takes place extracellularly. Moreover, exposure to free radical species generated by lipid peroxidation and aldehydes produced by MnP may lead to induce the expression of fatty acid desaturase genes. Therefore, we focus on the molecular relationship between lipid peroxidation and the biosynthesis of UFA, and we successfully cloned fatty acid desaturase genes from *C. subvermispora*. We are now trying to study biochemical and genetic bases of fatty acid desaturases and lipid-related metabolites involved in the selective lignin degradation by *C. subvermispora*.

REFERENCES

[1] Suutari, M. and Laakso, S. (1994) Crit. Rev. Microbiol., 20: 285-328.
[2] Aguilar, P. S. and de Mendoza, D. (2006) Mol. Microbiol., 62: 1507-1514.
[3] Kajiwara, S., Aritomi, T., Suga, K., Ohtaguchi, O. and Kobayashi, O. (2000) Appl. Microbiol. Biotechnol., 53: 568-574.
[4] Yamada, T., Shimoi, H. and Ito, K. (2005) J. Biosci. Bioeng., 99: 512-516.
[5] Enoki, M., Watanabe, T., Nakagame, S., Koller, K., Messner, K., Honda, Y. and Kuwahara, M. (1999) FEMS Microbiol. Lett., 180: 205-211.

Gene co-expresson network analysis in relation to cell wall formation and organic acid metabolisms of forest microorganisms

(Laboratory of Metabolic Science of Forest Plants and Microorganisms, RISH, Kyoto University)

Toshiaki Umezawa and Takefumi Hattori

It is becoming more important to establish a sustainable society, which depends on renewable resources. Because wood biomass is the most abundant renewable resource, studies of wood formation is the key to improve forest biomass production. In this context, we are involved in analyzing metabolic functions of forest plants and microorganisms from a wide variety of aspects, including organic chemistry, biochemistry, molecular biology, and metabolomics, in order to conduct basic investigations contributing cultivation and protection of forest resources. These projects are conducted in collaboration with Dr. Shiro Suzuki, Institute of Sustainability Science, Kyoto University.

1. Gene co-expression network analysis

During the last two decades, significant advances have been made in molecular biology of wood formation. For example, many genes involved in lignin biosynthesis have been cloned and their functions have been unequivocally identified. Having the genes in our hands, the major concern in tree biotechnology is the elucidation of comprehensive gene expression control mechanisms for cell-wall formation. Identification of transcription factors (TFs), as well as microRNAs, controlling expression of genes encoding enzymes involved in cell-wall formation is one of the most important steps. Following the completion of genome sequences of *Arabidopsis thaliana*, a large number of microarray data sets of *A. thaliana* gene expression are open to public, which can be exploited to analyze co-expression of genes. We are conducting gene co-expression network analysis starting with the genes encoding enzymes of the cinnamate/monolignol pathway providing monolignols. This allowed us to find out several genes encoding TFs which possibly control the gene expression of the pathway enzymes. Next, in order to confirm the roles of the TFs, we prepared transgenic *A. thaliana* cells where the individual TF genes were upregulated. Lignin characterization of the transgenic cells thus obtained and *A. thaliana* T-DNA tag line mutants with the target genes being downregulated are under way by the use of Forest Biomass Analytical System so that we can identify TFs which controls the metabolic flow of the cinnamate/monolignol pathway in *A. thaliana*.

2. Mechanisms for organic acid metabolism of wood-rotting fungi and ectomycorrhizal fungi

Biodegradation of wood components by wood-rotting (WR) fungi including white- and brown-rot basidiomycetes is important as a first process leading to humus production, which in turn contributes greatly to sustainable forest ecosystems. Oxalate excreted from WR fungi plays a wide variety of roles in the degradation owing to its various chemical natures. We have proposed that oxalate metabolism is an important biochemical device to produce energy for fungal growth of WR fungi. The peroxisomal glyoxylate (GLOX) cycle cooperatively play a role with mitochondrial TCA cycle in oxalate fermentation by which brown-rot fungus *Fomitopsis palustris* acquires energy for fungal growth on glucose. It was postulated that some of the common metabolites of the peroxisomal GLOX and mitochondrial TCA cycles are transported between peroxisomes and mitochondria in a constitutive and cooperative manner in terms of the oxalate biosynthesis. Furthermore, we have demonstrated that *F. palustris* has a biochemical system to decrease growth inhibitory effect caused by oxalate. We have isolated a cDNA *FpTRP26* from *F. palustris*, which conferred a specific resistance to oxalate on yeast *FpTRP26*-transformant.

Cytochemical and molecular approaches for enzymes and transporters involved in organic acid metabolism are being investigated for WR fungi. Furthermore, comprehensive study for elucidation of regulatory mechanisms for organic acid metabolism in WR and ectomycorrhizal fungi has just begun.

A molecular diagnosis for the resistant pine traits against pine wilt diseases

(Laboratory of plant gene expression, RISH, Kyoto University)

Hiroyuki Kuroda

Japanese pine forest has been severely suffered from pine wilt diseases and the dead trees are the biggest loss in biomass of Japan. Furthermore, the diseases have ignited in East Asia and Europe, causing political affairs. Pesticide application for controlling pine wilt diseases has gradually been diminished because of environmental concerns. New strategies are now required for controlling pine wilt disease, which is directly caused by pine wood nematodes. In the government-related facilities, survived pine trees have been collected from the natural pine forest stands, where they had been suffered from the pine wilt disease. Meantime, the pine EST libraries are available for analyzing gene expression under some stress in pine trees. The virtual full coding sequences, which may or may not represent substantial genes, are also easily obtained from the fragments. However, the expression data for pine wilt diseases in association with the resistant traits has little been accumulated. The author has focused attention on the resistant traits in Japanese red pine (*Pinus densiflora*).

In order to find a molecular clue, the expressed genes from a resistant tree have subtracted against the one from a susceptible tree after they had infected with the nematodes. In the course of the experiment, key processes were as follows: providing relevant plant materials (Fig. 1) for the resistant traits and the RNA preparations with reasonable quality and quantities. In the former case, the resistant traits against the nematodes are easily weakened by the pollination with susceptible pollen parents. The grown resistant family contains such weakened individuals since they are the seed descendants of a selected tree which carries resistant traits. The suspects had been under better control by counting nematode numbers after the infection. Thus the resistant tree was able to determine as the one which showed no nematode proliferation even after the nematode infection. In the latter case, resistant trees were more difficult to extract RNA, of which yield was always lower than the one from susceptible trees. Finally, the cDNA clones have successfully collected and over a thousand of sequenced clones have assigned for the public pine EST libraries.

The causes of the resistant traits may be compared to a gun. One component is corresponding to a kind of a trigger and the other is a kind of a bullet. The former trigger is a point mutation, which is usually expected to cause loss of function. The mutation may alter the metabolism, signal transduction and transport which are directly associated with the resistant traits. This direct resistance is the latter bullet case. The gain of function is possible in the latter case and it produces weapons which can defend against the worm and control them. In fact, obtained clones contain such families of "ecu and halberdier". The obtained sequences will provide molecular discrimination for selecting a resistant pine tree. The resistant tree selection is one of a key strategy for controlling pine wilt disease without environmental concerns. Further works for the diagnosis are now going on.

A view of pine nursery: the resistant families of Japanese red pine against the nematodes

The photo shows a nursery bed where the Japanese red pines with distinct resistance against the nematodes had been growing for two years after seeding.

Development of portable Raman lidars and application to field observations

(Laboratory of Atmospheric Sensing and Diagnosis, RISH, Kyoto University)

Takuji Nakamura

Atmospheric lidar (laser radar) is a technique of measuring atmospheric parameters by transmitting a laser beam and receiving scatter from the atmospheric molecules or aerosol/could particles. It is an active remote sensing technique which can observe temperature, aerosol characteristics, atmospheric constituents, wind velocities, etc., as a function of range. We started lidar observation at Shigaraki MU observatory, Shiga, Japan, in 2000, and have been observing atmospheric temperature in the troposphere, stratosphere and mesosphere, and water vapor mixing ratio (humidity) in the troposphere. The Raman scatter from the atmosphere, with a Raman shift of wavelength according to the species of molecules, is useful in measuring density of different atmospheric constituents. However, the scattering signal intensity is weaker by a factor of 10^3 to 10^6 or even more, and therefore the system needs high power laser and large aperture telescope. In order to study distribution and variation of water vapor mixing ratio at a various observation field, we have developed a couple of portable Raman lidars by limiting the observational range. The first portable Raman lidar system with a Q-switch pulsed Nd;YAG laser (532 nm, 0.6W) and a 35.5 cm Cassegrain telescope was developed in order to monitor water vapor mixing ratio at 200 m altitude for 24 hours a day in day and night. This lidar was also applied to profile water vapor mixing ratio up to 4-5 km at night. Not only vertical profiles, but horizontal humidity distribution over the natural forest around Shigaraki as well as water vapor in volcanic plumes at Mt. Aso has been successfully measured and its capability for field experiment has been proved. This system can be transported by a one-box type vehicle and can be operated with a power generator. Currently, this lidar is located at NiCT Ohgimi observatory in Okinawa and has been profiling water vapor in the sub-tropical region for more than one year. The second system has been developed in order to be carried only with man power without a vehicle. High sensitive GaAsP photomultiplier tubes could reduce the telescope size down to be 20.3 cm diameter without degrading the sensitivity. The system is mounted on the tripod and beam direction could be steered easily in azimuth and elevation. Small batteries and inverters can be used as a power source. The system has now finished a test observation in Mt. Aso, and will be used at other volcanoes where a vehicle is not accessible, as well as at the fields of the forest region where monitoring of atmospheric dynamics and substantial transport has been carried out. Such a portable lidar system would be applied to observation in the various fields where no past observations have been made.

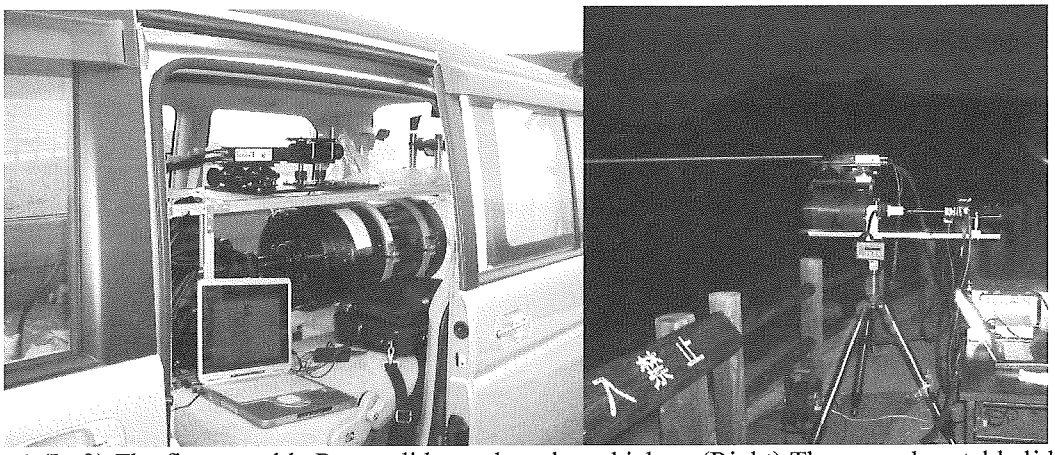

Fig. 1 (Left):The first portable Raman lidar on board a vehicle. (Right):The second portable lidar.

A satellite observation on the atmospheric ozone layer

Laboratory of Atmospheric Environmental Information Analysis, RISH, Kyoto University

Masato Shiotani

The earth system consisting of the atmosphere, the ocean, and the biosphere has been affected by natural and artificial perturbations. Resulting changes in the earth system become obvious in several places and in several parameters. Among those the ozone layer in the middle atmosphere is one of the most important regions to sense such changes. In recent years we have found several important variations in the middle atmosphere including the Antarctic ozone hole, and now we need synthetic understanding and extensive observations for these variations to project the future state of the earth system.

To monitor the atmospheric condition in the middle atmosphere with very high sensitivity Super- conductive Submillimeter-Wave Limb-Emission Sounder (SMILES) was designed on board the Japanese Experiment Module (JEM) of the International Space Station (ISS) as a collaboration project of Japan Aerospace Exploration Agency (JAXA) and National Institute of Information and Communications Technology (NICT). Mission Objectives are: i) Space demonstration of super- conductive mixer and 4-K mechanical cooler for the submillimeter limb-emission sounding, and ii) global observations of atmospheric minor constituents in the stratosphere (O_3, HCl, ClO, HO_2, HOCl, BrO, O_3 isotopes, HNO_3, CH_3CN, etc), contributing to the atmospheric sciences, especially to the ozone chemistry in the middle atmosphere. As a core of the science team we are devoted to this mission.

The SMILES observation is characterized as aiming at variation and its impact of radical species in the stratosphere. Based on its high sensitivity in detecting atmospheric limb emission of the submillimeter wave range, JEM/SMILES will make measurements on several radical species crucial to the ozone chemistry. Some of them have never be seen by any other satellite measurements, and the JEM/SMILES mission will be the first to detect them such as BrO. The SMILES will also try to observe isotopic composition of ozone. Unusually high enrichment in most of the heavy ozone isotopomers in the stratosphere has been puzzling problem, and the JEM/SMILES observation will provide us important findings to work out the puzzle.

As a result of some policy changes a new SMILES science team has been recently established and authorized in JAXA. The SMILES science team has been made up of scientists inside and outside JAXA including overseas scientists. As a consequence of the science team activity we try to form a research core of the earth and planetary atmospheric science in JAXA through coordination with, for example, PLANET-C (Probe of Venus Atmosphere) project. The system detail design and manufacturing of the proto-flight model (PFM) for JEM/SMILES is now being developed, and it is aiming at the launch scheduled in 2009 by the H-II Transfer Vehicle (HTV).

Further information about the SMILES mission including the mission plan can be found at the following URL.

`http://smiles.tksc.jaxa.jp/indexe.shtml`

Atmospheric observations with a ship-borne lower troposphere radar

(Laboratory for radar atmospheric sciences, RISH, Kyoto University)

Mamoru Yamamoto, Hiroyuki Hashiguchi, and Masayuki K. Yamamoto

Wind profilers are a powerful tool to obtain vertical profiles of three components of wind velocities and are widely used for not atmospheric researches but also operations for weather prediction. However observation data over the sea are still insufficient. We have developed a wind profiler for lower tropospheric observations over the sea (Ship-Borne Lower Troposphere Radar: SB-LTR), based on the L-band (1357.5 MHz) lower troposphere radar [1], which we previously developed. The SB-LTR was installed to the oceanographic research vessel MIRAI of JAMSTEC, Japan for test observations in March, 2004 (MR04-01), in December, 2004-January, 2005 (MR04-08), and in October-November, 2006 (MR06-05).

The SB-LTR system consists of five parts, which are a phased array antenna, an active module unit, a transmitter/receiver unit, a data acquisition unit, and a signal processing unit. An electromagnetic coupling coaxial dipole antenna is used as the antenna element [2]. The antenna can be divided into four sub-antennas. It is possible to operate the radar using one sub-antenna (whose size is 2 m x 2 m) for utilization in a relatively small installation space. It is possible to vary the beam direction by electronically steering the zenith angle within 45 degrees. A peak output power of 2 kW is obtained by 24 active transmitting modules.

The overview of the SB-LTR is shown in Figure 1. All equipment except for the antenna was stored in a container to avoid salt damage. A GPS navigational sensor and a three-axis angular sensor were deployed to provide necessary adjustments to wind profiles. During the observation, antenna beams were steered to vertical and 4 oblique directions with the zenith angle of 10 degrees. One cycle for 5 directions took about 2 s. Sub-pulse length was 1 us, which corresponds to the range resolution of 150 m. Time series complex data after conducting pulse-decoding and 64 coherent integrations were stored every 3.2 ms. The data such as roll, pitch, direction, speed, latitude, longitude of the ship simultaneously obtained were also stored for off-line analysis. Using the direction of ship head and the velocity vector of ship, we estimated wind profiles in stationary system. Figure 2 shows time-height cross-section of zonal winds observed with SB-LTR in MR04-08. Westerly wind was changed to easterly wind around December 24. During this period, a few MJO passed over, but the precipitation was not observed so frequently. In spite of relatively dry condition above 2 km (not shown), we could obtain wind profiles up to about 5 km.

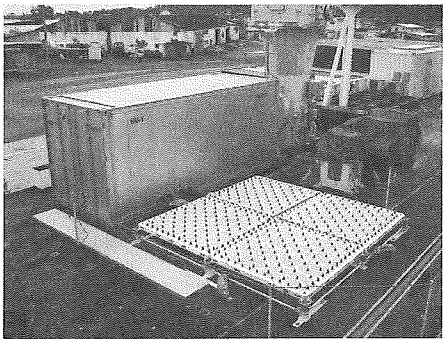

Figure 1. Overview of SB-LTR in MR04-08 cruise.

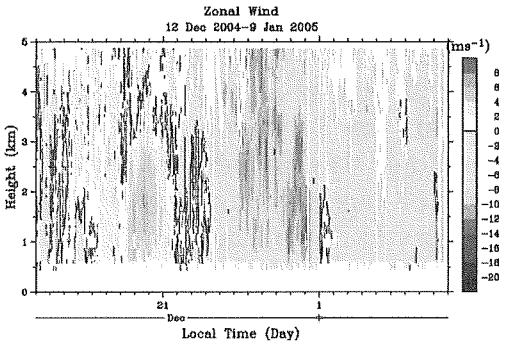

Figure 2. Time-height cross-section of zonal winds observed with SB-LTR during December 12, 2004-January 9, 2005.

REFERENCES

[1] Hashiguchi, H., S. Fukao, Y. Moritani, T. Wakayama, and S. Watanabe, A lower troposphere radar: 1.3-GHz active phased-array type wind profiler with RASS, *J. Meteor. Soc. Japan*, **82**, 915-931, 2004.

[2] Miyashita, H., H. Ohmine, K. Nishizawa, S. Makino, and S. Urasaki, Electromagnetically coupled coaxial dipole array antenna, *IEEE Trans. Antennas Propagat.*, **47**, 1716-1726, 1999.

Method of estimating humidity control capacity of materials

**(Laboratory of active bio-based materials,
RISH, Kyoto University)**

Toshiro Morooka

In Japan, to lower the influence of muggy weather on the living environment of a house, we have so far spent a lot of energy through air-conditioning. However, cutting down such energy consumption is desirable to cope with global warming: a house should be built in such a way that humidity can be controlled by the house itself and with as little artificial air-conditioning as possible. For this purpose, materials that can control humidity have been used in applications like interior wall materials, material for making closets, and materials under floors. However, before using these materials we have to understand their capability to control humidity precisely so that we can use them in a proper way. As a measure of estimating humidity control capacity of materials in an airtight room under sinusoidal temperature variation, we proposed the Cb value, which was the ratio of the range of variation of relative humidity in a steel box lined with material to the range in a steel box only. It was found that the Cb-value was affected by both the temperature variation over one period and the lined area in the box. From this, we could draw Cb-value contour diagrams of the period and the lined area for materials to understand the whole view of humidity control capacity of materials. They are exemplified in Figs. a and b for Japanese cedar and porous ceramics, respectively. Here, in order to show the extent of the lined area, the ratio of lined area (A) to the volume of steel box (V) , "A/V", is used. The overall impression of these two curves differed greatly. Noting the patterns of the contour lines, we saw that those for porous ceramics ran almost parallel to the horizontal axis. On the other hand, those for Japanese cedar ran from the top-left to the bottom-right, indicating that the map was symmetrical to the line passing through the origin, inclining at 45 degrees. From these results, we could conclude that humidity control capacity was higher for Japanese cedar than for porous ceramics in the range examined. In this way, in order to understand the material's humidity control capacity as a whole, we found that it was effective to draw each Cb-value contour map of each period and A/V covering their wide ranges.

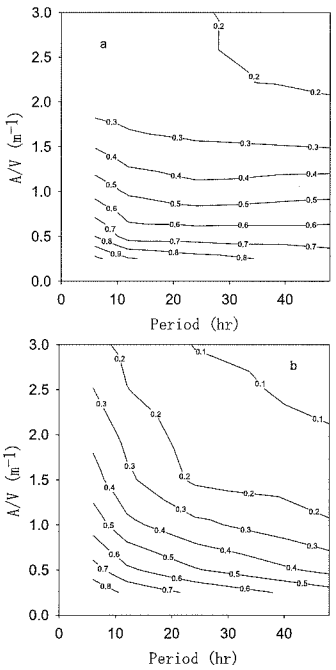

Figs. a and b : C-value contour diagrams of each period and A/V for porous ceramics (a) and sugi(b)

Evaluation of Aging Wood from Japanese Historical Buildings

(Laboratory of Sustainable Materials, RISH, Kyoto University)

Misao YOKOYAMA

In Japan there are so many historical buildings. Especially, the ancient capitals Kyoto and Nara have many traditional wooden buildings, some of which are listed as a World cultural heritage of the UNESCO or as a National Property of Japan.

Wood used for the building materials might change its properties during usages. Therefore, the aging of wood can be of critical importance to traditional carpenters, Buddhist sculptors, art craftsman, museum curators and conservators as well as scientists in the field of art history, architectures, conservation science and wood science. Carpenters have an empiric and old knowledge that leads them to know when a timber needs to be changed. They often estimate age of wood with their naked eye. Features often used are color, odor, density and hardness. Thus the experience and judgment of them is vital.

Wood materials perform differently under various conditions. The degradation of wood is, in general, classified into three categories, i.e., weathering bio-degradation and aging. Aging is defined as a slow oxidation process caused by oxygen in the air. Therefore, based on the temperature-time conversion law an accelerated aging test was performed by heat treatment.

The main purpose of this study is to evaluate the durability and degradation of wood; furthermore, it aims at obtaining an efficient and easy method to evaluate the strength of wood timbers in old structures like temples or shrines. This study aims at understanding and evaluating properties of an old timber.

First, Hinoki (*Chamaecyparis obtusa*) specimens were subjected to the heat treatment 180℃, 150℃, 120℃, and 90℃ respectively under various treatment time by normal oven method. An accelerated aging test was performed by heat treatment to obtain different levels of accelerated aging wood samples.

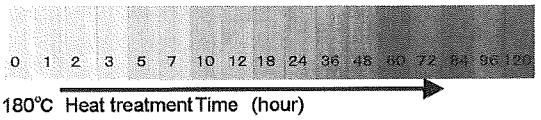

Fig.1 Antique-like appearance hinoki (*Chamaecyparis obutusa*) by the accelerated aging treatment

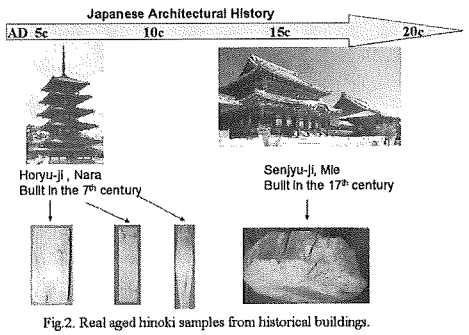

Fig.2. Real aged hinoki samples from historical buildings.

Secondly, naturally aged hinoki, some samples of Dr. J. Kohara old timber collections at the xylarium of RISH, were used. Oldest samples came from timbers of Horyuji Temple used in the 6th century. Horyuji Temple in Nara, at over 1300 years ago, is one of the oldest remaining wooden structures in the world. The age of these samples are measured by dendrochronology (Dr. Mitsutani, Nara National Cultural Properties Research Institute) and radioactive carbon chronology (Dr. Imamura, et al. National Museum of Japanese history), respectively.

A comparison will be lead between mechanical and chemical properties of naturally aged wood and that of heat-treated wood. These results can be used as the standards in comparison with the actual naturally aged wood materials. Future plan is to collect the old timbers from typical historical buildings to create a database of them, in the perspective of better understanding the history of wooden materials.

Development of Wooden Eco House Utilizing Natural Building Materials

Kohei Komatsu, Shinjiro Takino, Takuro Mori and Yasuo Kataoka*
(Laboratory of Structural Function, RISH, Kyoto University; *at present Cyubu University)
Shuichi Kawai, Masafumi Inoue** and Kenji Umemura
(Laboratory of Sustainable Materials, RISH, Kyoto University; **at present Tokyo University)
Yuji Imamura, Kunio Tusnoda, Tsuyoshi Yoshimura and Toshimitsu Hata
(Laboratory of Innovative Humano-habitability, RISH, Kyoto University)
Hiroyuki Yano, Toshiro Morooka
(Laboratory of Active Bio-based Materials, RISH, Kyoto University)

A two story experimental wooden house of 5.4m x 9.1m plane dimensions was completed in November 2006 as shown in Fig.1. This wooden construction is a result of our 6-year collective research activities for developing an idealized wooden structure which has minimum loads on the environment, and is composed of sustainable natural materials such as wood, mud and bamboo etc.

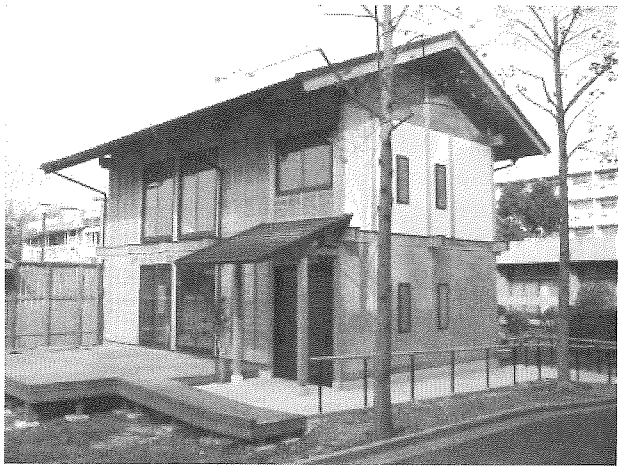

Fig. 1. Wooden Eco House completed in November 2006 in Uji campus.

Square timbers of 15cm x 15cm cross section sawn from 60 years old Sugi (Japanese Cedar, *Cryptomeria japonica*) logs were used for the continuous columns and sills. For short columns, 12cm x 12cm square sawn timbers were used.

All felled logs were initially dried in forest yards for about a few months with the leaves still attached so that free water could be released from the sapwood. After sawing, the square timbers were air-dried for about 6 months by laying them in a timber yard.

Figure 2 shows a perspective view of the wooden eco house in which various innovative attempts were made to recognize our research and development.

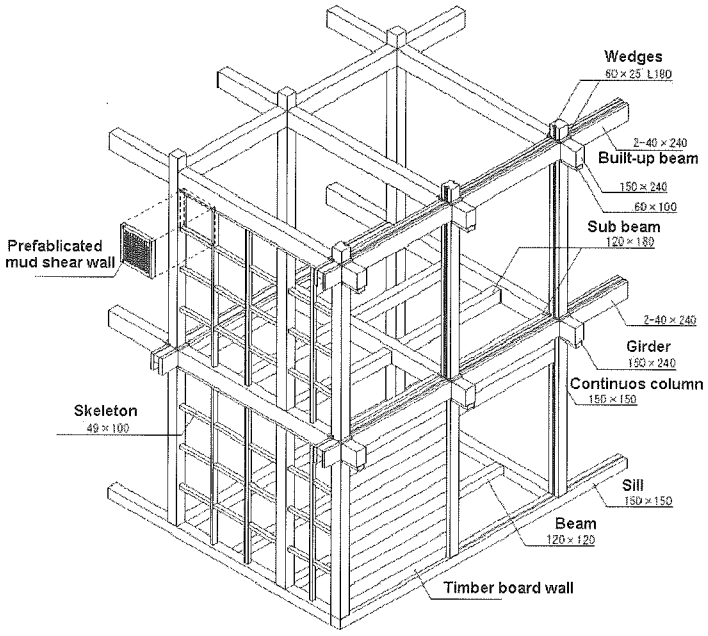

Fig. 2. A perspective view of the wooden eco house

For example, prefabricated small mud shear walls were introduced for shortening the on-site plastering job. Built-up beam system and timber board shear wall system were proposed for utilizing Sugi timber boards of 40mm thickness which were able to be supplied with sufficient quantity and dried relatively easily compared with square timbers. In addition to these structural aspects, living termite nests are being kept under the ground of 1st floor to investigate the process of real termite attack against wooden residential house. This very unique wooden house is now being utilized as a full-scale specimen for measuring not only structural but also living environment performances in timber dwelling house.

Research Projects on High-Performance Utilization of Wood for Outdoor Uses

Laboratory of Innovative Humano-Habitability, RISH, Kyoto University

Yuji Imamura

Wood has a long history of use in familiar products, and even now wood is the staple material for buildings and furniture. Recently, new applications of wood have been decks, garden furniture, house fences, play equipment, boardwalks, and signboards. Wood products are also widely used in public construction works on river and roads such as bridges, sound-insulating fence, and guard-rail. The increase in the outdoor uses of wood products arises from their warmth and amenity properties, good design characteristics and natural harmony with the surrounding scenery. The environmental friendliness of wood is due to its renewability as a natural resource, to the low energy consumption in processing, and because it is easy to recycle or dispose.

As proven by Horyuji Temple in Japan, which is the oldest wooden structure in the world, wood is almost an everlasting material. However, exterior wood, wood for outdoor uses is always exposed to weathering such as light or rainfall, and to biological deterioration by decay fungi or termites. For high-performance utilization of exterior wood products, not only structural reliability, but also durability and weathering resistance are highly required.

We are conducting the research projects on the high-performance utilization of wood for outdoor uses, which are the characterization of the wood surfaces exposed to sunshine and rainfall, the non-destructive detection of decay and insect attacks in wood, the development of maintenance system to provide the long-life to wood, and so on. Among them, two research topics are outlined in this page (1).

Phenolic Resin Treatment of Wood for Improving Weathering Properties

Phenol-formaldehyde (PF) resin treatment was applied to wood to improve weathering resistance against sunshine and rainfall for out-door use. Treatment of wood with aqueous solutions of PF resin-forming compounds gives bulked products of insoluble polymers which will not leach out in water. The molecular weight of the resin was proven to affect the biological resistance as well as dimensional stabilization in relation to the bulking of the wood cell walls, and resin with a molecular weight below 500 was evaluated to provide sufficient stability and biological control. The low molecular weight PF- resin was assumed to yield a polymer within the wood cell walls giving the greater biological resistance.

For outdoor use of wood products, weathering properties such as change of color, occurrence of surface checks, and retention of good surface characteristics are considered to be as important as dimensional stability and biological resistance. Among the factors responsible for natural weathering in wood, solar radiation is thought the most damaging, with water acting to wash away degradation products causing the surfaces to erode. PF–resin treatment improved the surface resistance of wood such as color stability, physical performance in cracking and hangnail test, and biological resistance after weathering.

Improvement of Liquid Penetration of Wood by Precompression Treatment

Impregnating wood with liquid chemicals is a common technique for enhancing various physical and biological properties, such as dimensional stabilization and decay resistance. However, it is not always easy to impregnate the liquid evenly and deeply into refractory wood specimens. Although several pretreatment processes have been developed to increase the permeability of wood, none are particularly practical or economical, except the conventional methods such as incision.

A new system for enhancing the penetration of liquid into wood using a precompression treatment was designed, and the effects of compressive deformation and recovery on liquid uptake were evaluated. Precompression with large deformation under appropriate moisture and heat conditions, with optimum press schedules effectively increased the penetration of liquid into refractory wood samples of practical sizes without producing any strength reductions. Fracture of pit membranes during compression with little damage to unpitted cell-walls was believed to improve liquid penetration with negligible compression defects.

REFERENCES

[1] Imamura, Y. (2006) Mokuzai-Kogyo-Tanshin(Rapid Report of Wood Industry-Japanese) 24(1):1-11

Relativistic Turning Acceleration of Resonant Electrons by Coherent Whistler-Mode Waves in a Dipole Magnetic Field

(Laboratory of Computer Simulations for Humanospheric Science, RISH, Kyoto University)

Yoshiharu Omura, Danny Summers, Hideyuki Usui

We report a very efficient process for accelerating high energy electrons by coherent whistler-mode waves in the Earth's dipole magnetic field, which we have found in our recent test particle simulations [1,2]. The efficient acceleration process takes place for weakly relativistic seed electrons of a few hundred keV. Under an assumption that the whistler-mode wave packets are excited near the equatorial plane of the inner magnetosphere and propagate away from the equator, the acceleration process becomes irreversible. With a sufficiently long whistler-mode wave packet of the order of one second, the energetic electrons are accelerated to a relativistic energy range of a few MeV through a single resonant trapping process. We call this particular acceleration process relativistic turning acceleration (RTA), which could be a viable mechanism for increasing relativistic electron fluxes in the outer radiation belt. Necessary conditions for RTA are a relatively large amplitude of whistler-mode waves, in the range of 50 pT to a few hundred pT, and an initial kinetic energy of trapped electrons in the energy range of a few hundred keV. The minimum energy of electrons accelerated by the RTA process, and the maximum energy attained by it are derived analytically, and verified by the test particle simulations.

The time scale of each RTA process is only of the order of a second. If a sufficiently large temperature anisotropy is maintained by continuous injection of high energy particles into the inner magnetosphere, successive chorus emissions are generated [3,4]. Then, a series of effective RTA processes take place, resulting in a rapid formation of a flux of relativistic electrons with a time-scale much shorter than that typically predicted by quasi-linear diffusion theory. RTA is a unique feature of the dipole magnetic field geometry. The process should also be operative in the magnetospheres of Saturn and Jupiter.

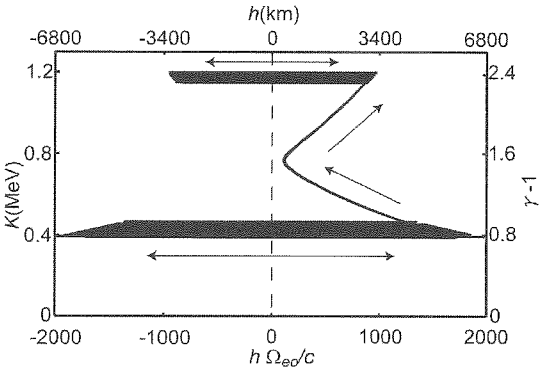

Figure 1. Trajectories of resonant electrons interacting with a coherent whistler-mode wave.

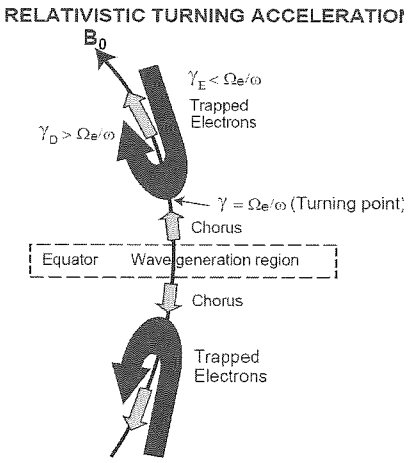

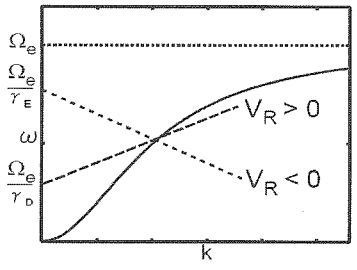

Figure 2. Schematic illustration of RTA (top panel) and the relativistic cyclotron condition for whistler mode wave (bottom panel).

REFERENCES

[1] Omura, Y., and D. Summers (2006), *J. Geophys. Res.*, 111, A09222, doi:10.1029/2006JA011600.

[2] Omura, Y., N. Furuya, and D. Summers (2007), *J. Geophys. Res.*, in press.

[3] Katoh, Y. and Y. Omura (2007), *Geophys. Res. Lett.*, 34, L03102, doi:10.1029/2006GL028594.

[4] Katoh, Y. and Y. Omura(2007), *Geophys. Res. Lett.*, inpress

Study on Wireless Power Distribution System for Buildings

(Laboratory of Applied Radio Engineering for Humanosphere, RISH, Kyoto University)

Naoki Shinohara, Tomohiko Mitani, and Kozo Hashimoto

We can apply the wireless power transmission (WPT) to the ground. Our research group advances two types of applications of wireless power transmission on the ground. One is a ubiquitous power source with weak wireless power density under $10W/m^2$[1]. The other is high power WPT to an electric vehicle[2] in closed transmitter and receiver and the WPT for wireless power distribution system for buildings as a new application of microwave power transmission (Fig. 1). $10W/m^2$ is limitation of safety of human body. Therefore, if there is no human, we can increase the wireless power which is limited by the system, mainly the limited by semiconductors. This system supplies electric power wirelessly by using building materials themselves as a microwave transmission line. The purpose of the present research is to confirm the feasibility and to clarify the technical problems. We have developed variable power dividers (Fig. 1) whose split ratios are from -10dB to -3dB. And we constructed the power distribution system that actively controls the distribution. We have examined the methods to take out microwave power from the deck plate waveguide. We analyzed methods using a coaxial probe and E-plane T-junction, and established the design technique. Finally, we did a practical examination of the whole system based on the abovementioned experiments. We designed the wireless power distribution system in detail, and explained its technical problems.

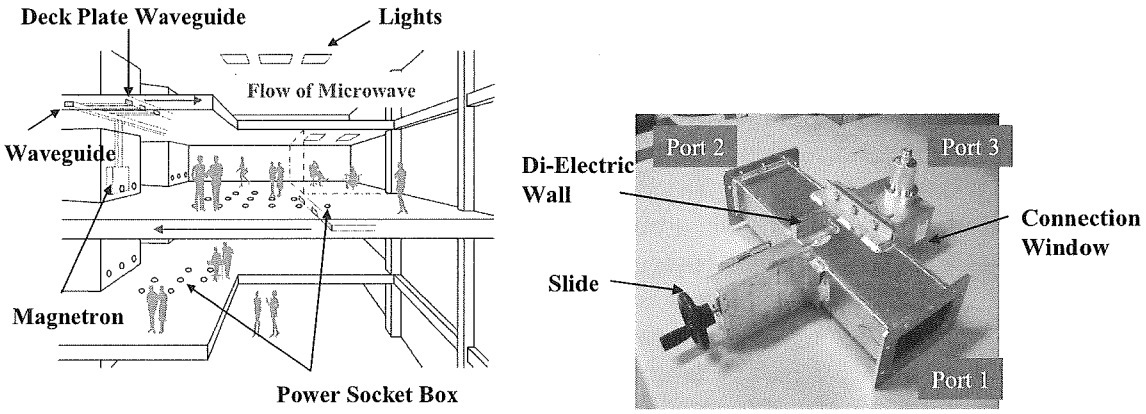

Fig. 1 Concept of Wireless Power Distribution System for Buildings and Developed Power Distribution System that Actively Did the Distribution Control

REFERENCES

[1] N. Shinohara, T. Mitani, and H. Matsumoto, "Study on Ubiquitous Power Source with Microwave Power Transmission", Proc. of URIS General Assembly, 2005, C07.5(01145)

[2] N. Shinohara, J. Kojima, T. Mitani, T. Hashimoto, N. Kishi, S. Fujita, T. Mitamura, H. Tonomura and S. Nishikawa, "Assessment Study of Electric Vehicle Charging System with Microwave Power Transmission II", Tec. Report of IEICE, SPS2006-18 (2007-02), 2007, pp.21-24 (in Japanese)

ACKNOWLEDGEMENT

This study is supported by Japan Science and Technology Agency. We corroborate with Kajima Technical Research Institute, Okayama University, and University of Tokushima.

Novel Space Environment Monitor, Instrument, and Space Propulsion Systems

(Laboratory of Space Radio Science, RISH, Kyoto University)

Hiroshi Yamakawa, Hirotsugu Kojima, and Yoshikatsu Ueda

1. Monitor system for Space Electromagnetic Environments (MSEE)

The main objective of the MSEE (Monitor system for Space Electromagnetic Environments) is to monitor the electromagnetic disturbances caused by human activities in space. It consists of the small sensor units distributed around the target space (Fig. 1). Our main activities on the development of the MSEE in 2006 are as follows: (a) Development of the analogue ASIC containing the differential amplifiers and A/D converters, (b) Simulation study on the location estimation method for each sensor unit.

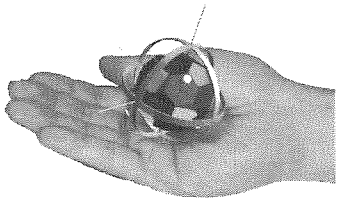

Fig. 1: Sensor unit of the MSEE.

2. Magneto-Plasma Sail (MPS) Space Propulsion System

An MPS (Magneto-Plasma Sail) is a unique propulsion system, which travels through interplanetary space by capturing the energy of the solar wind, which inflates a weak original magnetic field made by a super-conducting coil of about 2-10 m in diameter with an assistance of a high-density plasma jet. From our theoretical estimations, momentum transfer from the solar wind to a spacecraft with a coil is large enough if the plasma source is operated to inflate only the magnetic field away from the spacecraft. Our activities in 2006 are as follows: (a) Sizing (mass, dimension, current, etc.) of the super-conducting coil to produce magnetic field around the spacecraft, (b) Preparation of the experiment facility to measure magnetic field, temperature, current etc. around super-conducting coil.

3. Wave-Particle Correlator (WPC) Instrument for Spacecraft Observation.

For a practical application of a plasma wave instrument, a direct measurement system of wave-particle interactions is one of the important systems to the space science mission. WPC instrument can observe wave-particle interactions by calculation of the cross correlation functions between obtained waveforms and detected particles onboard. Our designed system is assembled in one FPGA (Field Programmable Gate Array) IC and data calibration and correlation method is programmed in FPGA.

On April 18, 2006, the Science and Technology Award by Ministry of Education, Culture, Sports, Science and Technology was resented to a space plasma study team of Hiroshi Matsumoto, Yoshiharu Omura, and Hirotsugu Kojima for "Discovery and Theoretical Analysis of Electrostatic Solitary Waves in Space Plasmas by a Scientific Satellite"

Electrostatic Solitary Waves (ESW) were observed by an innovative plasma wave instrument on board the Geotail satellite, launched in 1992. The formation process of the ESW were also reproduced by computer simulations, and its physical mechanism has been analyzed theoretically. ESW are identical to wave phenomena called Broadband Electrostatic Noise (BEN) which is a special wave frequency spectrum observed in the plasma sheet boundary layer of the Erath's magnetotail. The plasma wave observation by the Geotail satellite has revealed that the real characteristic of BEN is not a noise but coherent solitary waves resulting from a nonlinear evolution of an electron beam instability as verified in the computer simulation. The existence of such electron beam has also been confirmed in the observation by the Geotail satellite. The successful plasma wave observations by the Geotail satellite substantially influenced plasma wave observations by spacecraft launched after the Geotail satellite. Various types of ESW have been found in other regions of the magnetosphere, such as magnetosheath and auroral regions. The discovery of ESW has stimulated development of nonlinear theories of electrostatic potential structures and related numerical simulation studies.

Professor Shoichiro Fukao and Dr. Hiroyuki Hashiguchi received Minister's Prize for Science and Technology from the Ministry of Education, Culture, Sports, Science and Technology of Japan

In April 2006, Professor Shoichiro Fukao and Dr. Hiroyuki Hashiguchi of Research Institute for Sustainable Humanosphere, Kyoto University, and Shinichiro Watanabe of Mitsubishi Electric Corporation received Minister's Prize for Science and Technology from the Ministry of Education, Culture, Sports, Science and Technology of Japan for their outstanding contribution to development of lower-tropospheric wind profiling radar. The Minister's Prize for Science and Technology is to commend individuals who have made outstanding achievements in science and technology fields.

Professor Shoichiro Fukao received the Okawa Publications Prize

In November 2006, Professor Shoichiro Fukao received the Okawa Publications Prize for his outstanding book entitled, "Radar System studies for Atmospheric Remote Sensing," which was published by Kyoto University Press in March 2005. He received the prize with Kyosuke Hamazu of Mitsubishi Electric Corporation, coauthor of the book. The Okawa Publications Prize is to give public recognition and to promote outstanding publications in the field of information and telecommunications.

Mr. Hajime Nagata received Student Presentation Award (Aurora Medal) from the Society of Geomagnetism and Earth, Planetary and Space Sciences (SGEPSS)

Mr. Hajime Nagata received Student Presentation Award (Aurora Medal) from the Society of Geomagnetism and Earth, Planetary and Space Sciences (SGEPSS) for his outstanding presentation entitled, "Cirrus cloud observation in the tropical troposphere by the Equatorial Atmosphere Radar and the 95-GHz cloud profiling radar" at the 120th SGEPSS General Assembly in November 2006. The Student Presentation Award is a prize for students in geomagnetism and earth, planetary and space sciences, and presented for commendation of their excellent presentation at autumn meetings of SGEPSS.

An observational study of mesoscale phenomena with UHF wind profilers

Ahoro Adachi
Laboratory of Radar Atmospheric Science, RISH, Kyoto University

The understanding of the structure of the mesoscale phenomena is essential for weather forecasting since the mesoscale phenomena often dominate local weather in the region where they occur to the synoptic scale phenomena and sometimes produce severe storms. Recent progress in developing remote sensing tools like the Doppler radar has been leading to a rapid advancement of our understanding of mesoscale processes. The observational studies, however, always depend strongly on the available measuring equipment. Generally, the Doppler radar is available only for the phenomena that are accompanied by precipitation, conversely, other remote sensing tools like sodar and lidar are not available in precipitation. Wind profilers are one of the best tools for studying mesoscale phenomena, because they can observe the wind profile in all weather conditions. Moreover, the wind profilers provide the temperature profile when they are equipped with Radio Acoustic Sounding System (RASS). These observational capabilities of wind profilers assist to understand the dynamics of mesoscale meteorological phenomena. The aim of this thesis is to study the structures of mesoscale phenomena by use of the UHF L-band (about 1 GHz) wind profilers.

The L-band wind profiler was originally developed at NOAA [1,2] to provide high-vertical resolution wind measurements in the first few kilometers of the atmosphere from a few hundred meters above ground level. This lowest range gate is low enough to be supported by another measurement like a tower to the ground. In addition, recent progress of technology enables RISH to develop new L-band profilers to obtain continuous wind profiles in clear air up to 5 km on average [3]. This means that the L-band wind profiler could obtain whole structure of the mesoscale phenomena. Moreover, the L-band profiler is generally small enough to move to places where the mesoscale phenomena are expected to occur.

Even for the L-band wind profilers, observations at altitudes of a few hundred meters is, however, difficult because of hardware limitations and noise from both inside and outside of the system. In addition, the quality of the profiler data in clear air depends strongly on atmospheric conditions because of the small power aperture of the radar, since the clear-air echo becomes weak in cold and/or dry atmosphere. Moreover, the sensitivity of the L-band wind profilers to hydrometeors is different from those profilers operating at other frequencies. In this thesis, thus, the performance of L-band wind profilers is evaluated especially in observing the atmosphere from low altitudes, and their observational capabilities to facilitate understanding the dynamics of mesoscale meteorological phenomena are demonstrated.

A special focus of this thesis is the validation of the horizontal and vertical motion fields obtained from the profiler observations. In this thesis a five-beam wind profiler and a collocated meteorological tower are used to estimate the accuracy of four-beam and three-beam wind profiler techniques in measuring horizontal components of the wind at as low as 200 m in altitude. In the traditional three-beam wind profiler techniques, the horizontal components of wind are derived from two orthogonal oblique beams and the vertical beam. In the less used four-beam method, the horizontal winds are found from the radial velocities measured with two orthogonal sets of opposing coplanar beams. In this thesis the observations derived from the two wind profiler techniques are compared with the tower measurements. Results show that, while the winds measured using both methods are in overall agreement with the tower measurements, some of the horizontal components of the three-beam-derived winds are clearly spurious when compared with the tower-measured winds or the winds derived from the four oblique beams. These outliers are partially responsible for a larger 30-min, three-beam standard deviation of the profiler/tower wind speed differences (2.2 m s^{-1}), as opposed to that from the four-beam method (1.2 m s^{-1}). It was also found that the spatial variability of the vertical airflow in nonrainy periods or hydrometeor fall velocities in rainy periods makes the vertical beam velocities significantly less representative over the area across the three beams, and decreases the precision of the three-beam method. It is concluded that profilers utilizing the four-beam wind profiler technique have better reliability than wind profilers that rely on the three-beam wind profiler technique. Based on this result, the four-beam method is applied for the analyses of mesoscale phenomena in this thesis.

One of the unique capabilities of the wind profiler is to be able to rapidly sample the vertical velocity. Vertical airflow measurements are essential for understanding the structure of mesoscale phenomena

because vertical airflow could initiate and maintain clouds that produce mesoscale phenomena. However, there are few studies on estimating the accuracy of profilers in measuring the vertical velocity, although it has a significant influence on the estimation of horizontal wind [4, 5]. One of the reasons is that the vertical airflow has spatial and temporal variability due to convection [6], which makes the comparison difficult. The mesoscale events discussed in this thesis provide opportunities to observe mesoscale features with *in situ* and remote sensors simultaneously and enable to estimate the accuracy of profilers in measuring the vertical component of the wind. The results show that the vertical velocities derived from the wind profiler agree well with *in situ* vertical velocities measured by a sonic anemometer on the tower.

Three kinds of mesoscale phenomena with different weather conditions are analyzed with the wind profilers along with other observational equipments in this thesis. They are, a line-shaped convective system (LCS) with strong clear-air echoes in summer, a shallow gravity current with weak clear-air echoes in winter, and gusty winds within a typhoon with heavy precipitation.

The LCS is one of the mesoscale phenomena, which produces heavy rainfall in a local region where it occurs. The formation mechanism of the LCS is currently in dispute. One of the difficulties arises from the lack of observation in the clear-air region ahead of the LCS where conventional Doppler radar has not observed because of less hydrometeors. In this thesis, wind profiler data ahead of the LCS are analyzed to understand the formation of the LCS. The analysis revealed a horizontal convergence layer above a divergence layer in the clear-air region upwind of the LCS. The profiler observed upward airflow in the convergence layer and downward airflow in the divergence layer underneath. It is concluded that the upward airflow in the convergence layer and terrain effects forms the LCS from the analysis.

Observations from a wind profiler and a meteorological tower are utilized to study the evolution of a gravity current that passed over the MRI field site. Observations from the profiler/RASS and the tower-mounted instruments illustrate the structure of the gravity current in both wind and temperature fields. The profiler data reveal that there were three regions of waves in the vertical velocity field: KH waves above the feeder flow, lee-type waves in the head region of the gravity current, and the solitary wave formed from the elevated head of the gravity current. Profiler vertical-motion observations resolve this wave and enable to classify it as a Benjamin-Davis-Ono (BDO) type solitary wave. The ducting mechanism that enabled the solitary wave to propagate is also revealed from the wind profiler/RASS measurements.

Observations from the wind profiler and a Doppler radar were used to study the evolution of two thin-line echoes that occurred over the Kanto Plain as a typhoon (T0221) passed. The first thin-line echo formed on the edge of a region of low clouds between the typhoon center and a trailing outer rainband. The second thin-line echo developed ahead of an outer rainband of the typhoon in the area where the first thin-line echo had propagated. Both thin-line echoes were accompanied by gusty winds and followed by cold airflows, and both passed the MRI field site. Surface instruments at the MRI site recorded a peak wind gust of 31.6 m s^{-1} as the first thin-echo passed. The wind profiler indicated that the cold airflow behind the first boundary had characteristics unique to gravity currents, and the second boundary was associated first with strong updrafts and then with strong downdrafts. These results suggest that the first thin-line echo was caused by a gust front, and the second thin-line echo was caused by a solitary wave. In summary, it is confirmed that the use of wind profiler/RASS is invaluable in the study of mesoscale phenomena.

REFERENCES

[1] Ecklund, W. L., D. A. Carter and B. B. Balsley (1988) J. Atmos. Oceanic Technol. 5: 432-441

[2] Carter, D. A., K. S. Gage, W. L. Ecklund, W. M. Angevine, P. E. Johnston, A. C. Riddle, J. Wilson and C. R. Williams (1995) Radio Sci. 30: 977-1001

[3] Hashiguchi, H., S. Fukao, Y. Moritani, T. Wakayama and S.Watanabe (2004) J. Meteor. Soc. Japan 82: 915-931

[4] Strauch, R. G., B. L. Weber, A. S. Frisch, C. G. Little, D. A. Merritt, K. P. Moran and D. C. Welsh (1987) J. Atmos. Oceanic Technol. 4: 563-571

[5] Wuertz, D. B., B. L. Weber, R. G. Strauch, A. S. Frisch, C. G. Little, D. A. Merritt, K. P. Moran and D. C. Welsh (1988) J. Atmos. Oceanic Technol. 5: 450-465

[6] Gage, K. S., J. R. McAfee, D. A. Carter, W. L. Ecklund, A. C. Riddle, G. C. Reid and B. B. Balsley (1991) Science 254: 1771-1773

[7] May, P. T. and R. G. Strauch (1998) J. Atmos. Oceanic Technol. 15: 579-586

Studies on Orographic Rainbands Based on Combined Wind Profiler-Weather Radar Observations

Yasuko Umemoto
Laboratory of Radar Atmospheric Science, RISH, Kyoto University

The phenomena in the atmosphere are classified according to their horizontal scale. The scales of air motion encountered in cloud dynamics can be divided roughly into three ranges: the synoptic scale which exceeds about 2000 km in horizontal scale, the mesoscale which covers between about 20 and 2000 km in scale and the convective scale covering between 0.2 and 20 km (1). Convective clouds like thunderstorms as an isolated entity bring strong rainfall in 30 minutes ~1 hour and often occur in large groups and complexes. These complexes, referred to as Mesoscale Convective Systems (MCSs), are generally much larger than each cloud and of considerable scientific interest and practical importance. MCSs sometimes last for a long time through self-multiplication, which result in heavy rainfall in local area. It is important to understand MCSs very well, because they must be forecasted within several hours and it is difficult to forecast them in such a short time so far. MCSs also produce a large proportion of the earth's precipitation and thus are important from a climatological point of view. MCSs occur in a variety of forms such as multi-cell thunderstorms, supercell thunderstorms, squall lines and rainbands. When the generation mechanisms are considered, one important source of air motions in clouds is the flow of air over hills and mountains. While there are various types of orographic precipitation generated over and around the mountains (2), orographic precipitation of upslope or upstream triggering of convection often produce heavy rainfall and has been studied primarily over and around high mountains; e.g., the Rocky Mountains (3), Hawaii Islands (4), the Hokkaido Orofune mountain range (5), the southeast sides of the Kii Peninsula (6), Kyushu Yaku Island (7), and the Nagasaki Peninsula (8). However, the generating and developing mechanisms of these orographic precipitations have not been sufficiently clarified. It was difficult to obtain sufficient observational data over complex orographic and oceanic regions. Moreover time and space resolutions of operational observation by the Japan Meteorological Agency (JMA) have not been fine enough to investigate the MCSs.

A series of special observation campaigns, called "X-BAIU" were conducted over the East China Sea and Kyushu during the Baiu seasons from 1998 to 2002 (9). The purpose of this campaign was to investigate MCSs and disturbances in the Baiu front around Kyushu and the East China Sea. In these campaigns, X-band Doppler radars and wind profilers were installed. There had never been observations combining two or more the Doppler weather radars and two or more wind profilers done before. Wind profiler observations are well suited to examine detailed wind behavior including the vertical wind component associated with the MCSs (~100 km horizontal extent). Application of the wind profiler technique to the Baiu-frontal atmosphere was initiated by using a VHF-band profiler (the MU radar) (10, 11). In recent years, L-band wind profilers were developed in order to observe the lower troposphere (12). Wind profilers have the advantage that they can observe the wind behavior in no precipitation area, where typical weather radars cannot. However, the observation area is limited horizontally close to the radar. The JMA has operated the Wind profiler Network and Data Acquisition System (WINDAS) which consists of 31 wind profilers in Japan. In order to detect and predict severe storms, the interval of each site is 130 km on average.

To understand the structure of orographic rainbands and figure out mechanisms of their formation and development over coastal regions of Japan, detailed analyses of the orographic rainbands occurred in Kyushu in the Baiu season and in Shikoku in the summer season using various data sets are conducted. In order to understand the orographic rainband occurred over Kyushu, the rainbands extending northeastward from the Koshikijima Islands (Koshikijima line) observed on the south side of the Baiu frontal convergence zone on 28~29 June 1999 and 30 June~1 July 2002 during the field experiments "X-BAIU" are selected. The structures of the Koshikijima line are investigated based on observations by the C-band weather radars and the X-band Doppler radars. The Koshikijima line was consisted of some strong cellular precipitation clouds aligned in the southwest-northeast direction. The precipitation cells generated over the Koshikijima Islands propagated northeastward one after another in the rainband. The Koshikijima line with the length of 120~200 km and the width of 8~20 km had been maintained for about 11 hours. Vertical-temporal variations of wind around the Koshikijima line were indicated by the wind profilers and the X-band

Doppler radars. While the Koshikijima line appeared, strong southwesterly wind (~20 m/s) was predominant from the surface to 5 km altitude. The direction of the rainband agreed with the direction of the horizontal wind averaged below 3 km altitude. In addition, there was a strong shear normal to the rainband below 3 km altitude (13).

To understand the orographic rainband occurred over Shikoku, the rainband extending northward from the Muroto Cape on 1 August 2004 was selected. The rainband was generated on the north side of the Muroto Cape and stayed for about 20 hours after the typhoon Namtheun passed over Western Japan. The structure of the rainband was investigated by the C-band weather radars. The rainband had the length of ~100 km and the width of ~30 km, and consisted of some strong cellular precipitation clouds aligned in the south-north direction. The precipitation cells generated on the north side of the Muroto Cape propagated northward one after another in the rainband. Vertical-temporal variations of wind around the rainband were indicated by three wind profilers of the WINDAS. While the rainband occurred, strong southerly wind more than 15 m/s was predominant from the surface to 7 km altitude on the windward and leeward side of the rainband. The moving speed of cellular echoes in the rainband was almost consistent to the horizontal wind around 2 km altitude. In addition, there was a shear parallel to the rainband below 2 km altitude. Southeasterly wind was predominant below 2 km altitude on the east side of the rainband. Besides, updraft more than 0.4 m /s had been observed continuously in lower layer below 3 km altitude around the rainband.

Atmospheric conditions around the Koshikijima line and the rainband at Shikoku were examined by the upper-air sounding analyses. While these rainbands were observed, convectively unstable stratification, large Froude number (Fr) (>1), low Lifting condensation level (LCL) (below the top of the mountains around the rainband), large Convective available potential energy (CAPE) index and much water vapor were found in the lower layer. The generating process of these rainband is as follows: convective clouds were generated by effect of the geographical features and moved to the leeward side one after another by background wind. Then the precipitation cells formed the band-shaped rainfall. The direction of the rainband was result in the propagation of clouds, which was associated with the wind direction around 2~3 km altitude. In addition, generation and redevelopment of clouds by orographic effect and inflow on the leeward side of the rainband help the rainband to develop and form the long rainband. Even low mountains were capable of forming an organized precipitation band under the environmental fields in which there were a moist convectively unstable atmosphere, LCL was lower than the top of the mountains at the generating region, and there were both large Fr (>1) and strong wind in the lower troposphere. These results could be applied to not only the rainband in the present cases but also other region in other season.

REFERENCES

[1] Orlanski, I. (1975) Bull Amer Soc 56: 527-530
[2] Houze, R. A. (1994) Cloud Dynamics
[3] Yoshizaki, Y. and Y. Ogura (1988) J Atmos Sci 45: 3700-3722
[4] Smolarkiewicz, P. K., R. M. Rasmussen, and T. L. Clark (1988) J Atmos Sci 45: 1872-1905
[5] Iwanami, K., K. Kikuchi, and T. Taniguchi (1988) J Meteor Soc Japan 66: 497-504
[6] Sakakibara, H. and T. Takeda (1973) J Meteor Soc Japan 51: 115-167
[7] Kanada, S., H. Minda, B. Geng, and T. Takeda (2000) J Meteor Soc Japan 78: 47-67
[8] Yoshizaki, M., T. Kato, Y. Tanaka, H. Takayama, Y. Shoji, H. Seko, K. Arao, K. Manabe, and members of X-BAIU-98 Observation (2000) J Meteor Soc Japan 78: 835-856
[9] Kato, T., M. Yoshizaki, K. Bessho, T. Inoue, Y. Sato, and X-BAIU-01 observation group (2003) J Meteor Soc Japan 81: 993-1013
[10] Fukao, S., M. D. Yamanaka, T. Sato, T. Tsuda, and S. Kato (1988) Mon Weath Rev 116: 281-292
[11] Fukao, S., M. D. Yamanaka, H. Matsumoto, T. Sato,T. Tsuda, and S. Kato (1989) Pure Appl Geophys 130: 463-479
[12] Hashiguchi, H., S. Fukao, Y. Moritani, T. Wakayama, and S. Watanabe (2004) Bound Layer Meteor 74: 419-424
[13] Umemoto, Y., M. Teshiba, Y. Shibagaki, H. Hashiguchi, M. D. Yamanaka, S. Fukao, and X-BAIU-99 and X-BAIU-02 observational groups (2004) An Geo 22: 3971-3982

MF radar studies on the dynamics of the mesosphere and lower thermosphere

Kiyoshi Igarashi
Laboratory of Radar Atmospheric Science, RISH, Kyoto University

Studies on the dynamics of the mesosphere and lower thermosphere (MLT) received a big boost with the introduction of medium frequency (MF) radar. Compared to other systems MF radar is more economical and other merits such as simple nature of the system, convenient antenna configuration, high efficiency in continuous observation etc. has attracted a number of investigators. As a result, MF radars were installed at various locations around the globe. Combined usage of the datasets opened new avenues in collaborative studies and generated important information on mean winds, atmospheric tides, gravity waves and planetary waves. This thesis mainly deals with the analysis of MF radar data collected at the midlatitude stations Yamagawa (31.2°N, 130.6°E) and Wakkanai (45.4°N, 141.7°E) in Japan, and the high latitude station Poker Flat (65.1°N, 147.5°W), Fairbanks, Alaska, USA (Fig. 1). The Communications Research Laboratory installed these systems in the 1990s and since then has archived valuable datasets. This helped the author to undertake a systematic investigation on various dynamic features of the MLT region.

Analysis of the mean winds over Yamagawa and Wakkanai suggest that the circulation characteristics observed at these midlatitude stations are consistent with other midlatitude stations. Below 90 km, the mean prevailing zonal winds at both sites are dominated by westward/eastward motions in the summer/winter seasons. Meridional circulation at meteor heights is generally southward during most of the year and also extends to lower mesospheric heights during summer. The summer westward jet at Wakkanai is consistently stronger than at Yamagawa. However, the winter eastward winds have identical strength at both locations. Meridional winds also show larger values at Wakkanai. Harmonic analysis of mean zonal winds clearly demonstrates the dominance of annual oscillation over the other periods. Comparison of the observed winds and the HWM93 model winds shows interesting similarities and discrepancies. Climatological comparison of the mean winds at the MF sites and the MU radar site indicates latitudinal dependency of the summer westward jet which is also clearly evidenced in model studies. The analysis also revealed some signs of interannual variability of MLT mean winds.

Studies on the structure and variability of diurnal, semidiurnal, and terdiurnal tides in the midlatitude MLT region generated abundant information. Analysis of the semidiurnal tides indicates reasonable similarities in the variations over Yamagawa and Wakkanai. At both sites, the amplitude generally ranges from 5 to 15 m/s. The multi-year average indicates that the maximum amplitude is observed in August/September at both sites. The summer season is characterized by a large vertical wavelength, while the winter season has a comparatively smaller wavelength. Comparison of the observed semidiurnal tidal amplitude and phase parameters, and the GSWM-98 model values is generally not satisfactory. Diurnal tidal amplitude at Yamagawa and Wakkanai shows significant differences in strength. The amplitude is consistently larger at Yamagawa. Phase structures show better agreement between the sites. As in the case of semidiurnal tide, comparison of the diurnal tidal parameters and the GSWM-98 values reveals less satisfactory results. The interannual variability observed in both the semidiurnal and diurnal tides is larger in the Yamagawa data compared to the Wakkanai data. The semidiurnal and diurnal tidal phases around 90 km generally exhibit a bimodal state with the phase with an almost constant phase near the summer (June) and winter (December) solstices, and mark rapid transitions in the equinoxes. The duration of the winter constant phase is longer in the summer solstice than in the winter solstice. The terdiurnal tidal amplitude observed at Wakkanai exhibits strong day-to-day variability. Short-time variability confirms that the amplitude of terdiurnal oscillation can, on occasion, reach that of the diurnal and semidiurnal tides. The presence of dominant 8-h oscillation is observed in all seasons. However, a strong seasonal dependence is not observed in their amplitude variations. Amplitude values in the winter season are slightly larger than the corresponding values in the summer season. It was found that the terdiurnal amplitudes at Wakkanai are more comparable to the diurnal tidal amplitudes than the semidiurnal values. The dynamical behaviour of 12-, and 24-h oscillations during a time of strong eastward wind was investigated and the result revealed an anticorrelation between the magnitude of eastward mean wind and the zonal amplitude of the diurnal oscillation. It was also observed that the zonal amplitude of the diurnal oscillation is highly correlated with the diurnal oscillation amplitude of the geomagnetic declination, and also shows the strong decrease at the winter solstice.

Observations of planetary waves with quasi-2-day and 16-day periodicities are reported. Analysis of the quasi-2-day wave indicates similar wave features observed at Yamagawa and Wakkanai. The occurrence

of the wave event (probably the same) is seen at both stations during the same days. The wave is found every year with the maximum amplitude in the summer months. The meridional component has a larger amplitude than the zonal component. Comparing the amplitudes at the two stations, the values observed at Yamagawa are larger than those at Wakkanai. The amplitude appears to attain its maximum value at around 90 km at both stations. Substantial year-to-year variations are observed in the 2-day wave amplitude. The average wave period observed at Yamagawa and Wakkanai is roughly 48 hours. The study also explores the dependence of the 2-day wave on the background atmospheric circulation. The 16-day wave climatology observed at Yamagawa clearly shows some seasonal variations. The period from late autumn to spring is marked with larger wave activity, with the strongest waves observed in winter months. The maximum amplitude observed at Yamagawa was about 20 m/s, which is comparatively larger than the amplitudes observed at midlatitude stations. The height dependence of the 16-day wave suggests that the maximum amplitude is observed at altitudes below 80 km. The summer months are characterized by much weaker wave activity. The vertical wavelength appears to be larger in the winter months and shorter in the summer months. The study again confirms that the 16-day wave is highly sensitive to the background mean winds. Eastward motion of the background winds is a more favourable condition for the 16-day wave to penetrate to MLT heights. The wave features show some signs of interannual variability. Overall, the observed features of the 16-day wave at Yamagawa, which is located at the edge of the subtropical latitudes, show some correspondence with the results reported for midlatitude stations. Analysis of the critical frequency of sporadic *E* (*Es*) indicates quasi-periodic oscillations with a period of 2-16 days. The study shows a close relationship between planetary waves and the recurrent cycle of *Es* activity.

The dynamics of the arctic MLT region has been studied using the MF radar wind measurements conducted at Poker Flat, Alaska. The mean wind characteristics observed are fairly consistent with previous wind measurements obtained by the Poker Flat MST radar. The main feature of the zonal circulation is the annual variation with summer westward flow and winter eastward flow. The annual mean zonal wind has a westward motion at altitudes below 90 km. The annual mean meridional circulation has mainly southward motion at 70-104 km. There is very good agreement between the radar zonal winds and the HWM93 model winds. Comparison of the meridional winds shows some discrepancy. Tidal characteristics observed are also consistent with previous measurements. Semidiurnal tidal amplitude is largest in summer and weakest in winter months. The vertical wavelength is longer during the summer season compared to the winter season. Comparison with the GSWM-00 values produces mixed results. There is reasonable agreement between the observed and modelled phases. Diurnal tide amplitude is comparable in magnitude with that of the semidiurnal tide. Seasonal variation in amplitude is less evident. Again, comparison of the diurnal tidal parameters and the GSWM-00 values reveals some agreement and discrepancies. The overall scenario is that further effort is necessary for improvement of the models. Results of a comparative study of the wind fields in the MLT region over Poker Flat and Davis (69°S, 78°E) are also presented. The study confirms the existence of interhemispheric asymmetry of mean circulation in the high latitude MLT region.

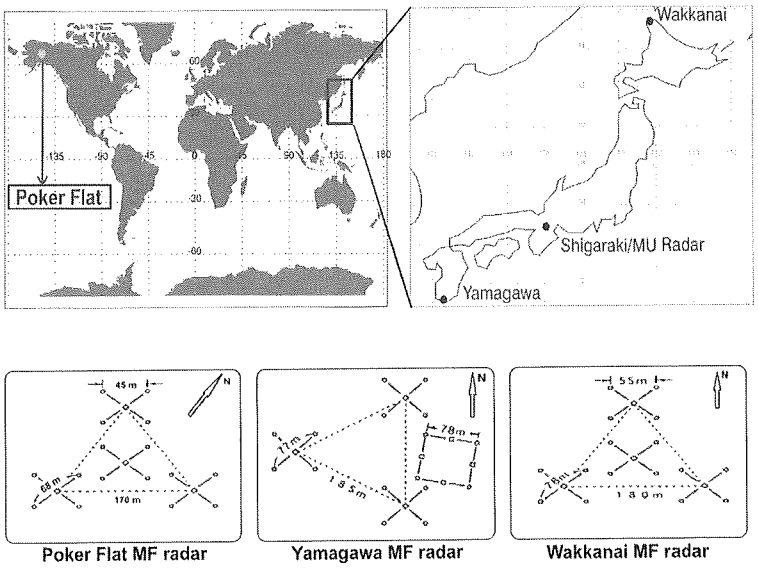

Fig. 1. Locations and antenna configurations of the Yamagawa, Wakkanai, and Poker Flat MF radars, including location of the MU radar at Shigaraki.

Wind observations around the tropopause over Sumatra, Indonesia by the Equatorial Atmosphere Radar

Masayuki Yamamoto
Laboratory of Radar Atmospheric Science, RISH, Kyoto University

Dynamical couplings between the stratosphere and the troposphere are the important factors that control the circulation of the Earth's atmosphere, and the tropics is one of the primary regions that tropospheric air enters into the stratosphere and vice versa. The boundary region between the troposphere and the stratosphere, which is called tropopause, is defined by the temperature lapse rate or temperature minimum. Altitude and temperature variations of the tropopause in the tropics have been studied to understand the mechanism of airmass exchange between the stratosphere and troposphere (stratosphere-troposphere exchange; hereafter STE). While the variations of the tropical tropopause have significant impacts on STE, recent studies have revealed that dynamical, photochemical, and microphysical processes in the region around the tropopause, which is called the tropical tropopause layer (TTL), are also important for clarifying STE. The TTL is generally defined as the layer between the level where cumulus activity generally terminates and the tropopause, and the air gradually changes from the tropospheric one to the stratospheric one with increasing altitude in the TTL.

The Indonesian Maritime Continent is one of the regions where deep cumulus convection occurs most frequently in the tropics. The Indonesian Maritime Continent is composed of five large islands (Sumatra, Borneo, Java, Sulawesi, and New Guinea) and many small islands surrounded by the warm sea. The topographic effects in the region cause the development of deep cumulus convection through local circulation (land-sea and mountain-valley breeze circulation). Though previous studies have pointed out that dynamical, photochemical, and microphysical processes associated with cumulus convection over the Indonesian Maritime Continent affect STE, many of these processes in the TTL remain unsolved due to the scarcity of observations. Observational data derived from a VHF Doppler radar, which is named the Equatorial Atmosphere Radar (hereafter EAR), installed at the Equatorial Atmosphere Observatory, Kototabang (0.20S, 100.32E, 865 m MSL), and has a capability to observe vertical profile of wind and turbulent motions, are used for investigating wind and turbulence features in the TTL over Sumatra.

An enhancement of turbulence by an equatorial Kelvin wave in the tropopause region has been shown using EAR and radiosonde data during November 2001. Significant enhancement of turbulence in the tropopause region (15-17 km) was intermittently observed for about 5 days (19-23 November 2001) in the spectral width of the radar echo power spectrum obtained by the EAR. The turbulence intensity was estimated with the spectral width data to show that the turbulence during the period was a factor of up to about 5 times larger in kinetic energy than that in other periods. Further data analyses using horizontal wind data derived from the EAR and temperature data derived from radiosondes indicated that the enhanced turbulence occurred in the region with weakened static stability and large vertical wind shear produced by tropopause-level Kelvin wave. This study is the first to confirm turbulence generations associated with Kelvin waves in the tropopause region.

Frequent occurrence of Kelvin-Helmholtz instability (KHI) around the tropopause has been shown. In November 2001, continuous strong eastward vertical wind shear (10-50 m/s/km) and westward wind (2-27 m/s) were observed in the region 0-1 km above the tropopause. During the same period, the Richardson number (Ri) calculated with horizontal wind derived from the EAR and temperature data derived from radiosondes was almost continuously less than 0.5 and sometimes less than 0.25, which indicates that KHI frequently occurs in that region. This study is the first observational evidence to show that KHI associated with strong vertical wind shear frequently occurs around the tropical tropopause over Sumatra.

From a case study from 5 to 9 May 2004, vertical motions in the TTL and their relationship to cumulus activity have been investigated using coordinated observation systems operated during the first observation campaign of the Coupling Processes in the Equatorial Atmosphere (CPEA) project (hereafter the first CPEA observation campaign). Before investigating the vertical motions in the TTL, features of wind, cloud, temperature, and humidity in the lower and middle troposphere have been investigated to reveal convective characteristics over the mountainous area of Sumatra. Data observed by the EAR, 1.3-GHz wind profiler, 9.445-GHz weather radar, radiosonde, and lidar installed at or near Kototabang are used. The period of 5-9 May 2004 is an initial phase of westerly wind burst (WWB) period of the first CPEA observation campaign. Convective events during 5-6 May, when precipitating clouds with relatively large radar reflectivity factor (greater than 15 dBZ) were observed at and around Kototabang, have been described. Cumulus activity around Kototabang showed a clear diurnal variability; shallow convective

precipitating clouds were dominantly observed in the early afternoon, and stratiform precipitating clouds were prominent in the nighttime. Raindrop size distribution retrieved by the EAR showed consistent results; smaller median diameter and shape parameter were observed in the early afternoon precipitation events. After 7 May, the 2.5-4.0 km westerly wind at Kototabang became large enough to be identified as WWB. Cumulus activity around Kototabang was suppressed after 7 May, as drier air (lower than 60% relative humidity) was transported from the Indian Ocean by lower-tropospheric westerly. Whereas the convective activity around Kototabang was suppressed, daily-averaged upward motions of 0.07-0.08 m/s were found at 2.5-4.0 km on 7 and 8 May, when strong westerly wind larger than 10 m/s were seen in 2.5-4.0 km. Further, the oscillatory motion of vertical wind with an amplitude of 0.1-0.2 m/s and a timescale of about 12 hours was observed at 2.5-5.5 km. Similar oscillatory motion was found in the 1.5-2.5 km zonal wind. These facts imply that the topography around Kototabang, which has steep mountains to the west, modulates the behaviors of the vertical wind. The vertical wind oscillation was suppressed around an altitude where westerly wind changed to easterly wind; this fact implies that horizontal wind change inhibits upward propagation of vertical wind oscillations. After 7 May, Ri of smaller than 0.25, which suggests an occurrence of KHI, was observed in the upper part of the westerly wind region (3.0-5.5 km). The small Ri was brought about by strong vertical wind shear (larger than 10 m/s/km) and/or weak vertical gradient of potential temperature (smaller than 3 K/km).

Vertical wind features from the middle troposphere to the TTL and their relationship to cumulus convection from 5 to 9 May have been investigated. During 5-6 May, the 3-hourly averaged vertical wind from the middle to upper troposphere (8-14 km) continuously showed upward motions up to 0.09 m/s. The averaged vertical wind during 5-6 May was 0.05 m/s. The upward motions were observed in the vicinity of deep convective events which were continuously seen over Sumatra within a synoptic-scale convectively active envelope, in addition to the diurnal variability of cumulus activity observed around Kototabang. After 7 May, when cumulus activity was suppressed over Sumatra, 3-hourly averaged upward motions of greater than 0.05 m/s almost disappeared. The averaged vertical wind during 7-9 May was 0.01 m/ s. Prominent downward motions in the TTL (above 14 km) were found in the vicinity of enhanced cumulus activity over Sumatra. During 5-6 May, downward motions up to about 0.11 m/s were observed above 14 km. Vertical winds caused by adiabatic processes were estimated using horizontal wind and temperature data derived from the European Center for Medium-Range Weather Forecasts (ECMWF) operational analysis; the estimations have revealed that a major part of the observed downward motions are explained by the leeward (southwestward) wind and leeward downward tilt of isentropes, both of which existed over the western Sumatra. The observed downward motions above 14 km during 5-6 May suggest that downward motions caused by leeward downward tilts of isentropes can be produced in the vicinity of convectively active region, and leeward downward tilts of isentropes suppress an upward transport of airmass into the TTL by producing downward motions in the TTL.

Fig. 1. Picture of EAR installed at Koto Tabang, West Sumatra, Indonesia

Analysis of pull-out resisting mechanism of Lagscrewbolt and application to wooden portal frame

Makoto Nakatani

Laboratory of Structural Function, RISH, Kyoto University

At present, moment-resisting connections for glulam constructions are widely constituted as drift-pin joints with insert-steel gusset plates, as well as bolted joints. These joint systems are trusted. However they require complex design calculations. Therefore, Lagscrewbolts® (LSB) were developed by Prof. Komatsu as a simple and economical timber connector [1]. Figure 1 show details of LSB. LSB has two threads: one is a screw type thread on the outside surface and the other is a bolt or nut type thread at one end of the shank. LSB is embedded into a glulam by the screw thread and connected to other pieces by the bolt or nut thread. LSB is expected to show high pull-out ability due to the shear resistance between the top thread and glulam.

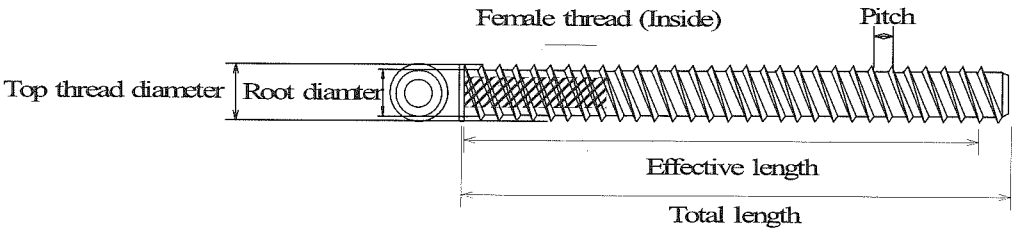

Fig.1 Details of Lagscrewbolt

A series of tests were conducted to clarify the effects of lead hole diameter, embedment depth, embedment direction and edge distance on the pull-out resistance of LSB. The results obtained were as follows: 1) the optimum lead hole diameter was defined. 2) Maximum pull-out load (P_{max}) vs. embedment depths, and slip modulus (Ks) vs. embedment depths showed positive correlations. However, the proportion of the load increasing decreases with increasing an embedment depth. 3) The maximum pull-out load (P_{max}) parallel to the grain was 0.75 times of that for perpendicular to the grain, and the pull-out slip modulus (Ks) parallel to the grain was 3 to 6 times of that for perpendicular to the grain. 4) The suitable edge-distance was thought to be more than $1.5d$ (d is top thread diameter of LSB) [2].

A theory on pull-out ability of an embedded LSB parallel and perpendicular to the grain direction was developed on the basis of Volkersen theory, which was originally developed for the shear stress analysis in rivet joints of aircraft technology [3]. Theoretical equations of P_{max} and Ks were derived as equation (1) and (2), receptivity. Shear strength fv and shear stiffness Γ, both are necessary parameters in the theoretical formular, were determined by pull-out test of thin specimens made of glulam, because thin specimens were assumed that the shear stress distribution was almost uniform. Effective area of glulam (A_w) of parallel and perpendicular to the grain, also necessary parameters, were determined, respectively. A_w of parallel to the grain was an area of a circle with radius $1.5d$ [4]. A_w of perpendicular to the grain was determined by an energy equivalent concept, the deformation energy by the theory of a beam on an elastic foundation [5] or the bending theory of a short beam as being equal to the deformation energy of work at the effective area of the glulam [6]. Verification experiment was conducted by using several types of LSB, in which top threat diameter were 25, 30 and 35 mm, and influences of various embedment depths ranging from 60 to 450 mm on the pull-out properties were examined. The developed theory predicted maximum pull-out load and slip modulus well.

$$\begin{cases} P_{max} = \dfrac{fv\pi d(E_wA_w + E_sA_s)\sinh kl}{k(E_wA_w\cosh kl + E_sA_s)} & (E_sA_s \le E_wA_w) \\ P_{max} = \dfrac{fv\pi d(E_wA_w + E_sA_s)\sinh kl}{k(E_sA_s\cosh kl + E_wA_w)} & (E_wA_w \le E_sA_s) \end{cases} \cdots(1) \qquad \begin{cases} Ks = \dfrac{\Gamma\pi d(E_wA_w + E_sA_s)\sinh kl}{k(E_wA_w\cosh kl + E_sA_s)} & (E_sA_s \le E_wA_w) \\ Ks = \dfrac{\Gamma\pi d(E_wA_w + E_sA_s)\sinh kl}{k(E_sA_s\cosh kl + E_wA_w)} & (E_wA_w \le E_sA_s) \end{cases} \cdots(2)$$

where, $k = \Gamma \pi d \left(\frac{1}{E_w A_w} + \frac{1}{E_s A_s} \right)$

and E: young's modulus, l: embedment depth, Subscript w: wood member, s: LSB.

Beam-column and column-base joints with LSBs using on optimum conditions were developed. The beam-column joint was composed of two LSBs, two M16 high tension bolts (HTB), and one steel plate. Two LSBs embedded from end of beam were connected to HTBs through a steel plate and a hole of column. Column-base joint was composed of two LSBs and two M16 HTBs. Two LSBs embedded from end of column were connected to M16HTBs which were regarded as parts of a base. The joint systems are very aesthetic constrictions, because LSBs and HTBs are hidden inside of beams and columns. Details of portal frame and test set-up are shown in Figure 2.

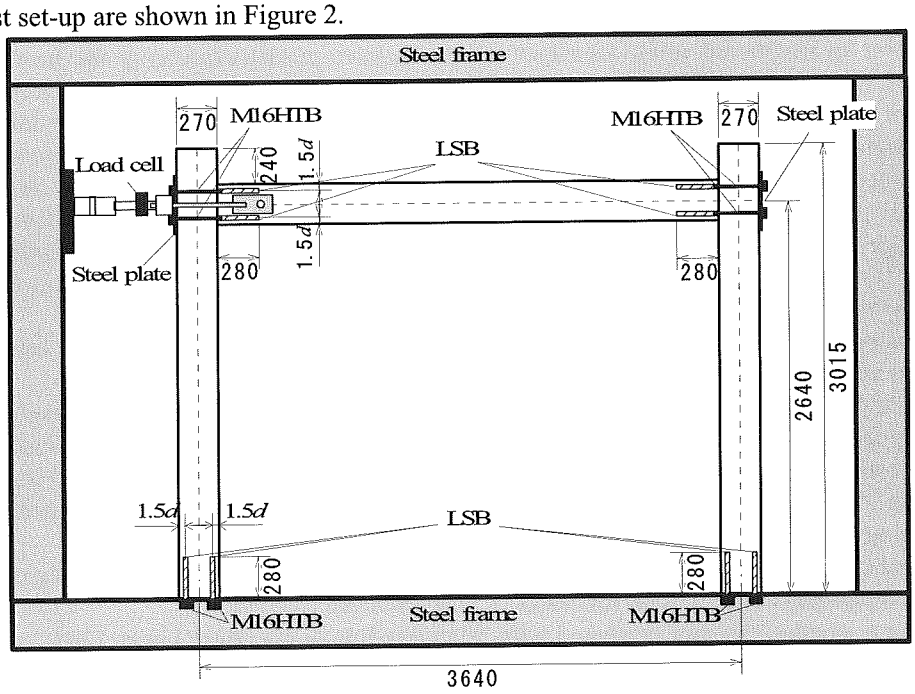

Figure 2 Geometry of wooden portal frame using LSB

Cyclic loads were applied at a beam by an oil jack. Figure 3 shows a test result and an analysis result of the portal frame. The analysis initial rigidity was predicted test results well. The analytical rigidity was derived from rotational rigidities of beam-column and column-base joints, which were derived from theoretical slip modulus of one LSB.

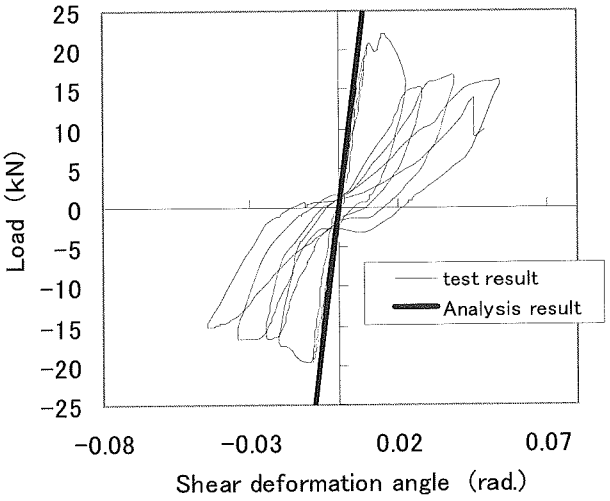

Figure 3 Test result of portal frame.

REFERENCES
[1] Komatsu K. (1997) Japanese Patent Application No.265314
[2] Nakatani M., Komatsu K. (2005) Mokuzai Gakkashi 51, 125-130.
[3] Volkresen O. (1938) Luftfahrtforshung 15, 41-47.
[4] Nakatani M., Komatsu K. (2005) Mokuzai Gakkashi 51, 311-317.
[5] Harada, M. (1951) Report of the Institute of Industrial Science, University of Tokyo 2(3), 1-38.
[6] Nakatani M., Komatsu K. (2006) Mokuzai Gakkashi 52, 160-167.

Improvement of Japanese traditional joint by using compressed wooden fastener

Kiho Jung

Laboratory of Structural Function, RISH, Kyoto University

Japanese traditional timber joint is characteristic joint method assembled and fastened by only timber parts them selves on the replace for usage of a nail, bolt and so on.

Recently, it has been more increasingly and widely used because it has good merits for environment system, low energy, and beautiful exterior in view.

Wooden fastener like as Komisen(squared peg), Kusabi(wedge), and wooden nail is well used to fix joint members in traditional joint. Japanese carpenters have used traditionally the hard wood like as maple or oak with high density because wooden fasteners have most important role in strength of joint.

Due to the performance of strength in traditional joint is almost dependent on embedding strength of the border between joint members, stiffness is heavily influenced by contact stress (pre-stress) and gap between joint members. Hence, the shrinkage of joint members has an influence on contact stress contributing to stiffness in the joint. It is a reason why traditional carpenters thought out anti-shrinkage-methods like as hammering around wooden fastener and roasting or frying with a heat before insertion and usage. Wooden fastener with compressed surface and low moisture content must play an important role in prevention of damages originated from shrinkage in the joint.

Ideal concept of this research was hinted and inherited from these traditional carpenter's skills (know-how) in the mechanism using recovery-property of compressed (densified) wood.

Recently, there were some reports about compressed wood for valid usage in low quality wood like as Japanese ceder(*Cryptomeria japonica*, density: 0.38) which is a very plentiful species in Japan. Originally, compressed wood was produced by relatively high temperature and needed to steam or resin treatment for stabilizing and fixation of its size because compressed wood's cells changed from round to flat will spring back by absorbing water molecule.

In this research, it was used this recovery property of compressed wood for preventing of relaxation of contact stress and gap between joint members in Japanese traditional joint.

Compressed wooden fastener produced with relatively low temperature under 130℃ and no fixation treatment will automatically spring back and recover its original volume to a certain level, and finally fill up the gap and give contact stress between joint members by cyclic humidity change of surrounding environment as shown in fig.1.

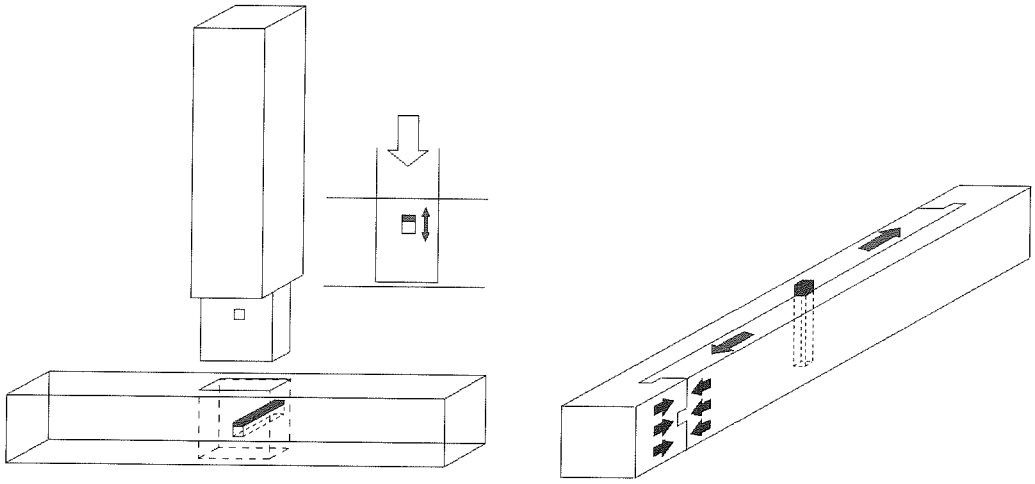

Fig.1. Improvement of contact stress using by recovery of compressed sugi on the Hozo komisen joint(Left) and Kanawa-Tugi joint(Right).

On the view of the capability in komisen material, 70% compressed wood with its high density over 1.1 has good properties in bending strength (250MPa in MOR, 30GPa in MOE) and compressive strength(43MPa).

Therefore, it was focused to study about the change of contact stress by cyclic humidity change, the anti-relaxation effect by recovery of the compressed sugi komisen, and the evaluation of pull-out strength at Hozo-komisen(traditional pegged mortise and tenon) joint inserted by compressed sugi komisen. And, it was focused to study about anti-relaxation effect by recovery of the compressed sugi komisen with contact stress test and creep test in Kanawa-tsugi(traditional beam to beam) Joint.

In result, it was verified that compressed sugi komisen has the anti-relaxation effect on contact stress between joint members in Hozo-komisen joint and Kanawa-tsugi jont. And, compressed sugi komisen improved strength of Hozo-komisen joint after long term cyclic humidity changes as shown in fig.2.

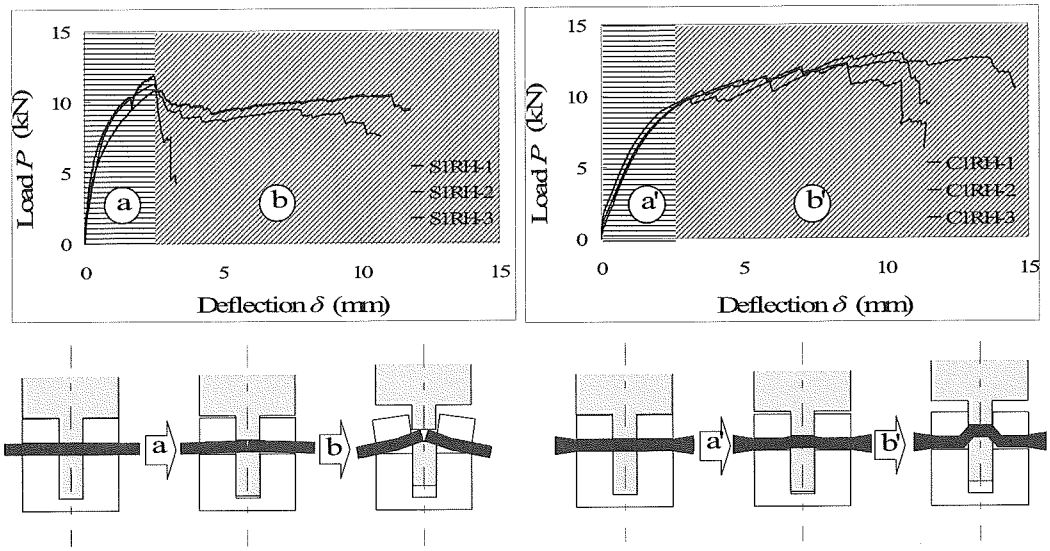

Fig.2. Load vs.Deflection in pull-out strength of Hozo-komisen join after controlling of 2 years cyclic humidity changes (Left: compressed komisen joint, Right: normal shirakashi joint).

The creep of Kanawa-tsugi joint inserted by compressed sugi komisen didn't accept any influence by cyclic humidity change in all cycles, however shirakashi komisen joint had been getting more increased from 2nd cycle as shown in fig.3

Finally, it was concluded that compressed wood have a good performance as types of key or wedge fastener received big cross-direction stress due to its anti-stress-relaxation in company with recovery property, however normal hard wood even high density wood give birth to the serious relaxation of stress in radial and tangential direction.

Compressed wood fastener, on view of valid usage in low quality wood and improvement for high-performance of joint, can be expected its practical application and adaptation in the role as fasten material.

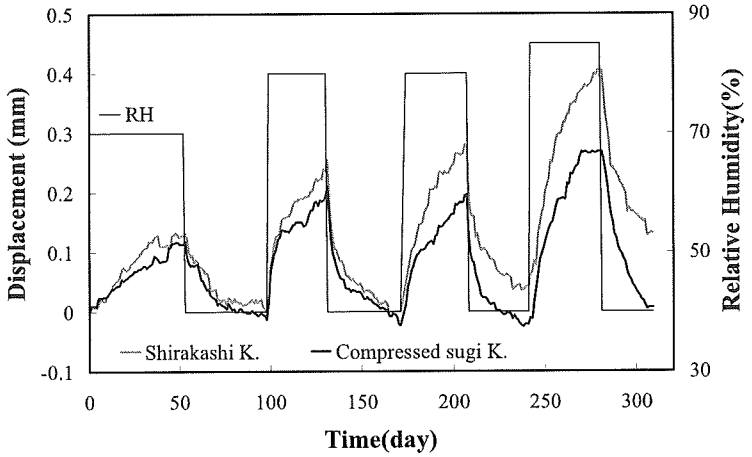

Fig.3. Schedule vs. deformation by cyclic humidity change for the time progress in Kanawa-tsugi Joint.

Evaluation of Shear performance of Earth wall in the Japanese traditional timber structure

Atsushi TABUCHI

Laboratory of Structural Function, RISH, Kyoto University

In this research, it was found out that shear performance of earth wall in Japanese traditional timber structure, and developed the way to evaluate the performance by using material constant.

(1)Evaluation of shear performance as material constant

An earth wall was constructed from mud, rice straw and bamboo. After mud was mixed with rice straw, it was molded on bamboo lath. In order to find out a behavior of bamboo lath in mud, interaction between mud and rice straw was focused on, and small size specimens which have 300 mm length, 300mm width and 70mm thickness were proved by lateral shear test. Fig.1 shows experimental set-up and dimension of a specimen. It was found out that shear stiffness was 4.0 N/mm^2.

And then a behavior and embedment of a bamboo as a lath of earth wall was evaluated by a theory of a beam on elastic foundation. In fact, it was assumed that a bamboo lath was a beam and mud was elastic foundation. This analysis showed that maximum deformation angle of bamboo lath was about 1/150 rad and this deformation angle could be ignored because of smaller value than a deformation of Nuki beam and other timber frames. As a result, it was found out that earth wall was integrated material with bamboo lath, a shear stiffness evaluated from above experiment was propriety.

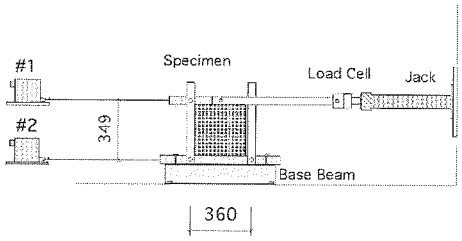

Fig 1: Experimental set up and dimensions

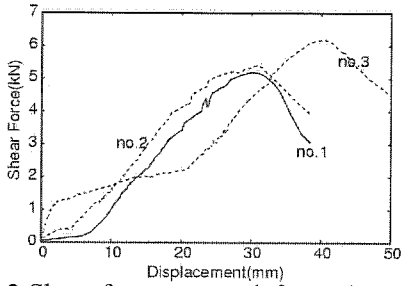

Fig2:Shear force versus deformation angle of element experiment

(2)Full scale lateral shear test of earth wall in case of Kyomachiya (town house of Kyoto) style

Figs 3 and 4 show experimental set-up and dimension of specimens. Keeping the typical module of Kyomachiya with 60mm thickness and 980mm column-to-column, Type-A had 1820mm column-to-column span and Type-B had 980mm width. Height of each specimen was 2500mm. These specimens were loaded on its beam laterally with tie rods in case of rocking rotation.

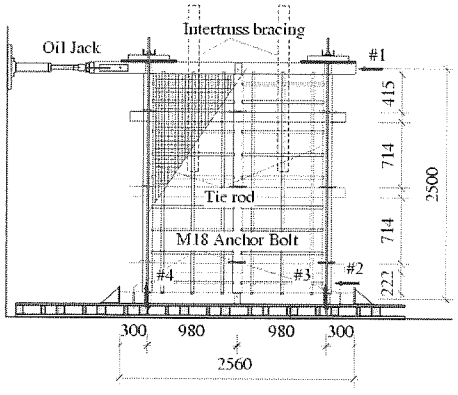

Fig3:Experimental set up and dimensions of type-A

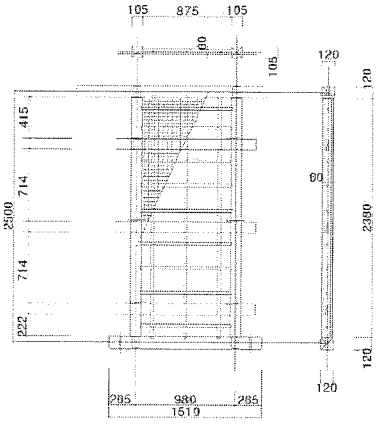

Fig4: Dimensions of type-B

Shear stress versus shear deformation angle curve is shown in Figs.5 and 6. These figures show that a maximum shear force of type-A was about 15kN and that of type-B was about 8.3kN. In addition, it was found out that shear stiffness of each type was similar. And the structural model of a timber frame was constructed using the theory of a beam on elastic foundation. According to this newly formulated model, the stiffness and strength of an earth wall in Kyomachiya can be evaluated simply.

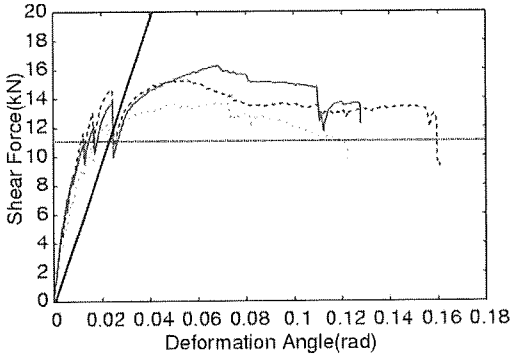

Fig5:Shear force versus deformation angle of type-A and results of physical model

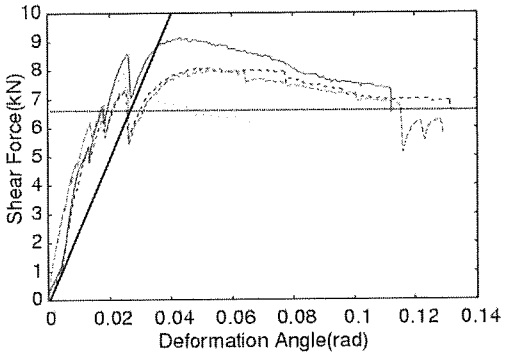

Fig6:Shear force versus deformation angle of type-B and results of physical model

(3)Lateral shear performance of kokabe-wall

Kokabe-wall, which has a opening under itself, is not anticipated as a shear wall (Fig.7). However, it has some strength. In that reason, timber frames with kokabe-wall were tested by lateral shear loaded. As the result, it was found out that the maximum load of a timber frame with kokabe-wall was about 1.9 times larger compared to those without it. The stiffness of timber frame alone was evaluated by using the physical characteristic model of embedment at Hozo (tenon) and Nuki-joint. Further, the stiffness of the kokabe-wall alone was evaluated by using shear stiffness and young modulus of earth wall. Final stiffness of the total structure was achieved by combining the two stiffness.

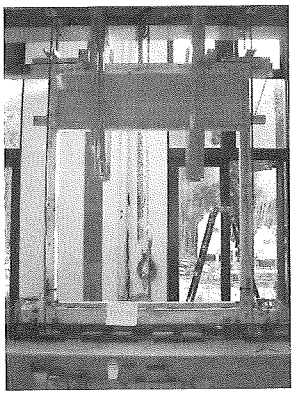

Fig7:Timber frame with kokabe wall

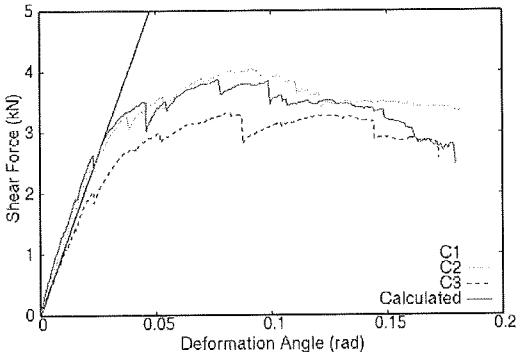

Fig8:Shear force versus deformation angle and calculated shear stiffness

(4)Conclusion

- Material testing was developed to evaluate a material constant of earth wall.
- It was found out that an embedment of bamboo lath to mud on earth wall could be ignored.
- It was proposed the newly formulated model by which a stiffness and strength of earth wall in Kyomachiya style could be evaluated simply.
- A stiffness of kokabe wall could be evaluated by using shear stiffness of earth wall and young modulus of timber.

Development of novel silicon carbide thermoelectric materials from carbonized wood

Masashi Fujisawa

Laboratory of Innovative Humano-habitability, RISH, Kyoto University

Research on the development of new energy sources has been quite vigorous due to concerns about environmental problems. Nonrenewable resources, such as fossil fuels, coal, fuel oil, and natural gas, will become increasingly scarce in the future. Moreover, air pollutants, such as nitrogen oxides, sulfur dioxide, VOCs and heavy metals, are discharged into the environment. Thermoelectric energy conversion technology has also attracted a great deal of attention. Thermoelectric energy conversion, which does not depend on hydrocarbons, is a type of clean power generation that directly converts thermal energy into electric energy. In particular, waste energy, which is discharged form factories and cars in great quantities, can be collected and recycled [1]. Considerable efforts have been devoted to the development of thermoelectric materials that can be used at high temperatures. Ceramic semiconductors have been investigated as thermoelectric materials for use at high temperatures. When the temperature difference is given between the two ends of a solid sample, a thermoelectromotive force is generated as free electrons and holes are moved from the hot side to the cold side.

SiC-based materials with high thermal, chemical and mechanical stabilities are candidate materials that may enable a thermoelectromotive forces to be generated at a high temperature range [2-6]. It has been reported that SiC composites have high figures of merit at high temperatures [7]. The objective of this study was to improve the thermoelectric properties of SiC composites obtained from carbonized wood. I focused on novel SiC thermoelectric materials that could be used at high temperatures.

Firstly, the development of SiC/C composites from wood-based carbon using the pulse current sintering method, as well as their electrical and thermal properties were investigated. SiC/C composites were investigated by sintering a mix of wood charcoal and SiO_2 powder (32-45 μm) at 1400-1800°C in a N_2 atmosphere with the pulse current sintering method. X-ray diffraction revealed the coating to be β-SiC. SEM and EDX confirmed that a 1 μm thick layer of β-SiC was formed on the surface of the wood charcoal pieces. The bulk density increased only slightly with sintering temperature and SiC content. The electrical resistance decreased slightly with sintering temperature but increased with SiO_2 content. The thermal conductivity increased with both sintering temperature and SiC content. By coating the wood charcoal in this rather natural way by such a ceramic layer we can use the SiC/C composite at least up to 1800°C, far beyond the carbon oxidation limit of 500°C. It is to be expected that the electrical and thermal conductivity of the SiC/C composite can be controlled by sintering temperature and the addition of SiO_2 [8, 9].

The thermoelectric properties of SiC/C composites were investigated. The thermoelectric properties of SiC/C composites sintered at 1400, 1600 and 1800°C in a N_2 atmosphere were investigated by measuring the Seebeck coefficient and the electrical and thermal conductivities. The Seebeck coefficient exhibited a p-type to n-type transition at a sintering temperature around 1600°C. The electrical conductivity showed a steady increase with temperature for all three sintering temperatures. For the thermal conductivity, the samples sintered at 1800°C showed high values at room temperature which strongly decreased with increase in measurement temperature. In total, thermoelectric properties were improved with an increase in measurement temperature. A maximum in the figure of merit of 3.38×10^{-7} K^{-1} was reached at 200°C in the sample sintered at 1400°C for 30 min. These results suggest good prospects of using SiC/C composites made from a mix of wood charcoal and SiO_2 powder as a thermoelectric material for high temperature applications [10].

Secondly, the porosity of porous SiC composites from wood-based carbon was investigated. Porous SiC ceramics have been investigated because of their even better thermoelectric properties [7]. Porous SiC composites by oxidizing a SiC/C composite sintered at 1400, 1600 and 1800°C under N_2 using a pulse current sintering device were developed. Raman spectroscopy revealed the presence of β-SiC and the successful removal of excess carbon. The pore size of the porous SiC sample sintered at 1600 °C was larger than that of the sample sintered at 1800 °C. The porous SiC ceramic had a much lower thermal conductivity than the non-oxidized SiC/C composite and is, therefore, a more promising material for thermoelectric applications.

The improvement of the thermoelectric properties of porous SiC composites was investigated. The thermoelectric properties of porous SiC composites sintered at 1600 and 1800°C in a N_2 atmosphere were investigated by measuring the Seebeck coefficient, the electrical conductivities and the thermal conductivity in the temperature range from 323 K to 973 K. The Seebeck coefficient of all samples showed n-type conduction and the absolute value of the Seebeck coefficient of the porous SiC samples with oxidation was much larger than those of the SiC/C samples without oxidation. The electrical conductivity of the SiC/C samples without oxidation was larger than that of the porous SiC samples with oxidation. The thermal conductivity of porous SiC samples with oxidation was much lower than that of SiC/C samples without oxidation, at least for the one at 1800°C. The thermoelectric properties improved at higher measurement temperatures (Fig. 1). A maximum figure of merit of 2.01×10^{-5} K^{-1} was obtained at 973 K in porous SiC samples sintered at 1800°C with oxidation. This meant a two orders of magnitude improvement in the value for the figure of merit over our previous results [10].

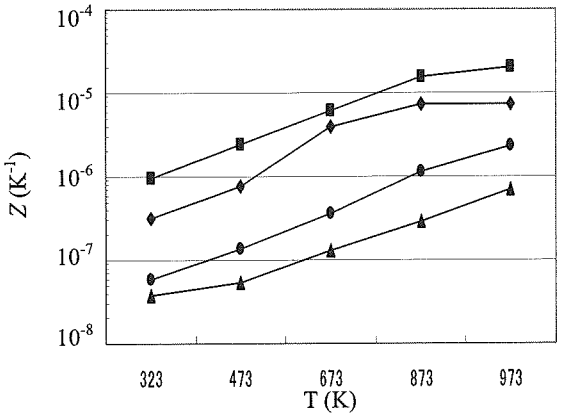

Fig. 1. Temperature dependence of the figure of merit of specimens sintered with and without oxidation. ▲ SiC/C composites sintered at 1600°C without oxidation; ● SiC/C composites sintered at 1800°C without oxidation; ◆ porous SiC composites sintered at 1600°C with oxidation; ■ porous SiC composites sintered at 1800°C with oxidation.

These results obtained in a series of current investigations add a valuable contribution to the development of thermoelectric materials used at high temperature. Porous SiC materials from carbonized wood can be used as thermoelectric materials for high temperature applications. Highly efficient thermoelectric generation can be realized by the application of novel SiC materials.

REFERENCES

[1] Funahashi, R., Mihara, T., Mikami, M. and Urata, S., 2005, 886, 493-498
[2] Banerjee, P.K., Pereira, J.M.T., Mitra, S.S. and Dutta, R., Journal of Non-Crystalline Solids, 1986, 87, 1-29.
[3] Pereira, J. M. T., Banerjee, P. K. and Mitra, S. S., Thin Solid Films, 1985, 127, 337-350.
[4] Nagels, P. and Gevers, M. R. R., Journal of Non-Crystalline Solids, 1983, 59/60, 65-68.
[5] Castro, V., Fujisawa, M., Hata, T., Bronsveld, P., Vystavel, T., Hosson, J. D., Kikuchi, H., and Imamura, Y., Key Engineering Materials, 2004, 264-268, 2267-2270
[6] Furuno, T., and Fujisawa, M., Wood and Fiber Science, 2004, 36(2), 269-277
[7] Koumoto, K., Shimohigoshi, M., Takeda, S., and Yanagida, H., J. Mater. Sci. Lett., 1987, 6, 1453-1455.
[8] Fujisawa, M., Hata, T., Bronsveld, P., Castro, V., Tanaka, F., Kikuchi, H., Furuno, T. and Imamura, Y., J. Eur. Ceram. Soc., 2004, 24, 3575-3580
[9] Fujisawa, M., Hata, T., Bronsveld, P., Castro, V., Tanaka, F., Kikuchi, H., Furuno, T. and Imamura, Y., Wood Research., 2003, 90, 15-16
[10] Fujisawa, M., Hata, T., Bronsveld, P., Castro, V., Tanaka, F., Kikuchi, H. and Imamura, Y., J. Eur. Ceram. Soc., 2005, 25, 2735-2738

Potential of didecyldimethylammonium tetrafluoroborate (DBF) as a novel wood preservative

Won-Joung Hwang

Laboratory of Innovative Humano-habitability, RISH, Kyoto University

Although chromated copper arsenic (CCA), the most effective and widely used wood preservatives in the past, had been a dominant wood preservative since it was develop in 1933, the use of CCA was recently banned or restricted in most of countries in the world, *e.g.* USA, Canada, Japan and Europe (1 - 3). Since CCA contains environmentally unfriendly heavy metals, it is quite natural for alternatives to replace that.

Chemical treatment is still the most reliable measure to ensure the longer service life of wood products with the aid of improved microclimate in the crawlspace of houses. Alkylammonium compounds (AAC's) such as didecyldimethylammonium chloride (DDAC), are one of the groups which are provided with low mammalian toxicity and environmental soundness (4). A novel didecyldimethylammonium tetrafluoroborate (DBF) (5, 6), one of the AAC's recently appeared in the market. However, little is known about its ability to protect wood from biodegradation. DBF is chemically constituted by a fungicidally effective alkyl chain (C_{10}-C_{10}) and water stable tetrafluoroborate (BF_4^-) as a counter ion. In this study, DBF was evaluated for its efficiency in protecting wood from decay fungi, subterranean termite and drywood termites. In addition, leachability of DBF from the treated wood and combined effect of DBF and wood extractives. The results were compared with those of the commercial wood preservative, DDAC.

Although microbial test showed that DBF was effective in inhibiting the microbial growth on the sapwood specimens of *Cryptomeria japonica* D. Don. and *Fagus crenata* Blume at ≥0.5-1%, and that DBF was superior to DDAC, it was concluded that DBF was not promising as a superficial protectant. Because decay and termite tests demonstrated that brush-on treatment did not meet the performance requirement of ≤3% mass loss (7) after accelerated aging cycles.

In the vacuum-impregnation treatment with DBF and DDAC, several wood species with different natural durability were treated at several retention levels, and then were served for the decay and subterranean termites test according to JIS K 1571 (7). Decay test using *Trametes versicolor* (L.:Fr.) Pilat (FFPRI 1030) and *Fomitopsis palustris* (Berk. Et Curt.) Gilbn.&Ryv. (FFPRI 0507) indicated that the toxic threshold values differed among wood species, *e.g.* in the case of DBF retention, 0.7-3.6 kg/m^3 in the heartwood of *C. japonica* and *Chamaecyparis obtusa* Endl., >6.5 kg/m^3 in the sapwood of *F. crenata*. DBF was proved to be as effective as DDAC in controlling fungal attack. The resistance against *Coptotermes formosanus* Shiraki was much enhanced by DBF impregnation and the lower DBF retentions were required to satisfactorily suppress termite activity. The required retentions of DBF were varied with durability levels of each wood species, and ranged from <0.07 kg/m^3 to 4.00 kg/m^3. Efficacy of DBF in controlling *Incisitermes minor* Hagen, western drywood termite activity as high as that of DDAC, and the required retention levels were >1.72 kg/m^3 and >4.50 kg/m^3 of DBF and DDAC for sapwood and heartwood of *C. japonica*, respectively.

Leachability of DBF was determined by chemical anslysis of the amount recovered from treated wood such as sapwood of *C. japonica* and *F. crenata* and heartwood of *C. japonica, C. obtusa, Pseudotsuga menziesii* (Mirbel) Franco and *Tsuga heterophylla* Sarg. after leaching and evaporation cycles. The results were compared with those of DDAC. Leachability was varied with wood species as expected and preservatives. DBF was generally more resistant against water leaching than DDAC after severe weathering cycles. The recovery rates ranged from 66% to 96% for DBF and from 47% to 96% for DDAC. The different leaching patterns of both preservatives might be reflected by pH of treatment solutions and other factors such as chemical structure, formulation constituents, biological and chemical characteristics of wood, *etc.*, although pH of treatment solutions and wood substrate did not fully account for the differences in the present research.

It has been generally known that heartwood is more durable than sapwood of the same wood species. This is dependent on heartwood extractives (8, 9). Therefore, it is thought that heartwood and sapwood differently act with preservatives, and reaction resultantly causes different levels of retention, distribution and fixation patterns of active ingredients. Wood extractives of two moderately resistant wood species were preliminarily evaluated their termiticidal properties. Filter paper test with extractives of *C. obtusa* showed

that termites was started dying soon after the initiation of the test in at 3.55% and 6.64% (m/m) retentions, and then reached 100% mortality after 12th and 8th, respectively. Similarity was seen in the case of *C. japonica* at 3.39 % and 6.51% (m/m) retentions. Wood block test demonstrated that termiticidal efficacy was seen remarkable at retentions of >6 kg/m^3. Impregnation of extractives from *C. japonica* and *C. obtusa* could meet performance requirement designated in JIS K 1571 (7) at the highest retention, 24 kg/m^3. The amount of extractives varied with wood species, and was well correlated with their natural durability (10). The combination of wood extractives and either DBF or DDAC contributed to the enhanced termite resistance in comparison with extracted wood specimens or extracted/DBF or DDAC-treated wood specimens. Wood extractives may provide the preservative-treated wood with an additional protective effect because of their recognizable biocidal characteristics. These results seemed to indicate a possible synergistic or combined effect between heartwood extractives of certain durable wood species and DBF or DDAC against termite attack. Therefore, the lower loadings of wood preservatives would be sufficient for protecting wood from termite attack, when durable heartwood portion is present in the wood substrate to be treated. Decay resistance of extracted wood specimens or extracted/DBF or DDAC-treated wood specimens should be discussed later to generalize these findings.

The current results undoubtedly supported that DBF was applicable to the preservative treatment of various wood species against biological degradation on the basis of the laboratory efficacy comparable to DDAC. DBF favorably outperformed DDAC in the control of microbial coverage on wood and fixation (leaching resistance). Since these are all based on laboratory evaluations, a field trial should be further planned to confirm the performance of DBF as an alternative preservative principally for the impregnation treatment of wood. Other options to widen the use of DBF should be discussed as well, for example, treatment of wood composites such as plywood, particleboard and fiberboard.

REFERENCES

[1] Cowan, J., and Banerjee, S. (2005) For Prod J 55(3): 66-70
[2] Ishida, H., Ito, T., Yamai, M., Matsusaka, H., and Tsunoda, K. (2004) International Research Group on Wood Preservation (IRG), IRG/WP 04-50215, Sweden
[3] Hywood company (2006) Internet homepage (www.hywood.co.jp/recycle)
[4] Angele, M. H. (1978) Seifen-Ole-Feffe,-Wachse-104: 433-436
[5] Tokkai No. 2003-321308. 2003. Sanyo Chemical Industries, Ltd
[6] Tokkai No. 2004-231592. 2004. Sanyo Chemical Industries, Ltd
[7] JIS K 1571-2004 Japanese Standards Association, Tokyo
[8] Schultz, T. P. and Nicholas, D. D. (2002) Phytochemistry 61: 555-560
[9] Taylor, A. M., Gartner, B. L., and Morrell, J.J. (2002) Wood and Fiber Science 34(4): 587-611
[10] JWTA (1990) Sekai no Yuyo Mokuzai-300 (300 useful wood species of the world) (in Japanese), (ed) Nihon Mokuzai kakou Gijyutsu Kyokai (Japan Wood Technology Association)

The invasive dry-wood termite, *Incisitermes minor* (Hagen), in Japan: infestation, feeding ecology and control strategies

Yuliati Indrayani

Laboratory of Innovative Humano-habitability, RISH, Kyoto University

The dry-wood termite, *Incisitermes minor* (Hagen), is a native to the western region of the United States, and is one of the five most economically important and destructive termites in that country (1,2). Because colonies of *I. minor* live entirely within sound dry wood, this pest insect is easily transported in infested wood products by means of various human activities. Japan is one of the major importers of wood and wood-based materials that can serve as a natural habitat of *I. minor*. The first infestation of *I. minor* in Japan was found in Tokyo, followed by appearances in the west Chiba Prefecture (3). Although *I. minor* has been spreading in Japan for more than 30 years, the detailed study of this pest termite has still not been done so far.

This research focuses on the dry-wood termite *I. minor* as an invasive termite species in Japan, and consists of 3 main parts, dealing with the distribution and infestation, the feeding ecology, and control strategies.

The infestation of *I. minor* in Japan was surveyed (4,5). The results of the survey showed that the infestations were sporadically found in Hyogo, Osaka, Wakayama, Toyama, and Fukui Prefectures. The majority of the infestation was detected by both fecal pellets and attacked timbers. Based on the present survey, roofing materials (39%) were the commonest attacked parts by *I. minor*. The second-most commonly attacked parts were exterior materials (23%) and followed by interior materials (20%). Materials beneath the floor (10%) floor materials (5%), and furniture (3%) were hardly attacked. We found also that the soil and timber treatments with termiticidal chemicals under the floor generally employed for the majority of Japanese houses to protect against attacks by subterranean termites, *Coptotermes formosanus* and *Reticulitermes speratus*, do not guarantee the protection against *I. minor* attacks which commonly start in roofing materials. These results suggest that upper housing timbers should be treated before construction to prevent the nesting of alates of *I. minor*.

In order to identify the parentage assessment of this invasive species, analysis of the individual DNA structure is conducted (6). There were two major clusters of *I. minor* based on their genetic structures living in Japan. Group I consisted of colonies of *I. minor* collected in Kozagawa Town and Nishinomiya City. The colonies collected in the remaining distribution area, including Sendai City, Tokyo, Yokohama City, Kokawa Town, Amagasaki City, were categorized into Group II. The present results provide evidence of multiple invasions of *I. minor* in Japan.

Due to wood is the food source of the pest termite species, the termite feeding behavior is one of the important research targets. Three patterns of feeding behaviors i.e. cutting, pulling, and collecting were observed in *I. minor* using a CCD camera and an AE detector (7). These were similar to those of *C. formosanus*. The other subterranean termite, *R. speratus*, showed only cutting and pulling actions. Among these species, *I. minor* showed the highest p-p amplitude regardless of patterns of feeding behavior. The body length and size of the mandibles of the termites might be correlated with the p-p amplitude of the AE signals of the termites, where *I. minor* have the biggest body length and mandibles among three species of termite.

Although many studies have reported testing methods of wood preferences by dry-wood termite, no standard testing methods for dry-wood termites have been established at present. A new method for testing wood preferences of dry-wood termites was suggested by the present study (8). Five Japanese timbers, four U.S. timbers and one Malaysian timber were evaluated for their resistance to *I. minor* using laboratory choice and no-choice feeding tests with holed specimens. A choice feeding test, combining all test samples, was suggested to be an appropriate method to determine the termite wood preference than no-choice tests in this study, with the higher survival rate in the choice feeding test after the experiment. From this experiment, the ranking of the resistance of the ten commercial timbers against *I. minor* was buna > karamatsu > sugi > western red cedar > Douglas-fir > rubber > western hemlock > hinoki > spruce.

Beside wood species, another factor influencing the feeding activity of termite is environment condition. The effect of ambient temperature and RH on the activity of *I. minor* has been investigated (9).

Among six temperatures (15, 20, 25, 30, 35, and 40°C) and four RHs (60, 70, 80, and 90%) conditions, the optimal temperature and RH for the feeding activities of *I. minor* were 35°C and 70%, respectively. The higher AE events in 24 combinations of six temperatures and four RHs were observed at 35°C-70% and 35°C-80%. The hottest temperature (40°C) caused termites to become moribund, and their feeding activity decreased rapidly. The coolest temperature (15°C) did not kill the termites, but did reduce the feeding activity.

In recent years, the introduction of bait system that use fewer chemicals to the methods of subterranean control has encouraged the application of the system to eliminate *I. minor* colonies (10). The application of a gel formulation against *I. minor* must be considered, since this strategy is less hazardous to the environment. Though the basic effectiveness of the gel was confirmed by the present laboratory experiments, the higher deviation in mortalities of termites in replications was observed. Therefore, the search for special attractants that spread into the whole attacked areas should be conducted to attain the satisfactory remedial treatments.

REFERENCES

[1] Su, N.Y., and Scheffrahn, R. H. (1990) Sociobiology 17:77-94
[2] Cabrera, B.J. and Scheffrahn, R. H. (2004) http://edis.ifas.ufl.edu/ BODY_IN526
[3] Mori, H. (1976) Shiroari (Termite) 27:45-47 (in Japanese)
[4] Indrayani, Y., Yoshimura, T., Fujii, Y., Yanase, Y., Okahisa, Y., and Imamura, Y. (2004) Jpn J Environ Entomol Zool 15 (4):261-268
[5] Indrayani, Y., Yoshimura, T., Fujii, Y., Yanase, Y., Fujiwara, Y., Adachi, A., Kawaguchi, S., Miura, M., and Imamura, Y. (2005) Sociobiology 46:45-64
[6] Indrayani, Y., Matsumura, K., Yoshimura, T., Imamura, Y., and Itakura, S. (2006a) Mol Ecol Notes 6 (4):1249-1251
[7] Indrayani, Y., Yoshimura, T., Yanase, Y., Fujii, Y., Matsuoka, H., and Imamura, Y. (2007a) Sociobiology 49:121-134
[8] Indrayani, Y., Yoshimura, T., Yanase, Y., and Imamura, Y. (2007b). J Wood Sci (in press)
[9] Indrayani, Y., Yoshimura, T., Yanase, Y., Fujii, Y., and Imamura, Y. (2006b) J Wood Sci 53 (1):76-79
[10] Indrayani, Y., Yoshimura, T., and Imamura, Y. (2007c) (Submitted to J Wood Sci)

BIODEGRADABILITY OF GAMMA-IRRADIATED WOOD AND ITS APPLICABILITY TO THE TERMITE MANAGEMENT

Noriaki Katsumata

Laboratory of Innovative Humano-habitability, RISH, Kyoto University

There were no remarkable changes/modifications of the cell wall surfaces of spruce, beech and popular based on the early microscopic observations (1), when they were gamma-irradiated at 500 kGy. The similar results were reported on the gamma-irradiated pine wood (2). Since lignin is more stable than cellulose in the wood cell wall against gamma irradiation, the former is degraded little even at the dose of gamma irradiation which causes degradation of wood cellulose (3). High doses of gamma irradiation decrease the degree of polymerization of cellulose (4), resulting in the changes of physical and mechanical properties. These reports suggest that a drastic change of wood cell wall is induced by gamma irradiation the range between 100 kGy and 1 MGy.

Although lignin remains intact and the degree of polymerization of cellulose decreases at low gamma-irradiation (4), the decay resistance of white oak, red oak, sweetgum and Douglas-fir against a brown-rot fungus, *Poria monticola* did not go down (5). Unfortunately, there has been no information about termite resistance of the gamma-irradiated wood. As the strength of cellulose material is related to the DP of the cellulose (6), gamma-irradiated wood is easily bitten and taken by termites due to the relatively lower DP of cellulose. If gamma irradiation helps termites eat more wood, the gamma-irradiated wood might be suitable for the substrate of bait toxicant in the termite management system, because an ideal substrate is highly resistant to microbial infection (decay and sapstaining fungi and molds) and vulnerable to termites at the same time. Since some microbial infection obviously discourages the termite to gain an access to bait stations and in contrast, low termite resistance is likely to attract termites.

The gamma-irradiated *Cryptomeria japonica* sapwood was tested for its biological resistance and potential as the substrate of toxicants in termite bait system. Laboratory evaluations clearly showed that the decay resistance of *C. japonica* sapwood did not change after gamma irradiation due to the unchanged matrix of cell wall. On the other hand, a decreased degree of polymerization of cellulose by gamma irradiation resulted in the raised feeding activity of the subterranean termite, *Coptotermes formosanus* in the no-choice laboratory test. This discovery that gamma irradiation of wood enhanced termite feeding definitely insisted on the necessity of further research to discuss the applicability of gamma-irradiated wood to the bait substrate in termite management program.

Additional laboratory evidences indicated the superiority of the gamma-irradiated wood as the bait substrate to nondurable and moderately durable timbers such as heartwood of *Pseudotsuga menziesii*, *Larix kaempferi* and *Chamaecyparis obtusa* in both no-choice and comparative choice tests using termites from multiple colonies. Although the variation of termite feeding activity and survival rates among test termite colonies had been anticipated, the experimentation did not show any conspicuous effect of termite colonies. Both no-choice and multi-choice tests always indicated that *C. japonica* sapwood gamma-irradiated at 200 kGy always outperformed any other wood species tested.

The gamma-irradiated *C. japonica* was finally examined for its potential as the bait substrate (matrix) for termite management. Noviflumuron or hexaflumuron, insect growth regulators (IGRs), was impregnated into the gamma-irradiated wood, and *C. formosanus* workers were forced to eat the treated wood blocks. The termite workers were then fed on untreated filter paper to record the number of dead termites with time. The gamma irradiation favorably helped termites eat more wood with noviflumuron or hexaflumuron in. The results of this bioassay clearly demonstrated that both IGRs did not lose their slow-acting and low dose-dependent characteristics required as the bait toxicant.

All these results strongly support that gamma-irradiation at 200 kGy is feasible in converting nondurable wood into more suitable substrate of bait toxicants, and that further studies should be planned to demonstrate the usefulness of gamma-irradiated wood in the field where alternative food source is always available. The gamma-irradiated wood should be examined in terms of its attracting and/or arresting ability as well under the field conditions to establish environmentally benign termite management as a result of the commercialization of gamma irradiation technology.

REFERENCES
[1] Polčin, V. J. and Karhánek M. (1964) Holzforschung 18: 102-108
[2] Burmester, A. (1966) Materialprüf 8: 205-211
[3] Seifert, K. (1964) Holz Roh Werkst 22: 267-275
[4] Siau, J. F, Meyer J. A. and Skaar C. (1965) For Prod J 15: 162-166
[5] Scheffer, T. C. (1963) For Prod J 13: 208
[6] Teszler, O., Kiser L. H., Campbell P. W. and Rutherford H. A. (1958) Text Res J 27: 456-462

Biodegradation of moso bamboo with special references to some chemical and physical properties

Yoko Okahisa

Laboratory of Innovative Humano-habitability, RISH, Kyoto University

Bamboo had been used as a building material for centuries in Japan. Japanese traditional buildings use many bamboo materials for wall-supporting materials or interior materials. Recent changes in people's life-style and in architectural design have resulted in the decrease of bamboo usages in Japan [1]. However, new housing materials made from bamboo have been developed and new building methods employing bamboo have also been proposed.

To explore the trends and changes in the modern utilization of bamboo, a postal questionnaire survey on the architectural uses of bamboo in Japan was carried out. In general, there was a big opinion gap between architects and dealers regarding the architectural uses of bamboo. The majority of the architects regarded the ornamental aspects of bamboo as important, but most of the dealers pointed out that the mechanical and biological aspects should be considered in using bamboo as a housing material. The architects also claimed that improvements in bamboo processing have made it easier to work with. On the other hand, the dealers pointed out that the susceptibility to insect attacks and the occurrence of cracks were the most important problems to be solved [2]. In this dissertation, the bio-deterioration characteristics of bamboo were investigated.

The biologically perishable properties of bamboo are assumed to be mainly caused by its high sugar and starch contents, which are excellent foods for fungi or insects. Therefore, a simpler and faster method for analyzing the sugar and starch contents of moso bamboo is designed. Many methods have been proposed to extract sugar and starch from plants. Among them, the Ethanol extraction - Perchloric Acid hydrolysis method (EPA method), which extracts sugars from plants by using 80 % ethyl alcohol and solubilizing starch by using dilute perchloric acid, is commonly used for estimating the sugar and starch contents of bamboo [3]. However, this method takes a lot of time and is reported to be relatively unreliable. A facile but reliable method is thus strongly needed. The performance of the Alkaline extraction - Glucoamylase hydrolysis method (AG method), which extracted sugars and starch by using sodium hydroxide and hydrolyzed starch by using glucoamylase and α-amylase, was compared with that of the EPA method for analyzing the sugar and starch contents of moso bamboo (*Phyllostachys pubescens* Mazel) and the author concluded that the AG method was superior to the EPA method by taking into account of the time performance [4].

When the free glucose and starch contents of moso bamboo were determined by this newly designed method [4], the free glucose contents were generally lower in the upper culms, and the starch contents were highest in the middle culms (6 m-section). Both contents were generally higher in the inner part of each culm. This characteristic localization of free glucose is likely to be associated with the distribution of the particular nutrient storage cells, i.e., parenchyma cells. On the other hand, it is suggested that the starch content of moso bamboo depends not only on the ratio of parenchyma cells but also on the density of starch grains in the cells [5].

Some reports have indicated that bio-deterioration of bamboo depends on the season when it is cut [6]. Previous investigations mainly focused on the damage to bamboo caused by the attack of mold or *Dinoderus minutus* Fabricius, a serious insect pest to bamboo [7]. Termites and decay fungi cause serious damages to building and construction materials in Japan. However, no detailed study on the biological degradation of bamboo by termites and decay fungi has been conducted so far. There fore, the potential of termite and fungal attacks against moso bamboo in correlation with the seasonal changes in the free glucose content and starch contents, which were measured by the AG method were evaluated. Regarding the seasonal fluctuation of the free glucose and starch contents of moso bamboo, the free glucose contents were generally lower in autumn and winter than those in spring and summer, whereas the lowest starch contents were obtained in August and the contents increased almost linearly up to February and March. There was no special correlation between the free glucose or starch contents and the consumption by the pest termite, *Coptotermes formosanus*, even though higher mortalities were obtained in the bamboo-fed termites than in the wood fed ones. On the other hand, a positive correlation between the free glucose contents and mass losses of the samples at the 4 m- and 8 m-heights from the bottom by the decay fungus, *Trametes versicolor*

was observed. For the starch, no influence on fungal attack was found [8].

Workers of *C. formosanus* attacked only the radial section of the moso bamboo by laboratory no-choice tests. Previous studies indicated the damages of bamboo by *D. minutus* only appeared on the inner side of bamboo, which was soft and contained starch [3]. Therefore, evaluation of the potential of termite attack against moso bamboo in relation to two surface characteristics, hardness and roughness was conducted. As a result, it was suggested that termite attack against moso bamboo was closely related to the surface roughness of the material [9].

In Japan, a traditional drying method called "hagarashi" in Japanese have been applied to wood for improvement of the biological durability and heartwood color after drying. In this method, wood is felled down and retained for a long period without lopping until drying by the water transpiration. Some reports stated that this process reduced the moisture and starch content of wood [10]. The "hagarashi" process was applied to moso bamboo specimens to evaluate its potential for bamboo drying. The free glucose content of the "hagarashi" samples decreased faster than that in the samples stored at room temperature, but the starch content of the "hagarashi" samples decreased slower. The application of this process showed both the positive and negative effects on the biological characteristics of moso bamboo [11].

REFERENCES

[1] The Inquiry of the Ministry of Agriculture and Fisheries (2002) Bamboo J No.19: 67 (in Japanese)
[2] Okahisa, Y., Azuma, M., and Hikita, Y. (2005) Wood Preservation 31(2): 57-62 (in Japanese)
[3] e.g.) Ninomiya, S, and Kotani, K. (2002) Wood Preservation 28 (4): 135-143 (in Japanese)
[4] Okahisa, Y., Yoshimura, T., and Imamura, Y. (2005) J Wood Sci 51(5): 542-545
[5] Okahisa, Y., Yoshimura, T., Sugiyama, J., Erwin, Horikawa, Y., and Imamura, Y. (2007) J Bamboo Rattan (submitted)
[6] e.g.) Hamaguchi, T. (1953) J Jpn For Res 35 (3): 85-87 (in Japanese)
[7] Okahisa, Y., Yoshimura, T., and Imamura, Y. (2006) J Wood Sci 52 (5): 445-451
[8] e.g.) Hirano, Y., Shinoda, S., Arima, T. (2003) Mokuzai Gakkaishi 49 (6): 437-445 (in Japanese)
[9] Okahisa, Y., Yoshimura, T., Imamura, Y., Fujiwara, Y., and Fujii, Y. (2005) Jpn J Environ Entomol Zool 16(2): 85-89
[10] e.g.) Hayashi, Y., Ohara, S., Furuta, M., Kurosu, H., Kitamura, Y. (1988) Mokuzai Gakkaishi 34(11): 934-941 (in Japanese)
[11] Okahisa, Y., Yoshimura, T., and Imamura, Y. (2007) Bamboo J No.24: 27-32

Study on Beam Forming and Direction-of-Arrival Measurement for Solar Power Satellite

A. K. M. Baki
Laboratory of Applied Radio Engineering for Humanosphere, RISH, Kyoto University.

An area of continuing uncertainty is the "energy resources". A huge and clean power source is needed for sustainable economic activities. One source of huge and clean power is the space solar power. Solar Power Satellite (SPS) can send enormous power to the Earth as the form of microwave (MW). Precise MW power beam steering is a most critical goal for SPS because without precise beam steering the higher efficiency of MW power can not be assured at the rectenna location. Retrodirective beam control system is a proposed method of precise beam directing.

Microwave Power Transmission (MPT) system designers must be concerned with Beam Collection Efficiency (BCE), Side Lobe Levels (SLL), size, weight, and cost among many other factors. It is needed to improve the MPT efficiency in order to reduce the SPS costs. BCE and Maximum Side Lobe Level (MSLL) are used for an evaluation of the MW beam. Reduction of SLL is of paramount importance especially for the MPT in order to achieve the highest possible BCE and to reduce interference to other communication systems. If all antennas are uniformly excited then the main beam will carry only a part of the total energy due to higher SLL. SLL are decreased and BCE is increased by adopting edge tapering for SPS. However, tapering the excitation causes thermal problem and it is a complicated task to maintain different power levels. Isosceles Trapezoidal Distribution (ITD) edge tapered antenna, which is a new concept, is studied for the first time for SPS as an optimization. ITD is better than full edge tapering and uniform amplitude distribution. It was found that the highest BCE and lowest SLL are possible to achieve in ITD edge tapering [1], [2]. Different amplitude distribution systems like uniform, Gaussian, Dolph-Chebyshev and the newly derived ITD method have been compared. The SLL reduction in ITD is even higher than those of other kinds of edge tapering.

The ITD has never been experimented any other places before. Only a small number of antennas from each side of the phased array antenna are tapered in this method. ITD edge tapering is almost uniform so it is technically better. The power density at the center of the array of the ITD system can be made lower than that of the Gaussian or similar kinds of distributions for the same power transmission. Therefore thermal behavior at the center of the ITD edge tapered phased array antenna is better than that of the Gaussian and other kinds of edge tapering. The higher BCE and better SLL performance than those with uniform distribution can be achieved in ITD with phase error and under unit failed condition.

A statistical method of achieving minimum SLL with random element spacing was also studied. Different properties of large antenna arrays with randomly, uniformly and combined spacing (uniform with little perturbation) of elements were studied. A new unified approach in searching for reducing SLL by exploiting the interaction of deterministic and stochastic element spacing was studied. The models indicated an advantage with respect to side lobes in the large area around the main beam and strongly reduced SLL in the entire visible range.

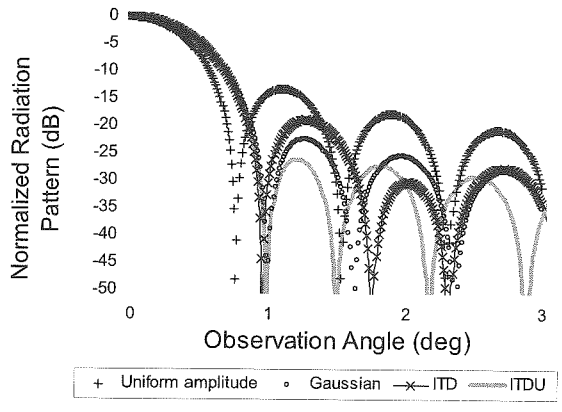

Figure 1 Normalized radiation patterns for phased array antenna of uniform amplitude, -10 dB Gaussian tapering, -10 dB ITD and -10 dB ITDU. 33 elements from each side were tapered in ITD. 30 elements from each side were tapered in ITDU and 40 elements from each side were of unequal spacing in ITDU.

Though it is possible to reduce SLL with statistically thinned array or combined stochastic algorithm but it does not guarantee higher BCE and needs edge tapering to achieve high efficiency. The performance of ITD was further improved from the perspective of both Maximum Side Lobe Level (MSLL) and BCE by using unequal spacing of the antenna elements [1]. The MSLL for ITD with Unequal element spacing (ITDU) was found to be the lowest (Figure 1) when it was compared with Gaussian, ITD and uniform amplitude distribution [1], [3]. The MSLL of ITDU is much lower than that of ITD. Moreover the BCE is found to be the highest in newly derived ITDU. The unequal spacing was derived from the ITD concept and by using the sinc function. The estimation of

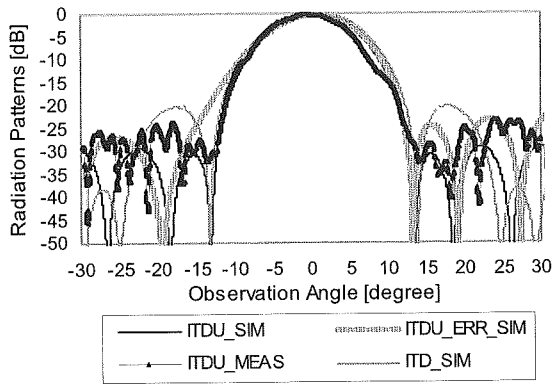

Figure 2 Simulated, measured and simulated (with error) radiation patterns of ITDU and simulated radiation pattern for ITD with 11 phased array antenna elements. (Experimental verification is done after submitting the dissertation).

unequal spacing is very easy. The unequal element spacing is chosen within such a range so that no grating lobe in the observation range of $\pm 90^{\circ}$ is formed due to unequal spacing with ITD. Both ITD and ITDU are new concepts. The merits of ITDU over ITD and Gaussian edge tapering were also studied [1]. Experimentation on ITDU was also done and it was found that the experimental results agree well with the simulation results (Figure 2). The experimentation on ITDU is also done for the first time and it was done no where before.

Detection of accurate phase and Direction of Arrival (DOA) of incoming pilot signal in SPS system is an important part of accurate beam forming. Imperfect knowledge of pilot signal receiving antenna spacing can cause DOA detection error. The displacement of antenna element spacing may occur after launching the satellite due to thermal expansion of the antenna or other reasons. The DOA error increases as the phase detection error increases. There are several sources of phase detection error such as element spacing error, ionospheric effect, antenna gain and phase errors. MUSIC and Time-Frequency MUSIC (TF-MUSIC) based DOA detection requires accurate knowledge of array element spacing and their performance can degrade substantially when there is a discrepancy between exact and presumed array element spacing. The effect of pilot signal receiving antenna spacing error on DOA was studied and a possible solution of element spacing calibration was investigated by using two reference signals in a time-sharing manner. TF-MUSIC method of DOA detection can increase the effective SNR and can detect the DOA of closely spaced signals. Therefore the TF-MUSIC for DOA detection in SPS was also studied. An experiment on simultaneously calibrating the antenna gain and phase errors and detection the DOA of two pilot signals were performed and the method is named as Calibrated_MUSIC (C_MUSIC) in the thesis. C_MUSIC was better than general MUSIC. TF_MUSIC was also tested by considering antenna gain and phase errors and the method is named as Calibrated TF_MUSIC (CTF_MUSIC). It was found that the CTF_MUSIC performed better (Figure 3) than C_MUSIC [1], [4]. The DOA errors were less and peaks were sharper in CTF_MUSIC than C_MUSIC.

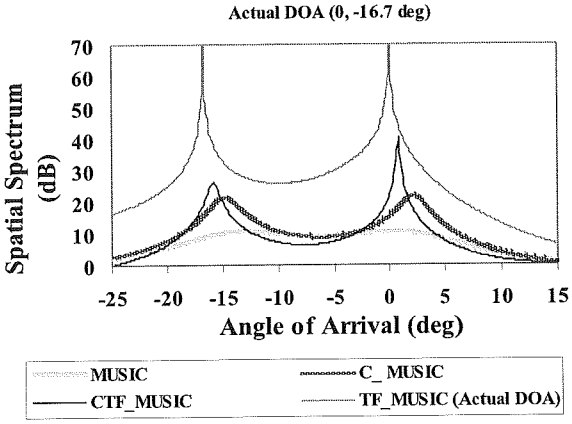

Figure 3 Spatial spectrum of MUSIC, C_MUSIC, and CTF_MUSIC of measured incoming signals and TF_MUSIC of actual (simulated) incoming signals (without any error). CTF_MUSIC performs better than MUSIC and C_MUSIC in real situations.

The effect of ionospheric total electron content (TEC) on the DOA of SPS pilot signal was studied and it was found that this effect can be neglected.

REFERENCES

[1] A. K. M. Baki, "Study on Beam Forming and Direction-of-Arrival Measurement for Solar Power Satellite", A Ph D dissertation submitted to the Faculty of Engineering of the Kyoto University, Kyoto, Japan, 2006.

[2] A. K. M. Baki, N. Shinohara, H. Matsumoto, K. Hashimoto, and T. Mitani, "Study of Isosceles Trapezoidal edge tapered phased array antenna for Solar Power Station/Satellite", IEICE TRANS. COMMUN., VOL.E90-B, NO.4 APRIL 2007.

[3] A.K.M.Baki, Kozo HASHIMOTO, Naoki SHINOHARA, Tomohiko MITANI, and Hiroshi Matsumoto, "Isosceles-Trapezoidal-Distribution Edge Tapered Array Antenna with Unequal Element Spacing for Solar Power Satellite", IEICE Trans. Comm. (submitted), 2007.

[4] A.K.M.Baki, Kozo HASHIMOTO, Naoki SHINOHARA, Tomohiko MITANI, M. Matsumoto, and Hiroshi Matsumoto, "Direction-of-Arrival Measurement and Beam Pointing Accuracy for Solar Power Satellite", IEICE Trans. Comm. (submitted), 2007.

Study on Electrostatic Waves in the Terrestrial Bow Shock Region via Spacecraft Observations

Koichi Shin
Laboratory of Applied Radio Engineering for Humanosphere, RISH, Kyoto University

Plasma waves observed in the Earth's bow shock region are presented in this thesis. Plasma waves play a very important role for acceleration, dissipation and thermalization of the electrons and ions. We, especially, focus on electrostatic waves whose frequency ranges are near 1 kHz which is commonly between the electron plasma frequency and the ion plasma frequency in the bow shock region.

One of the topics is electrostatic quasi-monochromatic (EQM) waves. Geotail plasma wave observations show the existence of intense EQM waves in the downstream region of Earth's bow shock [1]. Fig. 1 show that observed waveforms are quasi-monochromatic and their electric field oscillates parallel to the ambient magnetic field and appears at frequencies between the electron plasma and ion plasma frequencies. Although these waves have been believed to be Doppler-shifted ion acoustic waves, the typical plasma parameters observed in the downstream region do not support the generation conditions for ion acoustic waves. The existence of cold electron beam-like components accompanying EQM waves are examined based on the waveform and statistical analyses using Geotail plasma wave and particle observations. Based on linear dispersion analyses using realistic plasma parameters, it is explained that the cold electron beams cause destabilization of electron acoustic waves at frequencies consistent with those of observed EQM waves [2]. The results of observations and linear analyses suggest that EQM waves are generated by the destabilization of the electron acoustic mode.

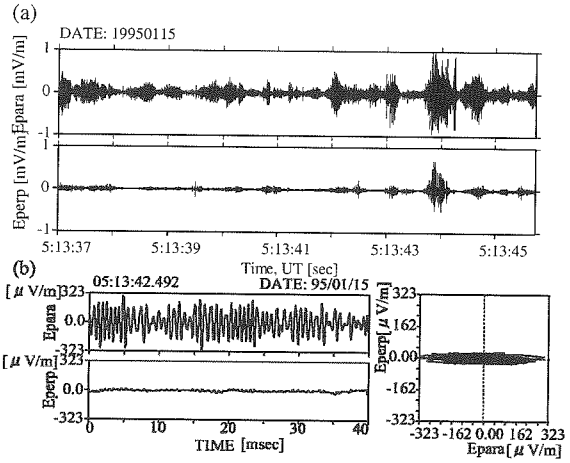

Fig. 1: (a) Waveforms of the EQM waves of the parallel (top panel) and the perpendicular (bottom panel) components with respect to the ambient magnetic field observed in the downstream region of the bow shock during the period from 5:13:37.000 UT to 5:13:45.500 UT on January 15, 1995. (b) Expanded waveforms (left panels) and corresponding hodograph (right panel) for the period of 40 milliseconds from 5:13:42.492 UT.

Next main topic is electrostatic solitary waves (ESW). We observed ESW in the upstream region of the terrestrial bow shock by the Geotail spacecraft [3] (Fig. 2). The ESW are mostly observed at a foreshock region. The foreshock region is separated into electron foreshock and ion foreshock regions dominated by energetic electrons and superthermal ions, respectively. The Geotail waveform observations show the existence of ESW in both electron and ion foreshock regions. To understand the wave features of ESW, we perform the waveform analyses and analyses of the spatial distribution of ESW. Results show that occurrences and amplitudes of ESW decrease as the distance from the bow shock transition increases. In the electron foreshock region, observations of the ESW correlate with electron beams away from the bow shock. We roughly estimate the potential depth of ESW as 0.15 eV using observed parameters. Potential depth is roughly few percent of the ambient electron temperature, similar in situation to the magnetotail ESW. In the ion foreshock region, ESW are simultaneously observed with superthermal ions reflected by the bow shock. We find two types of ESW which have different polarization in the ion foreshock region based on the orientation of their bipolar waveforms. To distinguish the characteristics of the different polarization ESW, we examine the spatial distribution of the occurrence frequency of the ESW both upstream and downstream propagating ESW (Fig. 3). The upstream propagating ESW are observed farther from the bow shock than the downstream propagation ESW. Furthermore, we examine the shock normal dependence and the Alfven Mach number dependence of the occurrences of ESW in the ion foreshock region. Results show that ESW observed in the quasi-parallel shock have characteristics different from those observed in quasi-perpendicular shock. The most plausible generation mechanism of the first type of ESW is Buneman instability based on the reflected superthermal ions and background electrons. A possible

mechanism of the second type of ESW is positive potential which is propagated from the foreshock region to the bow shock, or negative potential generated by the reflected superthermal ions.

Furthermore, we observed ESW that have oblique potential structures with reference to the ambient magnetic field in the upstream region of the bow shock (Fig. 4). To understand the wave features of these ESW, we conducted the waveform and statistical analyses using wave form capture data onboard the Geotail spacecraft. The results of the statistical analyses show that the ESW with oblique potential structure are frequently observed in the vicinity of the bow shock, and the occurrence of those decreases as the distance from the bow shock increase. We conceive that generation of these ESW is highly dependent on bow shock conditions. Further, we examine the dependence of occurrence frequency of ESW and angle between the shock normal and electric field vector of the ESW. The ESW whose electric field vectors are parallel to the shock normal direction are observed mostly (Fig. 5). One of the possible generation mechanisms of oblique potential structures with the bi-polar pulses is that the oblique potential is generated by the two-stream instability with ion and electron components.

REFERENCES

[1] Shin, K., H. Kojima, H. Matsumoto, and T. Mukai, Electrostatic Quasi-monochromatic Waves Downstream of the Bow Shock: GEOTAIL Observations, *Frontiers of Magnetospheric Plasma Physics, COSPAR Colloquia Series, 16*, 293-296, 2005.

[2] Shin K., H. Kojima, H. Matsumoto and T. Mukai, Electrostatic quasi-monochromatic waves in the downstream region of the earth's bow shock based on Geotail observations, *Earth Planets Space*, 2006 (accepted for publication).

[3] Shin K., H. Kojima and H. Matsumoto, Characteristics of Electrostatic Solitary Waves in the Earth's Foreshock: Geotail Observations, *Journal of Geophysical Research*, 2007 (submitted).

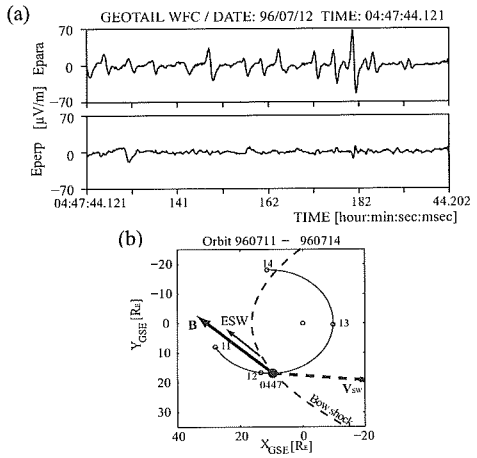

Fig. 2: (a) ESW waveforms of the parallel (upper panel) and perpendicular (lower panel) electric field component observed in the electron foreshock region on July 12, 1996. (b) Geotail orbit for the period of July 11, 1996 to July 13, 1996 in the Geocentric Solar Ecliptic (GSE) Coordinate System. Solid and dotted arrows show the directions of the ambient magnetic field (**B**) and the solar wind ion bulk flow (**V**sw), respectively.

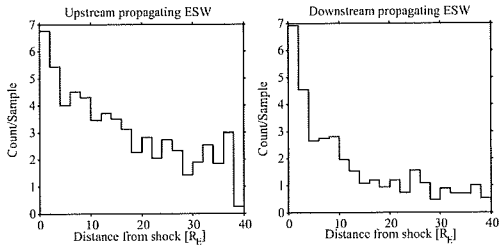

Fig. 3: Histograms of the occurrences of the (a) ESW propagating to the upstream region and (b) the ESW propagating from the bow shock with respect to the distance from the bow shock along to the ambient magnetic field.

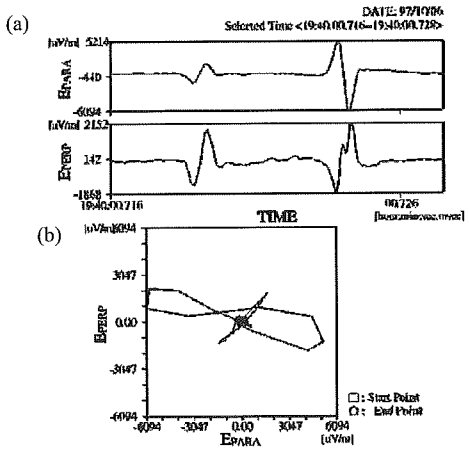

Fig. 4: (a) Waveforms of the parallel (upper panel) and perpendicular (lower panel) electric field with respect to the ambient magnetic field observed in the upstream region of the bow shock during the period from 19:40:00.716 UT to 19:40:00.728 UT on October 06, 1997 by the WFC receiver, and (b) corresponding hodograph of the observed electric field.

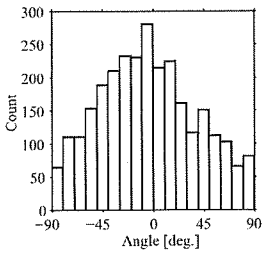

Fig. 5: Histogram of the occurrence frequency of the ESW that have oblique potential structure with respect to the angle between the shock normal and electric field vector of the ESW. Electric filed vectors of most ESW are close to the shock normal direction.

Populus euphratica in Niya site ~Scientific assessment of deterioration and aspects in humane studies~

Suyako Mizuno
Laboratory of Biomass Morphogenesis and Information, RISH, Kyoto University

Niya site is located near the center of the Silk Road in the district of Minfeng lying in the Xinjiang Uighur Autonomous Region of the People's Republic of China. The southern half of the region is the vast Tarim basin, which spreads for 550 km from north to south and as much as 1000 km from east to west, mainly constituted by the Taklimakan Desert so called "Sea of Death". Set 100 km from Minfeng at the southern tip of the Taklimakan, Niya is believed to have flourished from the 1st century BC to the 4th century AD, and has been identified as the Jingjue Kingdom referred to in the Han Book. Occupying an extensive area of approximatery 25 km from north to south and 7 km from east to west, the Site comprises about 100 ruins of dwellings, garden, agricultural fields and a huge number of dead trees. Niya site is praised as the "Pompeii of the Silk Road" because of its great historical importance buried under ground and kept remained. The extraordinary archeological excavation of NIya site and carbon 14 dating made it clear that housing pillars still standing after 2000 years and almost all of the trees were *Populus euphratica* Olivier (koyo). Because of its strong salt tolerance, koyo is used as a afforestation tree for Taklimakan desert today.

Koyo excavated from Niya site have been exposed to the ultraviolet rays of the sun, strong wind and dry climate for 2000 years. Therefore the surface of wood samples are discolored to almost white. In addition a series of many cracks along the longitudinal direction are obvious. Among our collection, samples from 3 kinds of eras (190, 1558～1667, 1900～2354 years-old) are subjected to physiochemical analysis. As a standard material, a present Koyo from China was used for comparison.

The samples examined were all anatomically identical with present koyo wood from China. However, there found considerable differences in physical properties, such as Young's moduli, loss tangent (tanδ). Particularly, in the static three-point bending test, Niya samples were much inferior in terms of fracture toughness, which strongly suggests that the sample became fragile by aging. This was also corroborated by the straight fracture line and the flat fracture surface of the Niya wood.

As mentioned above, the surface of the Niya wood were all discolored, probably due to degradation of lignin components by the ultraviolet irradiation. However, no significant spectroscopic differences in functional groups of carbohydrate regions were not detected, when a few millimeters from the surface was analyzed. Therefore, the major factor of deterioration in Niya wood was considered to be "thermal", more than UV and biological deterioration.

Such features of deterioration are quite similar to those reported for aged wood from the traditional Japanese constructions, where the deterioration "aging" is said to be caused by oxidation, i.e. thermal process.

Synthesis and functional analysis of ceriporic acid, extracellular metabolite of selective white rot fungus *Ceriporiopsis subvermispora*

Hitoe Shimizu
Laboratory of Biomass Conversion, RISH, Kyoto University

Wood is mainly composed of cellulose, hemicelluloses and lignin. Most white rot bacidiomycetes simultaneously degrade polysaccharides and lignin. In contrast, a selective white rot fungus *Ceriporiopsis subvermispora* decomposes lignin with minimum damage of cellulose. Important mechanisms for the selective white rot include lignin degradation by low molecular mass agents and inhibition of cellulose degradation by the cellulolytic active oxygen species, hydroxyl radicals (·OH). Previously we reported that production of hydroxyl radicals and cellulose depolymerization were inhibited by ceriporic acid B (1-nonadecene-2,3-dicarboxylic acid), an extracellular metabolite of *C. subvermispora* [1-3]. On the other hand, it was known that this fungus secretes oxalic acid [4], which accelerates hydroxyl radical production at certain molar ratios of oxalate/Fe^{3+} [5]. In the present study, we analyzed effects of ceriporic acid B on hydroxyl radical production and cellulose degradation by the Fenton reaction system in the presence and absence of oxalic acid.

Hydroxyl radicals were produced by the Fenton system containing Fe^{3+}, H_2O_2 and a reductant in the presence and absence of ceriporic acid B and oxalic acid. Depolymerization of cellulose by the Fenton system was then evaluated by measuring decrease in viscosity of cellulose. In the presence of oxalic acid, hydroxyl radical production and cellulose degradation were accelerated at the equimolar ratio of oxalate and Fe^{3+}. However, addition of ceriporic acid B inhibited the hydroxyl radical production and cellulose degradation at all the molar ratio employed. These results indicate that ceriporic acid B inhibited cellulose degradation, in the presence and absence of oxalic acid.

C. subvermispora secretes (*Z*)-10-nonadecadiene-2,3-dicarboxylic acid (ceripoirc acid C), in addition to 1-nonadecene-2,3-dicarboxylic acid (ceriporic acid B) and 1-heptadecene-2,3-dicarboxylic acid (ceripoirc acid A) [6,7]. In the present study, (*Z*)-10-nonadecadiene-2,3-dicarboxylic acid (ceripoirc acid C) and its (*E*)-isomer was synthesized by the Grignard reaction for structural and functional analysis of the extracellular metabolites.

REFERENCES

[1] Watanabe, T., Teranishi, H., Honda, Y., Kuwahara, M. (2002) *Biochem. Biophys. Res. Commun.* **297**: 918-923.
[2] Rahmawati, N., Ohashi, Y., Watanabe, T., Honda, Y., Watanabe, T. (2005) *Biomacromolecules*, **6**: 2851-2856.
[3] Ohashi, Y., Kan, Y., Watanabe, T., Honda, Y., Watanabe, T. (2007) *Org. Biomol. Chem.*, **5**: 840–847.
[4] Urzur, U., Kersten, P. J., Vicuña, R. (1998) *Appl. Environ. Microbiol.*, **64**: 68-73.
[5] Valera, E., and M. Tien, (2003) *Appl. Environ. Microbiol.*, **69**:6025-6031
[6] Enoki, M., Honda, Y., Kuwahara, M., Watanabe, T. (2002) *Chem. Phys. Lipid*, **120**: 9-20.
[7] Amirta, R., Fujimori, K., Shirai, N., Honda, Y., Watanabe, T. (2003) *Chem. Phys. Lipids*, **126**: 121-131.

Ligninolytic free radicals in selective white rot

Yukiko Uno
Laboratory of Biomass Conversion, RISH, Kyoto University

There is a growing demand to produce fuels and chemicals from biomass to solve the problems of global warming and deficiency of fossil fuels because the biomass feedstock is produced by fixation of carbon dioxide by the photosynthesis of plants. In enzymatic conversion of lignocellulosics it is necessary to decompose the network of lignin prior to the enzymatic hydrolysis because lignin makes the access of cellulolytic enzymes to cellulose difficult. Thus, effective pretreatments are needed for enzymatic saccharification and fermenataion of lignocellulosics. Physical, physicochemical, thermochemical, chemical and biological pretreatments have been studied to decompose the network of lignin. Natural processes that occur during fungal biodegradation of wood have a great potential to decompose the lignin network. Treatments of lignified plant materials with selective lignin-degrading fungi (white rot fungi) assist to expose cell wall polysaccharides to increase accessibility of cellulolytic enzymes to the cell wall polysaccharide.

A selective white rot fungus, *Ceriporiopsis suibvermispora* is able to degrade lignin selectively without intensive damage of cellulose. In the selective delignification, extensive delignification was observed without penetration of extracellular enzyme into wood cell wall regions [1]. This phenomenon indicates that low molecular mass oxidant play an important role for the selective delignification. In incipient stage of wood decay, this fungus secretes manganese peroxidase (MnP) and lipids, and catalyzes the MnP-dependent lipid peroxidation [2,3]. In lipid peroxidation, carbon-centered ($R^{\bullet}$), alkoxyl ($RO^{\bullet}$) and peroxyl ($ROO^{\bullet}$) radicals are produced by chain reactions. However, little is known about reactivity of these free radicals to lignin. In the present study, $ROO^{\bullet}$, $RO^{\bullet}$ and both radicals were generated by decomposing organic peroxides with transition metal complexes. We analyzed reactivity of $RO^{\bullet}$ and $ROO^{\bullet}$ radicals with non-phenolic β-*O*-4 lignin model compounds by electron spin resonance (ESR) and gas chromatography/mass spectrometry (GC-MS).

REFERENCES

[1] Messener K., Srebotnik E. (1994) *FEMS Microbiol. Rev.*, **13**: 351-364.
[2] Enoki, M., Watanabe, T., Nakagame, S., Koller, K., Messner, K. Honda, Y., Kuwahara, M. (1999) *FEMS Microbiol. Lett.*, **180**: 205-211.
[3] Watanabe, T., Katayama, S., Enoki, M., Honda, Y., Kuwahara, M. (2000) *Eur. J. Biochem.*, **267**: 4222-4231.

Energy conversion of wood biomass using ligninolytic activities of basidiomycetes

Kenta Yano
Laboratory of Biomass Conversion, RISH, Kyoto University

To prevent serious global warming by emission of carbon dioxide from fossil fuels, it is an urgent task to produce energy and chemicals from carbon-neutral renewable resources. The development of conversion systems from lignocelluloses into biofuels and chemicals has received much attention due to immense potentials for the utilization of renewable resources. Since lignin makes the access of cellulolytic enzymes to cellulose difficult, it is necessary to decompose the network of lignin prior to the enzymatic hydrolysis. Thus, effective pretreatments are needed for enzymatic saccharification and ethanol production from wood. To this end, biological pretreatments with lignin-degrading fungi possess a great potential if the fungal treatment could decompose the network of lignin with minimum loss of polysaccharides. There have been many proposals for thermal pretreatments of wood. These include steam explosion, microwave irradiation and ethanolysis. However, extent of enzymatic saccharification of softwood after these pretreatments was much lower than that of hardwood and non-wood lignocellulosics. Therefore, combination with catalysts like sulfuric acid and SO_2 has been examined to apply the thermal pretreatments to softwood. However, use of toxic chemicals like sulfuric acid decrease the advantage of environmentally-friendly process, enzymatic saccharification. In this context, development of pretreatments without the use of toxic chemicals with low energy input has been required for producing ethanol and methane by enzymatic saccharification and fermentation.

In the present study, we propose a new pretreatment process using selective white rot fungi and microwave solvolysis. We screened white rot fungi capable of degrading lignin in Japanese cedar wood because the softwood species shares over 60% of forest plantation in Japan. We isolated a new strain (*Phellinus* sp. SKM2102) which exhibited high pretreatment effects comparable to those of the best biopulping fungus, *Ceriporiopsis subvermispora*. In cultures of *Phellinus* sp. SKM2102, positive reaction was found in Bavendamn test with guaiacol and gallic acid. This fungus secreted manganese peroxidase and manganese-independent peroxidase as a major ligninolytic enzyme. Although the pretreatment effects of *Phellinus* sp. SKM2102 was higher than that of *C. subvermispora*, decrease in total weight and hollocellulose content in the Japanese cedar wood chips was lower than that of *C. subvermispora*. *Phellinus* sp. SKM2102 consumed fatty acids (C16～C18) in Japanese cedar wood at an incipient stage of decay within 20 days, and produced long-chain fatty acids (C20 over) after 20 days. Methane fermentation was accelerated by fungal treatment with *Phellinus* sp. SKM2102. The strain exhibited accelerating effects on enzymatic saccharification of Japanese cedar wood in combination with microwave solvolysis. Ethanol was produced from the enzymatic digests of the pulp fraction by *Saccharomyces cerevisiae* without intensive fermentation inhibitation. Thus the new strain was effective for the pretreatments of Japanese cedar wood.

Cloning and repression of *ku70* in *Pleurotus ostreatus*

Yoichiro Yano
Laboratory of Biomass Conversion, RISH, Kyoto University

INTRODUCTION

White rot fungi belong to basidiomycetes and degrade plant cell wall lignin. They produced a family of extracellular ligninolytic enzymes, but function of each isozyme has not been not clearly elucidated yet, besides numerous enzymatic and biochemical analyses. Differential expression control in transcriptional level has been reported, however, a reverse-genetics technique would be more effective to clarify the role of each isozyme in biodegradation of lignin. To establish a reverse-genetic technique in basidiomycetes, it is required to develop an efficient gene targeting system. Gene targeting is to substitute a specific gene in the genome by homologous recombination (HR) in the living cell and will make it possible to evaluate the physiological role of an interested gene. HR is major repair pathways for DNA double strand breaks (DSB) in yeasts. In the HR pathway, the DSBs are repaired through regions homologous to each other. However it is generally considered that another repair pathway, non-homologous end joining (NHEJ) is predominant in somatic cells of multi cellular eukaryotes. In the NHEJ pathway, DSBs in chromosomes are repaired by joining two broken ends of DNA irrespective of their sequence homology. For the establishment of an efficient gene targeting system, it is necessary to repress the NHEJ pathway and to exaggerate the HR.

Recently, there were reports that deletion of an essential gene *ku70* for the NHEJ system increased greatly the efficiency of gene targeting in ascomycetes, *Neurospora crassa* [1] and *Aspergillus oryzae* [2]. In this study, the development of the gene targeting system by the repression of *ku70* was tried in basidiomycete *Pleurotus ostreatus*.

MATERIALS and METHODS

Degenerated primers for amplification of *P. ostreatus* gene fragment encoding for KU70 (*Poku70*) were designed with CODEHOP strategy [3], using highly conserved amino acid sequence among known KU70 proteins. Using these primers, a DNA fragment was amplified by PCR and cloned into pGEM-T vector. Then, a whole gene fragment was cloned using inverse PCR technique and full-length cDNA fragment was amplified by RACE methods and RT-PCR. Sequence analysis, phylogenic analysis and predicted molecular modeling of *Poku70* were done. To repress *Poku70*, we tried antisense RNA and RNAi methods. We constructed recombinant plasmids which contain a full-length or partical *Poku70* cDNA fragments in the antisence direction under the control of *P. ostreatus sdi1* promoter and terminator (p07uk series). Moreover, we constructed derivative plasmids which of p07uk series by inserting an intron from *P. ostreatus mnp2*. We also constructed RNAi plasmid which contains a partial cDNA fragment and intron followed by the same cDNA fragment in the antisense direction under the control of *P. ostreatus sdi1* promoter and terminator. Co-transformation of *P. ostreatus* by PEG/$CaCl_2$ protocol was carried out using antisense plasmids or RNAi plasmid as well as plasmids which contain a drug resistant marker gene.

RESULTS and DISCUSSION

The length of the cording regions of *Poku70* was 1947 bp which may code a peptide of 648 aa. Although the amino acid identities between *Po*KU70 and other KU70 proteins were not so high (20-30%), it was suggested that *Po*KU70 has highly conserved domains among KU70 proteins such as N-terminal α/β domain, β-barrel domain and SAP domain. Furthermore, the predicted molecular modeling of *Po*KU70 was extremely similar to 3D structure of human KU70.

We have not isolated recombinant *P. ostreatus* strains containing the antisense or RNAi sequences among the drug resistant transformants so far analyzed. Further experiments will be continued to repress *Poku70*.

REFERENCE

[1] Ninomiya Y., Suzuki K., Ishii C. and Inoue H. (2004) *Proc. Natl. Acad. Sci.* USA, **101**: 12248-12253
[2] Takahashi T., Masuda T. and Koyama Y. (2006) *Mol. Gen. Genomics*, **275**: 460-470
[3] Timothy M. R., Jorja G. H. and Steven H. (2003) *Nucl. Acids Res.*, **31**: 3763-3766

Characterization of genes involved in the lignin degradation from a new white-rot fungus, *Phellinus* sp. SKM2102

Taro Yoshida
Laboratory of Biomass Conversion, RISH, Kyoto University

The production of ethanol from lignocellulosics has received much attention due to immense potential for conversion of renewable biomaterials into biofuels and chemicals. Since lignin makes the access of celluloytic enzymes to cellulose difficult, it is necessary to decompose the network of lignin prior to the enzymatic hydrolysis. Recently, we have isolated a new white-rot fungus which has been characterized as the best fungus for the pretreatments of enzymatic saccharification of Japanese cedar wood. The fungus, designated *Phellinus* sp. SKM2102, exhibits high pretreatment effects for enzymatic saccharification of wood similar to those of a selective lignin-degrading fungus, *Ceriporiopsis subvermispora* [1]. The former exhibits less weight decrease in holocellulose than the latter. However, profiles of their metabolites, such as fatty acids, are different, reflecting the differences in gene expression involved in the fatty acid metabolism of these strains. Therefore, we focus on the fatty acid metabolism, especially the biosynthesis of unsaturated fatty acids because unsaturated fatty acids are precursors of lipid peroxidation in the selective lignin degradation by *C. subvermispora* [2]. On the other hand, we have found that strain SKM2102 possesses activities of ligninolytic enzymes, such as laccase and manganese peroxidase [3]. In order to establish basic understandings of the lignin-degrading system, we cloned fatty acid desaturase, laccase and manganese peroxidase genes from *Phellinus* sp. SKM2102 by PCR-based method.

REFERENCES

[1] Baba, Y. (2006) Div. Appl. Life Sci., Graduate School of Agric Sci., Kyoto Univ., Master thesis.
[2] Enoki, M., Watanabe, T., Nakagame, S., Koller, K., Messner, K., Honda, Y., and Kuwahara, M. (1999) *FEMS Microbiol. Lett.* **180**, 205-211.
[3] Yano, K. (2007) Div. Appl. Life Sci., Graduate School of Agric Sci., Kyoto Univ., Master thesis.

Characterization of *O*-methyltransferases involved in lignin and lignan biosynthesis

Yu Kitamura
Laboratory of Metabolic Science of Forest Plants and Microorganisms, RISH, Kyoto University

An *Arabidopsis thaliana* gene, At5g54160, was annotated as a caffeic acid *O*-methyltransferase CAOMT (= 5-hydroxyconiferaldehyde OMT, CAldOMT) (AtOMT1) gene based on its high sequence homology to *Populus tremuloides* CAOMT. However, Muzac et al. reported that a recombinant AtOMT1 did not methylate caffeic acid, whereas the protein methylated efficiently a flavonoid, quercetin [1]. Later, Goujon et al. reported that an At5g54160-knockout *Arabidopsis* mutant lacks syringyl unit in the lignin, again suggesting that the gene is involved in syringyl lignin biosynthesis [2]. In this study, the author identified firmly the *bona fide* function of At5g54160 gene as *AtCAldOMT* based on biochemical characterization of the recombinant protein and lignin analysis of an At5g54160-knockout T-DNA tag line mutant

Sakakibara et al. established a pathway from matairesinol to yatein which is a typical heartwood lignan and a key precursor to the antitumor lignan, podophyllotoxin in *Anthriscus sylvestris* [3]. The conversion involves four reactions steps, two of which is methylation of phenolic hydroxyl groups of lignans, probably catalyzed by lignan OMT(s). Umezawa et al. has reported the first molecular cloning of the gene encoding lignan OMT from *Carthamus tinctrius* maturing seeds [4], which catalyzes regioselective methylation of matairesinol to give rise to arctigenin, but not isoarctigenin. Taking advantage of this gene sequence, the author tried to isolate OMT genes in biosynthesis of podophyllotoxin and yatein in *Podophyllum peltatum* and *Anthriscus sylvestris*.

References

[1] Muzac, I., Wang, J., Anzellotti, D., Zhang, H., Ibrahim, R.K. (2000) Arch. Biochem. Biophys 375: 385–388.
[2] Goujon, T., Sibout, R., Pollet, B., Maba, B., Nussaume, L., Bechtold, N., Lu, F., Ralph, J., Mila, I., Barriere, Y., Lappierre, C. (2003) Plant Mol. Biol. 51: 973-989.
[3] Sakakibara, N, Suzuki, S, Umezawa, T, Shimada, M (2003) Org. Biomol. Chem. 1: 2474–2485.
[4] Umezawa, T., Li, L., Nakatsubo, T., Wada, S., Sakakibara, N., Suzuki, S., Chiang, V.L. Manuscript in preparation.

Physiological and cytochemical studies on an oxalic acid-producing enzyme, glyoxylate dehydrogenase, of copper-tolerant wood-rot fungus *Fomitopsis palustris*

Kumiko Okawa
Laboratory of Metabolic Science of Forest Plants and Microorganisms, RISH, Kyoto University

Brown-rot fungus *Fomitopsis palustris* accumulates large amounts of oxalate during wood decay. The fungus detoxifies copper-containing wood preservatives by forming insoluble copper oxalate. In addition, *F. palustris* acquires biochemical energy for growth by oxalate biosynthesis. Thus, the elucidation of mechanism for oxalate biosynthesis is important for the understanding of carbon metabolism of the fungus and the development of new wood preservatives.

The oxalate formation is catalyzed by oxaloacetase (OXA, EC 3.7.1.1) and cytochrome *c*-dependent glyoxylate dehydrogenase (GLOXDH) in *F. palustris*. In this study the authors attempted to elucidate a possible role of GLOXDH in the fungal growth under the gluconeogenetic condition. Furthermore, the subcellulare localization of the GLOXDH in *F. palustris* was investigated by immunoelectronmicroscopy.

Studies of metabolic control of lignin biosynthesis by use of *Arabidopsis thaliana* cultured cells

Shohei Wada
Laboratory of Metabolic Science of Forest Plant and Microorganisms, RISH, Kyoto University

Lignin is one of the major components of wood, and changing lignin structures and concentrations strongly affect characteristic traits of wood. Therefore, to elucidate integrated mechanisms for lignin biosynthesis is important in cell-wall biotechnology.

Plant metabolisms including lignin biosynthesis are largely controlled by a variety of transcription factors. To identify the function of transcription factors involved in lignin biosynthesis, it is very useful to employ the newly developed gene co-expression network analysis by use of microarray data sets of *Arabidopsis thaliana*. By exploiting this strategy, in our laboratory, a transcription factor (referred to as transcription factor A in this study) was tentatively identified as a candidate, which controls syringyl lignin biosynthesis.

The aim of this study is to identify firmly the function of transcription factor A by characterizing lignins of transgenic *A. thaliana* T87 cells in which the expression of the gene encoding transcription factor A is upregulated. However, conventional methods for lignin analysis, which were optimized for secondary xylem tissues of wood, have not yet been optimized for plant cultured cells including the T87 cells. Hence, in this study, methods for analyzing lignin structures (thioacidolysis and nitrobenzene oxidation methods) and for determining lignin contents (acetyl bromide and Klason methods) were optimized for *A. thaliana* T87 cells. Then transgenic *A. thaliana* T87 cells were subjected to lignin analysis under the condition established above, and it was firmly confirmed that the transcription factor A can upregulate syringyl lignin biosynthesis.

ACKNOWLEDGEMENTS

The author is grateful to Professor Daisuke Shibata and Dr. Nozomu Sakurai and Dr. Yoshiyuki Ogata of Kazusa DNA Research Institute for providing *A. thaliana* microarray date and transgenic and nontransgenic *A. thaliana* T87 cultured cells.

Functional analysis of *Oryza sativa* monooxygenase genes involved in Coenzyme Q biosynthesis

Takumi Kuchiya
Laboratory of Plant Gene Expression, RISH, Kyoto University

Coenzyme Q (CoQ) is a lipid-soluble electron carrier required for the respiratory chain in the many organisms. In eukayote, its preferable localization in cells is mitochondrial inner membrane. It's the main function of CoQ is to accept electrons from the NADH- and succinate-coenzyme Q reductases and to donate them to the bc_1 complex. It is known that CoQ content in human tissues peaks at the age of 20 and decreases thereafter, which is especially prominent the case in heart cells, and CoQ is therefore used clinically for the treatment of certain heart diseases. Several new biological activities has been discovered and further potential uses of CoQ for improving human health have recently been reported, i.e. CoQ confers mild symptomatic benefits for patients with Alzheimer's, Parkinson's and Huntington's diseases. Recently, CoQ has also been used in cosmetics and food supplements to prevent the accumulation of active oxygen species utilizing its strong antioxidative activity, and which caused a dramatic increase in demand and consequently a severe worldwide shortage of CoQ.

The biosynthetic rout of CoQ have been mostly investigated using various mutants of *Saccharomyces cerevisiae* and *Escherichia coli* that are deficient in production of CoQ. The benzoquinone ring of coenzyme Q6 of yeast a polyprenyl side chain six isoprenoid units. At least nine yeast genes (*COQ1–9*) were defined by complementation studies bored on the growth defect on glycerol media. However, in higher plants the synthesis of CoQ have not been well characterized.

This study suggests that a bifunctional enzyme exists in the rice genome involved biosynthesis of CoQ. We clarified its biochemical properties by use of yeast mutants, and the subcellular localization of this enzyme in plant cells.

The pine *O*-methyltransferase involved in stilbenoid biosynthesis

Tetsurou Morinaga
Laboratory of Plant Gene Expression, RISH, Kyoto University

Pine wilt diseases gave severe damages on Japanese pine forests, and it has been gradually decreasing after 1980s. Meanwhile, they are spread into other East Asian countries. The diseases are caused by pine wood nematode, which is transmitted by a pine sawyer. The pesticides and nematicides have been applied for the disease control. However, it has been criticized from an environmental point of view. Moreover, the disease is not completely controlled by these efforts because of the wide target area in the forests and mountains. On the basis of these backgrounds, alternative control strategies for pine wilt diseases are now expected.

In the genus *Pinus*, the stilbenoids, pinosylvin and its monomethyl ether are major constitutive phenolic constituents in the heartwood. Both compounds accumulate upon biotic and abiotic stress, which may function as phytoalexins in the tree. Especially, pinosylvin monomethylether showed strong nematicidial activity, of which LD_{50} was at 4ppm [1]. This is about 10-fold high comparing with the case of pinosylvin, suggested that pinosylvin monomethylether biosynthesis is a good target to control pine wilt diseases. This reaction would be catalyzed by an *O*-methyltransferase (OMT), which transfer methyl group from *S*-adenosyl-L-methionine to pinosylvin, to produce pionsylvin monomethylether [2].

We had already cloned five O-methyltransferase (OMT) cDNAs from the seedlings of *Pinus densiflora*. They belong to a type II OMT family, and are divided into two sub-groups. For the OMT cDNAs, we have established a pET32Xa/LIC expression system with *E. coli* OrinagmiB (DE3) pLysS. They can be produced in a soluble form probably because of thioredoxin tag. The OMTs are purified with a good yield and with a single band on SDS-PAGE gel through a Ni-NTA agarose column. The OMTs are finally obtained in soluble forms after removal of the attached tag. OMT is rich in SH groups and easily miss-folded without activity in some cases. For example, loblolly pine OMT with the activity has hardly obtained in *Escherichia coli* and form inclusion body [3]. Here, the purified soluble OMTs with mass production will provide insight of the folding studies for the 3D structure and the activity. Further studies on the cDNA translates will elucidate their functional roles.

REFERENCES

[1] Suga, T. et al.: Phytochemistry 33, 1395-1401, 1993.
[2] Chiron, H. et al.: *Plant Molecular Biology* 44, 733–745, 2000.
[3] Li, L. et al.: *Proc. Natl. Acad. Sci.. USA* .94, 5461–5466, 1997.

Characterization of dark-inducible genes involved in naphthoquinone biosynthesis in *Lithospermum erythrorhizon*

Kyoko Yamamoto
Laboratory of Plant Gene Expression, RISH, Kyoto University

Lithospermum erythrorhizon Sieb. et Zucc. (Boraginaceae) is a perennial herbal plant rarely found in Japan, Korea, and China. Roots of this medicinal plant appear strong red-purple, as its root bark (cork layers) contains a large amount of red naphthoquinone pigments, shikonin derivatives. Many studies demonstrated that shikonin and its derivatives showed various pharmacological activities, i.e. antibacterial, anti-inflammatory, wound-healing, tumor-inhibiting, etc. From this plants, a cell culture system was established, which produced higher amount of shikonin derivatives than the intact plants. The production system of shikonin by the cell cultures was applied for its industrial production by Mitui Petrochemical Industries as the first example of the production of secondary metabolites by plant cell cultures. The biosynthetic route of shikonin and its regulation mechanism have also been intensively studied with cell cultures as a model of clear inducible system of secondary metabolites in plants.

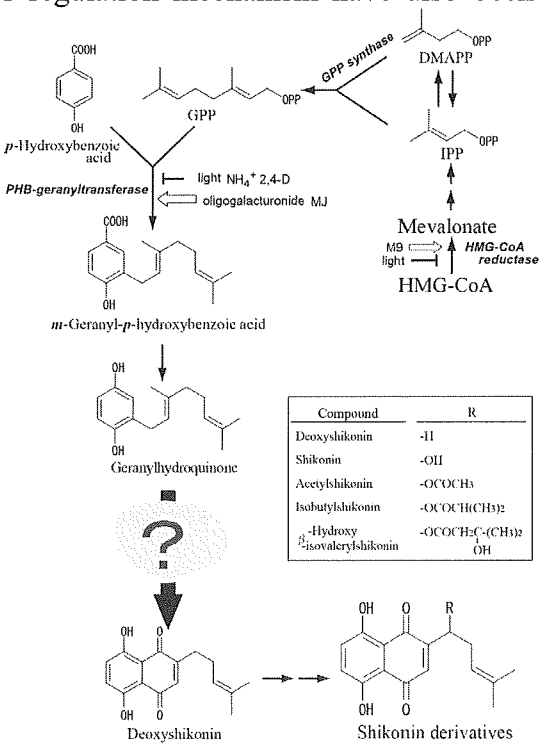

Shikonin molecule is formed *in vivo* from geranyldiphosphate derived from mevalonate pathway and *p*-hydroxybenzoate (PHB) *via* shikimate pathway. The coupling of these pathways is achieved by a membrane-bound enzyme, PHB-geranyltransferase (LePGT), which functions as a regulatory enzyme for shikonin production. The geranylated PHB is then convertes to geranylhydroquinone, which forms a naphthalene ring leading to the production of shikonin. However, the biosynthetic reactions responsible for the formation of naphthalene ring are not clarified yet. In the present study, we have attempted to identify enzymes involved in the naphthalene formation as well as their substrates and reaction products using *L. erythrorhizon* cell cultures as a model system. Results obtained from this research will provide crucial information of the mechanism of polycyclic ring formation involved in secondary metabolites, such as anthraquinones.

First, PCR-selected subtraction was applied to *L. erythrorhizon* cultured cells, in which cDNA samples of dark-grown cultures (shikonin-producing) and of cell cultures under illumination (non-producing) were used as the tester and the driver DNAs, respectively. The dark-inducibility was evaluated by dot-blot analysis in each gene for ca. 1,000 clones, and we obtained 240 clones whose expression was promoted more than 5-times in the dark. In these clones, adding to preciously identified biosynthetic genes, e.g. LePGT, we have found some strong dark-inducible genes as candidates of the naphthalene-forming enzymes.

Characteristics of Atmospheric Gravity Wave Activity in the Polar Regions Revealed by GPS Radio Occultation Data

Hayato Hei

Laboratory of atmospheric sensing and diagnosis, RISH, Kyoto University

Using GPS radio occultation (RO) temperature data, we have studied the climatological behavior of atmospheric gravity waves in the lower stratosphere in both the Arctic and Antarctic regions. We used level-3 version 004 GPS RO data obtained by the CHAMP satellite from May 2001 to December 2005, which are processed by GFZ Potsdam. From the temperature profiles, we have calculated the background mean temperature, T_0, Brunt-Väisälä frequency squared, N^2 and temperature fluctuations, T' with vertical wave length shorter than 7 km and then determined E_p at 12-19 km, 19-26 km and 26-33 km. The E_p values are estimated every one month in a cell with 20°×10° in longitude and latitude and we determined the monthly mean E_p as a function of longitude, latitude and time (month) between 12-33 km.

In the Arctic region, E_p shows a clear annual variation with maximum in winter (December-February), which is consistent with the annual variation of vertical component of E-P flux, F_z estimated from the global objective analysis data. The large F_z value indicates higher planetary wave activity, which results in distortion of the polar vortex. Then, the unbalanced flow due to the distortion of the polar vortex can excite gravity waves through geostrophic adjustment. Our study has confirmed similarity in the horizontal distribution of E_p and the polar night jet. A good correlation between E_p and the divergence of EP-flux, ∇F, suggests that the active planetary wave generates gravity waves through planetary wave transience and/or breaking.

In the Antarctic region, E_p gradually increases from July to August/September and reaches maximum in early spring (September-October) before decreasing rapidly. Time derivative of V in term of month coincides with the peak of E_p, and the horizontal distribution of E_p has a very similar structure with V. An example is shown in Figure 1. These results suggest that the E_p enhancement is closely related to the decay of the polar vortex. Because ∇F correlates well with the E_p enhancement, planetary wave transience and/or breaking seems to be related to the gravity wave generation. In winter, considering a good correlation between E_p and F_z similar to the Arctic result, we assume that gravity waves are also generated by the planetary wave activity via geostrophic adjustment.

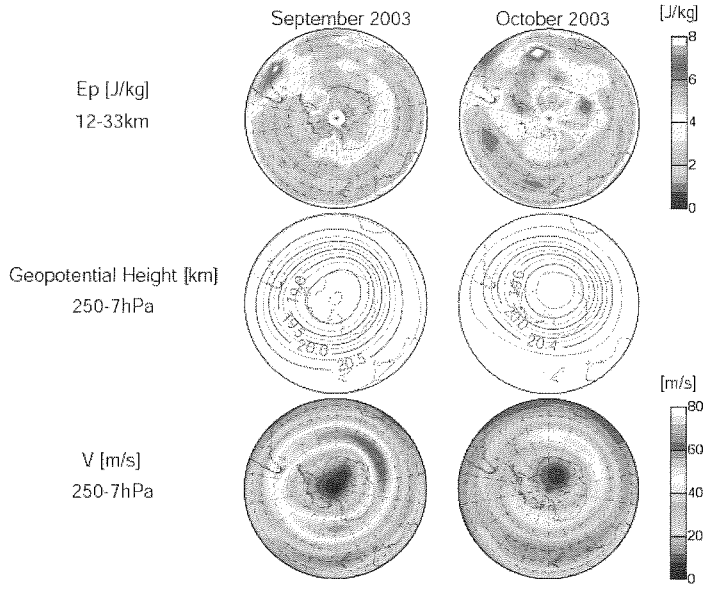

Figure 1. Distribution of E_p at 12-33 km (top), geopotential height at 250-7 hPa (middle) and V at 250-7 hPa. Right and left panels are the distribution in September 2003 and October 2003.

Frequency domain interferometric imaging to monitor detailed temperature profiles with the MU radar-RASS measurement

Atsushi Matsugatani

Laboratory of Atmospheric Sensing and Diagnosis, RISH, Kyoto University

INTRODUCTION

Atmospheric temperature, which is closely related with atmospheric buoyancy, is one of the most important parameters to characterize atmospheric behavior. Although the tropospheric temperature generally decreases with height, the detailed temperature variation plays an important role in the generation of various meteorological phenomena. Development of the temperature measurement technique with good height and temporal resolutions are very important for unveiling the thermodynamics of the meteorological phenomena. This study was devoted to improve height resolution of Radio Acoustic Sounding System (RASS), which is a radar remote-sensing technique to monitor temperature profiles by detecting the Bragg scattering from the acoustic wavefronts. In this study, a Frequency domain Interferometric Imaging (FII) technique, which is an adaptive technique for multiplied operational frequency array, was applied to RASS with Middle and Upper atmosphere (MU) radar (MU radar-RASS), aiming to improve the height resolution from 150 m to 50 m.

APPLICATION OF FII TECHNIQUE TO RASS ECHO

The FM-chirped acoustic pulse is employed to satisfy the Bragg condition in the wide height range for the RASS observation. The RASS echo is effectively scattered in the region of where the Bragg condition is satisfied. Since the effective scattering region of RASS echo propagates upward with time, we can improve the height resolution by extracting the FII results to an adequate period. Note, however, that the Doppler velocity of RASS echo is biased due to the effects of the radar range gate shape and the temperature profile. The effect was compensated using the model of the range gate function and temperature profiles with a constant lapse ratio. The simulation study to apply FII to RASS echo revealed that the inversion layer is successfully reproduced in the FII results. The discrepancy between the model and retrieved temperature is smaller than 0.2 K. For the MU radar-RASS imaging observation, the expected range resolution and the precision of range selectivity are estimated as about 50 m and less than 1 m, respectively.

THE MU RADAR-RASS OBSERVATION USING IMAGING TECHNIQUES

The MU radar-RASS imaging observation campaign was conducted on October 29-31, 2006. Continuous detailed time-height variations of temperature within the radar range gate were retrieved from the MU radar-RASS imaging data.

Left panel of Figure 1 shows the temperature profile between 0853 LT and 0919 LT on October 29, 2006. The horizontal dashed line shows the reference of the conventional height resolution of 150 m. The FII result shows the clear inversion structure with the minimum temperature at 1.85 km and the positive lapse ratio at 1.85-1.90 km. The structure agrees very well with the simultaneous radiosonde result (dot-dash line). The result at 18 LT on October 30, 2006 is shown in the right panel, showing the increase of temperature at 1.95-2.05 km and the decrease at 2.3-2.35 km. Temperature variation within the radar range gate agrees very well with the simultaneous radiosonde results.

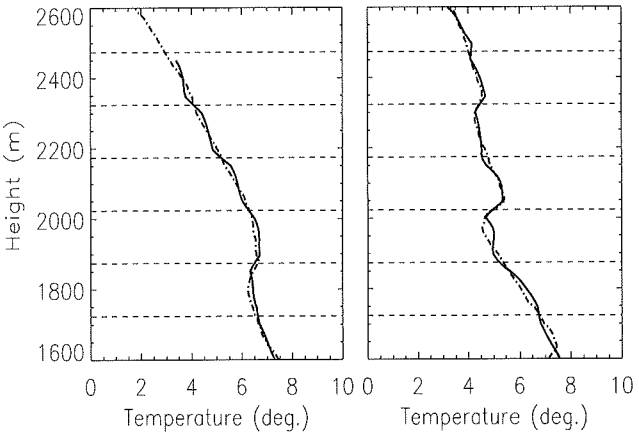

Figure 1: (Left panel) The temperature profiles of FII results (solid line) averaged over the period of 22.5 minutes from 0853 LT to 0919 LT on October 29, 2006. The simultaneous radiosonde result is also plotted in dot-dash line. The dash lines show the conventional range resolution of 150 m. Right panel is the same as left one except the results at 18 LT on October 30, 2006.

Characteristics of scattering layers in the troposphere revealed by simultaneous observations with a Raman/Mie lidar and the MU radar

Tomoaki Takai

Laboratory of atmospheric sensing and diagnosis, RISH, Kyoto University

INTRODUCTION

Atmospheric turbulence causes diffusion of substances which induce the climate change such as greenhouse effect. However, observations to reveal relationships between atmospheric turbulence and humidity or clouds are very limited. Both an MST (Mesosphere, Stratosphere, Troposphere) radar and a Raman/Mie lidar are remote sensing techniques for measuring atmospheric properties with high altitude and time resolutions. An MST radar observes atmospheric turbulence and wind velocity. A Raman/Mie lidar measures humidity, temperature and backscattering ratio. The MU radar has a capability of FII (Frequency domain Interferometric Imaging) observation that can investigate fine-scale turbulence structure with a height resolution smaller than 30[m]. A new data acquisition system was installed in the lidar system in Shigaraki MU observatory to improve the height resolution as small as 9[m]. We have carried out simultaneous observations with the Raman/Mie lidar and the MU radar to investigate relationships between atmospheric turbulence and humidity.

EXPERIMENTAL SETUP AND DATA PROCESSING

The MU radar was operated on 5 frequencies and the power distribution in each 150[m] range gate was estimated by applying the filter-bank Capon method. The antenna beam was pointed toward zenith and one or 4 oblique direction at 10 degrees. For lidar observation, analogue detection mode has been used to observe Mie-scattered signals even below 2.5[km] altitude.

RESULTS

Fine-structure of turbulence and humidity was examined by the lidar with a resolution of 50[m] and 30[sec] below 4.0[km] due to higher resolutions by enough signal-to-noise ratio. The thin layered structures observed by the MU radar were compared with the parameters derived from the lidar and we found that the peaks of height derivative of backscattering ratio (|dBS/dz|) or humidity (|dqdz|) corresponded well with the peak of radar signal intensity . The height differences between the maxima of radar echo power and the peaks of |dBS/dz| or |dq/dz| were within 30[m] (Fig 1), and the agreement lasted for more than 270 minutes (Fig 2). This correspondence was also observed even where isotropic turbulence echoes were dominant. Results in this study suggest that intense radar echo layers are mainly produced by large gradients of refractive index in this height range. The remarkable relationship between radar echo power and |dBS/dz| indicates development into the new sensing technique.

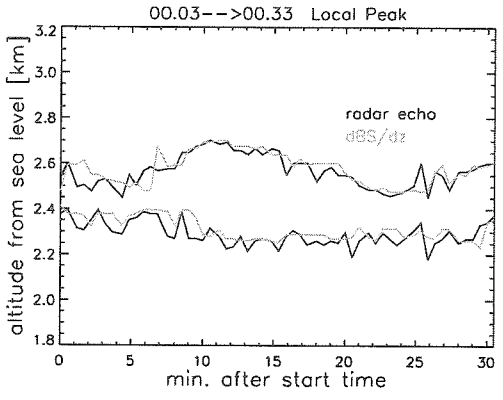

Figure 1. The relations between the positions of the maxima of radar echo power (black lines) and the peaks of |dBS/dz| (orange lines) between 0:03 to 0:33 on November 15, 2005.

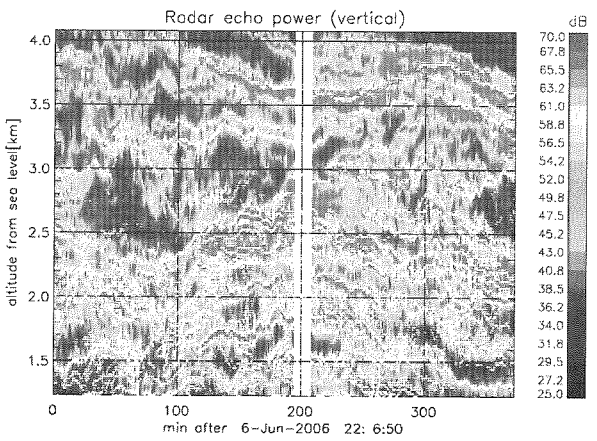

Figure 2. Time-height variations of the radar echo power between 22:06 on June 6 to 4:14 on June 7, 2006. The time resolution is 42 seconds. White dots indicate the positions of the peaks of |dBS/dz|.

Ozone variations in the atmospheric boundary layer over the eastern tropical Pacific

Haruo Kuribayashi

Laboratory of Atmospheric Environmental Information Analysis,
RISH, Kyoto University

It is known that the eastern tropical Pacific is a characteristic region where the sea surface temperature (SST) is low and its seasonal variation is large. Here a thin layer of the temperature increase with altitude in the lower troposphere is often observed in the latter half of the year. This is called an inversion layer that is very stable and supposed to prevent vertical mass transport. However, only typical meteorological parameters such as temperature and relative humidity have been studied so far (*Bretherton*[2004]). In this study, we investigate seasonal variations of the inversion layer and its relation to vertical profiles of water vapor and ozone using high-resolution ozonesonde data which are semi-regularly obtained at San Cristobal Island, Ecuador (0.92S, 89.6W) in the eastern tropical Pacific.

In March the temperature decreases with altitude, while in September the inversion layer is often observed at about 1000m. Then we defined the inversion layer as a layer in which the potential temperature increases over 2.0K in a 100m height range, and calculated a frequency of inversion layer formation in each month. Figure 1 shows the result together with the seasonal variation of SST. The high formation frequency of the inversion layer was closely related to the low SST. It is also found that relative humidity just below the inversion layer was as much as 90% in the latter half of the year, suggesting the presence of low level clouds. At the same time horizontal wind speed has a maximum at 400- 500m and a minimum just above the inversion layer.

Figure 2 shows a time-height section of monthly mean ozone mixing ratio. From February to April, ozone mixing ratio was relatively low below 3000m and there is a minor maximum around 1000- 2000m. By contrast, from July to November ozone mixing ratio was almost constant below the inversion layer. This might be due to vertical mixing caused by the strong wind shear around this time. Moreover, there is a local minimum of ozone just above the inversion layer. Considering that low level clouds exist persistently just below the inversion layer, photodissociation may become intense just above the inversion layer because of the solar reflection by clouds (*Madronich* [1987]). Taken with a wind speed minimum there, air parcel can stay this region for a long time, and then ozone would be destructed easily.

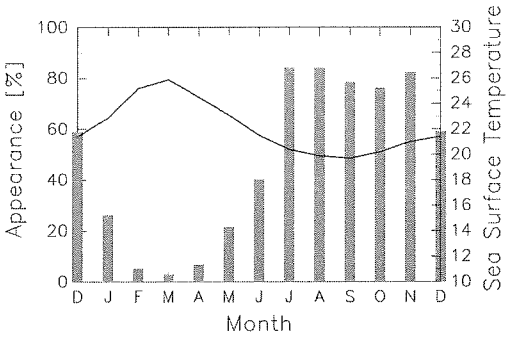

Figure 1: Frequency of inversion formation

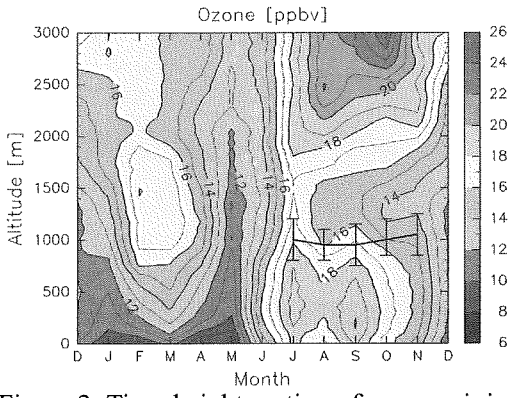

Figure 2: Time-height section of ozone mixing ratio

REFERENCES
[1] Bretherton, S., The EPIC 2001 Stratocumulus Study, *BAMS*, July 2004.
[2] Madronich, S., Photodissociation in the Atmosphere: 1. Actinic Flux and the Effects of Ground Reflections and Clouds, *J.Geophys. Res.*, 92, 9740- 9752, 1987.

Study of low-latitude *E*-region irregularities related to the background ionosphere and neutral wind field with the Equatorial Atmosphere Radar

Takamichi Kawamura
Laboratory of Radar Atmosphere Science, RISH, Kyoto University

In the equatorial ionospheric *F*-region, equatorial spread *F* (ESF) frequently with field-aligned irregularities (FAI) occurs in the nighttime. Since the bottomside of the equatorial *F*-region couples to the low-latitude *E*-region through the geomagnetic field, the low-latitude *E*-region has a significant effect on the equatorial and low-latitude ionosphere. In this study, we studied the relationship between *E*-region FAI (*E*-FAI) and neutral wind based on the data from Equatorial Atmosphere Radar (EAR), meteor radar and ionosondes. Observations were conducted in March - August 2005. National Institute of Information and Communications Technology operated three ionosondes located along the geomagnetic meridian including the EAR site.

Comparing data between the EAR and meteor radar, zonal velocities of FAI were found to agree quite well with the neutral winds below 94km. We also found that *E*-FAI echoes were frequently observed in association with the occurrence of sporadic *E* (*Es*) layers. Altitudes of their co-occurrence were different in time.

FAI echoes were observed in the low latitude valley region (120km～140km) between the upper *E*-region and the lower F_1-region. We compared altitudes of the echoes mapped to the dip equator and the height of the bottomside of the ESF. These two altitudes agreed quite well each other (See Figure1). We estimated downward electric fields from the zonal velocities of *E*, *F*-FAI, and found similar values 1～3 mVm^{-1} in all regions. As a result of this investigation, we could quantify the several aspects of the *E* - *F* coupling processes in the geomagnetically low latitude ionosphere.

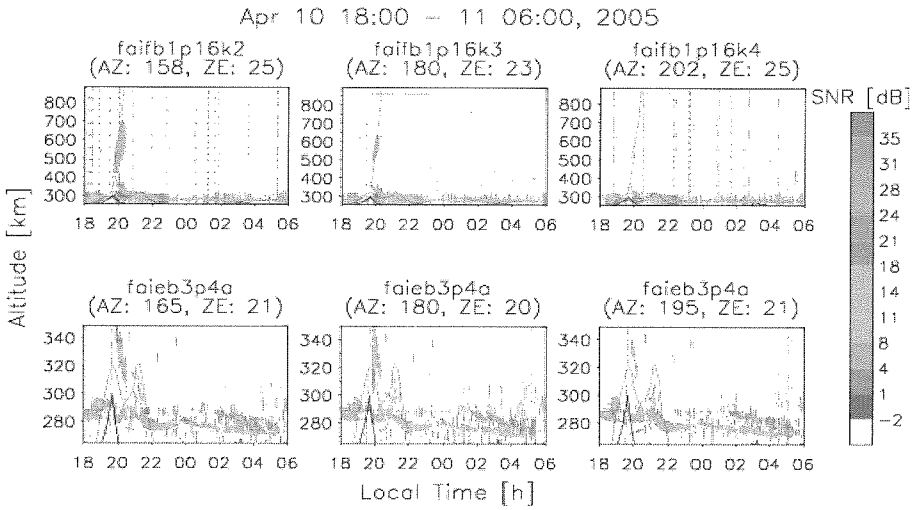

Figure 1: Time-height (after mapping to dip equator) cross-section of FAI echoes observed with the EAR during 18-06LT on April 10, 2005 and time variation of the bottom of *F*-layer.

REFERENCES

[1] Yokoyama, T., A. K. Patra, S. Fukao and M. Yamamoto: Ionospheric irreguralities in the low-latitude valley region observed with the Equatorial Atmosphere Radar, J. Geophys. Res., Vol.110, p.A10304 (2005)

[2] Patra, A. K., T. Yokoyama, M. Yamamoto, T. Nakamura, T. Tsuda and S. Fukao: Lower E region field-aligned irregularities studied using the Equatorial Atmosphere Radar and meteor radar in Indonesia, J. Geophys Res, Vol.112, p.A01301(2007)

Cirrus cloud observation in the tropical troposphere by the Equatiorial Atmosphere Radar and the 95-GHz cloud profiling radar

Nagata Hajime
Laboratory of Radar Atmosphere Science, RISH, Kyoto University

Cirrus clouds existing in the upper part of the troposphere consist almost entirely of ice particles, and play a significant role in regulating the radiation balance of the earth-atmosphere system. In this study, features of vertical air motion (V_{air}) in tropical cirrus clouds and its relationship to particle falling velocity ($V_{particle}$) are investigated. V_{air} and reflectivity-weighted $V_{particle}$ (V_Z) relative to the ground were respectively observed by 47-MHz and 95-GHz Doppler radars. They were operated at Equatorial Atmosphere Observatory, Kototabang, West Sumatra, Indonesia (0.2°S, 100.32°E, and 865 m MSL).

A case on 14 November 2005 is intensively studied. On that day, cirrus clouds existing in the outflow region of convective system were observed from 2030 LT to 3130 LT. Figure 1a shows a scatter plot between V_{air} observed by the 47-MHz Equatorial Atmosphere Radar [*Fukao et al.*, 2003] and V_Z observed by the 95-GHz cloud profiling radar developed by National Institute of Information and Communications Technology (NICT) [*Horie et al.*, 2000]. It is clear that V_Z, a velocity relative to the ground, contains fluctuations due to upwelling and downwelling of V_{air}. Figure 1b shows a scatter plot between V_Z and radar reflectivity factor observed by 95-Ghz radar (Z_e). A negative correlation between V_Z and Z_e is observed. Though V_Z tends to show consistent changes with Z_e, it contains large fluctuations. Figure 1c shows a scatter plot between (V_Z - V_{air}) and Z_e. By eliminating fluctuations by V_{air}, a negative correlation between (V_Z - V_{air}) and Z_e becomes clearer, which indicates that the fluctuations in Figure 1b occurred due to upwelling and downwelling of V_{air}. These results indicate that V_{air} observation by VHF Doppler radar is indispensable for observing particle falling velocity ice particle in cirrus clouds.

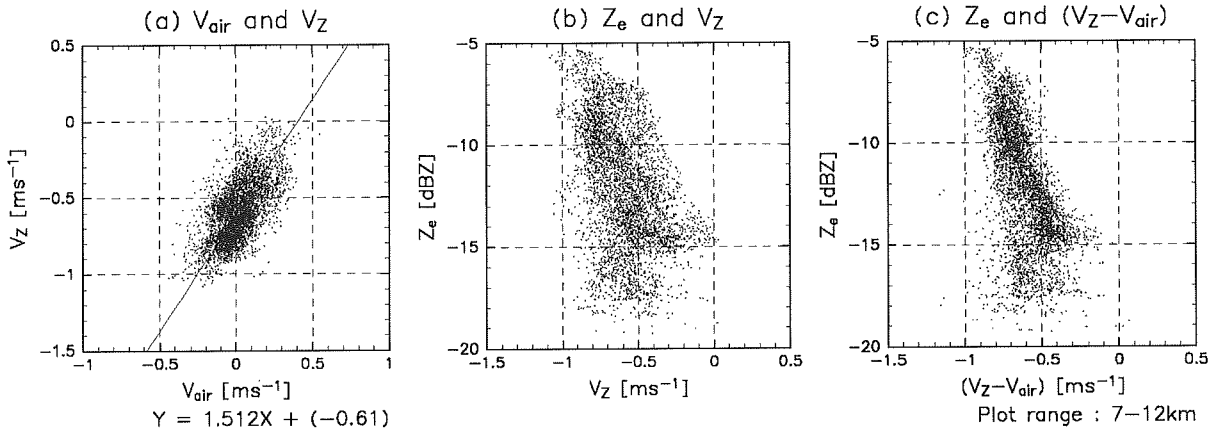

Figure1: Scatter plots between (a) V_{air} and V_Z, (b) V_Z, and Z_e, (c) (V_Z - V_{air}) and Z_e, in an altitude range of 7–12 km.

REFERENCES

[1] Fukao, S., H. Hashiguchi, M. Yamamoto, T. Tsuda, T. Nakamura, M. K. Yamamoto, T. Sato, M. Hagio and Y. Yabugaki: The Equatorial Atmosphere Radar (EAR): System description and first results, *Radio Sci.*, 38(3), 1053, doi:10.1029/2002RS002726, 2003.

[2] Horie, H., T. Iguchi, H. Hanado, H. Kuroiwa, H. Okamoto and H. Kumagai: Development of a 95-GHz airborne cloud profiling radar (SPIDER) -- Technical aspects --, *IEICE Trans. Communications*, Vol. 83, No.9, pp.2010--2020, 2000.

3D imaging observations of atmospheric turbulence layers with the MU radar imaging observation system

Tomohiro Yamaguchi
Laboratory of Radar Atmosphere Science, RISH, Kyoto University

Atmospheric turbulences have been studied by the MU radar standard observation mode, which shows time-height variations of turbulences with resolutions of about 1 minute and 150 m altitude. In 2004, the MU Radar Imaging Observations System has been installed to the MU radar, which allows to us make simultaneous observations of SDI (Spatial Domain Interferometry) and FII (Frequency Interferometry Imaging) techniques with much better range-angular resolutions [1].

We conducted the SDI/FII simultaneous observations on 13th November 2005. The data were first analyzed with each of SDI and FII with the Capon method. FII analyses showed that there are many thin turbulence layers within 1 range (150 m), which can not be detected by the normal standard observation mode. SDI analyses showed that several thin turbulences have some tilts, and these tilts varied in time in a few minutes like a wave, which indicated that these turbulences was not a flat plane but had wave-like structures. We then expanded the data analysis to use the three-dimensional imaging technique. Example of the analysis is shown in Figure 1. We found a scattering layer that has thickness of less than the range resolution (Figure 1, left panel). Scattering positions revealed from the three-dimensional analysis showed that, in time, center positions of the echoes moved from west-northwest to east southeast within the range of 150 m thick. That indicates that there are some angular distributions of turbulences within 1 range, in addition, we found some turbulences motion along background wind. The features were not well detected by conventional SDI and FII techniques.

These results show that simultaneous observation of SDI and FII techniques with the MU radar new system can detect detail information of three-dimensional strictures of atmospheric turbulences including their time variations with much better height-angular resolutions than normal standard observation mode.

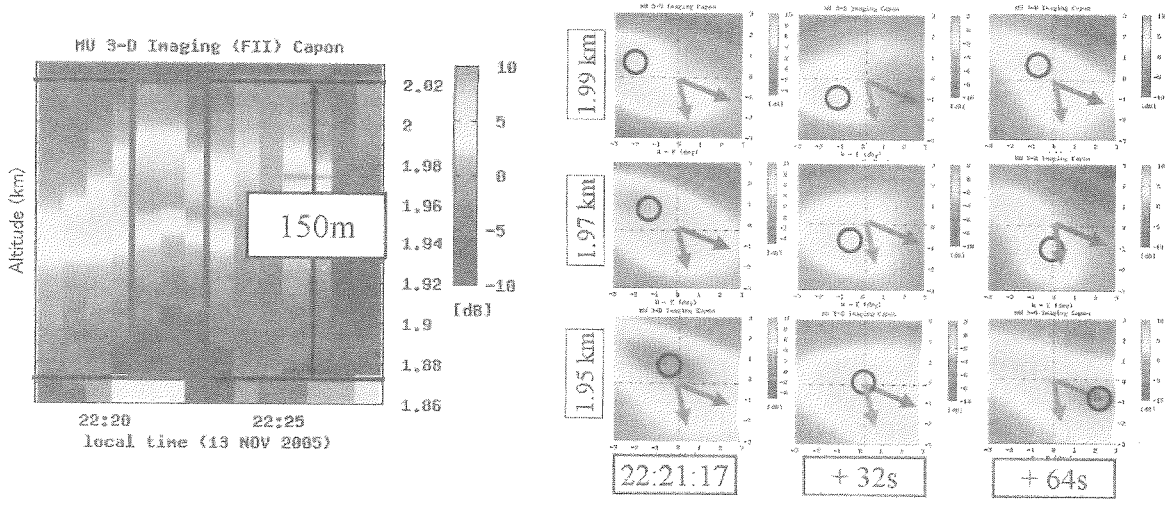

Figure 1: Result form three-dimensional radar imaging. Time-height distribution of echo power within one range gate of 150 m thick (left panel). Angler distribution of echo power at 22:21:17 LT and after at 1.95 km, 1.97 km, and 1.99 km (right panel). In each panel circles denote center position of the echoes, and two angles show directions of wind velocity (east-southeastward) and wind shear (south-southeastward), respectively.

REFERENCES

[1] Luce, H., G. Hassenpfulug, M. Yamamoto and Fukao, S., High-resolution vertical imaging of the troposphere and lower stratosphere using the new MU radar system, *Ann. Geophys.*, 24, 791—805, 2006.

The development of cellulose nanofiber / alkoxysilane hybrid material

Fumio Asagaki
Laboratory of Active Bio-based Materials, RISH, Kyoto University

INTRODUCTION

The sol-gel process is a technique to hydrolyze and polycondense alkoxysilanes like tetraethoxysilane (TEOS) into polysiloxane (Si). By using this technique, it is possible to make organic-inorganic hybrid compounds at low temperature. In this research, transparent alkoxysilane, which is resistant to high temperatures but is extremely fragile (brittle), was combined to cellulose nanofibers (CNF), and the effects of this reinforcement in the hybrid material were evaluated at various fiber contents.

MATERIALS and METHODS

The starting material was microfibrillated cellulose (MFC) produced by Daicel Chemical Industries, Ltd., a mechanically fibrillated kraft pulp. CNF was obtained by further fibrillating a 1wt% MFC water suspension through a grinder (MKCA6-3, MASUKO SANGYOU Co., Ltd.).

A 0.2wt% CNF water suspension was filtered using a membrane filter and CNF sheets were obtained after drying. CNF sheets were immersed in a solution of silanol derived from TEOS or methyltrimethoxysilane (MTMS). Thereafter, the impregnated chemical compounds were hydrolyzed by drying for 15 minutes at room temperature and polycondensed by drying for additional 15 minutes at 120℃ or 140℃. In this way, about 85wt% fiber content hybrid materials (CNF/Si hybrid and CNF/SiMe hybrid) were obtained.

Alternatively, CNF was added to a solution of silanol derived from MTMS, and a given amount of the stirred solution was put into petri dishes. Subsequently, those were hydrolyzed by drying for 2 days at room temperature. After drying for 2 days at 50℃, those samples were drawn from the petri dishes and were polycondensed by heating for 1 day at 140℃. Thus, hybrid materials with fiber contents of 0wt%, 1wt%, 3wt%, 5wt%, and 10wt% were obtained.

RESULTS and DISCUSSION

By combining CNF sheets and transparent alkoxysilane, the regular transmittance of hybrid materials at 589nm was over 80% (Fig.1). The fracture strain of CNF/Si hybrid and CNF/SiMe hybrid increased over 2.5 times (Fig.2). These results suggest that hydroxyl groups of cellulose were bound covalently to Si or SiMe. The fracture strains of low fiber content hybrid materials increased from 0.7% to 1.3% at an addition of only 1wt% CNF, then tensile strength and fracture strain increased accordingly to the increase of CNF content (Fig.3). This is attributed to the fact that CNF formed a complex with SiMe at a nano scale level as CNF was evenly dispersed in SiMe.

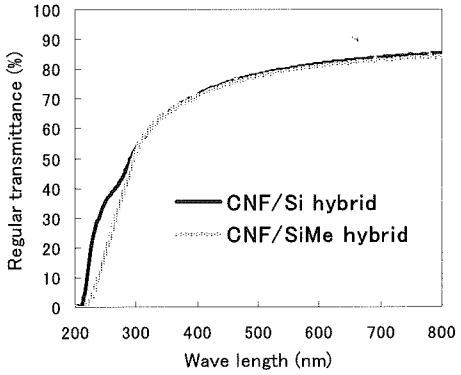

Fig.1 Regular light transmittance of high fiber content hybrid materials

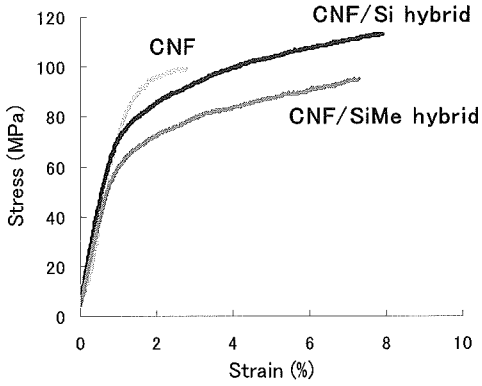

Fig.2 Stress-strain curves of high fiber content hybrid materials

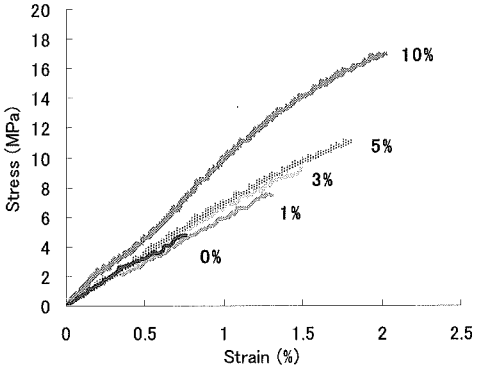

Fig.3 Stress-strain curves of low fiber content hybrid materials

Development of a board containing bark-tannin with cellulose nanofibers as a binder

Manabu Kamada
Laboratory of Active Bio-based Materials, RISH, Kyoto University

INTRODUCTION

Tannins, one of the polyphenols, have many attractive capabilities such as protein adsorption, antioxidant, metal chelating and antifungal properties. The purpose of this research is to develop a novel material utilizing these abilities of tannin. In this study we made a composite consisting of *Acacia mangium* bark powder with a large content of condensed tannin, artificial zeolite having a porous structure with the ability to control humidity, and cellulose nanofibers as a binder.

MATERIALS and METHODS

Manufacture of composites

Artificial zeolite (Kimura Chemical Plants Co., Ltd) was mixed in a water suspension of 1wt% cellulose nanofibers (DAICEL CHEMICAL INDUSTRIES, LTD.). The water was removed from the blend by filtration and centrifugation and the *Acacia mangium* bark powder was added and mixed on a Laboplasto-Mill equipped with a twin rotary roller mixer (Toyo Seiki Seisaku-sho, Ltd.). The mixing was carried out for 15min at a rotary speed of 70rpm at room temperature. A moderate amount of water was added to this mixture and a cold dewatering press molding with a die was performed. By drying it at 55℃ for one day and 110℃ for another day the composite was obtained. Based on preliminary experiments, the ratio of cellulose nanofiber was adjusted to 10wt% of the composite.

Performance evaluation of composites

(A) Bending strength property: Specimens were cut from the composite into predetermined sizes. Bending strength test was performed with an Instron 3365.

(B) Humidity conditioning property: Relative humidity change was measured in a steel box(23.5×23.5×35cm) enclosing the composites, which was put in a climatic chamber. The C value was calculated from the results. The C value was defined as the ratio of the amplitude of humidity changes in the steel box with the composites to that in the empty steel box.

(C) Antioxidant property: 10mg of the ethyl docosahexaenoate (DHA) and 10mg of the ethyl stearate (reference substance) were dispensed in vial containers. Those and the composites were put into a desiccator set in a chamber at 20℃. In addition, a desiccator without the composite was also prepared. The quantity of non-oxidized DHA in the vial containers collected periodically was measured by gas chromatography. The antioxidation property was evaluated by comparing the quantity of non-oxidized DHA with that of ethyl stearate.

RESULTS and DISCUSSION

The results of the composites consisting of 10wt% cellulose nanofibers, 30wt% bark powder and 60wt% artificial zeolite are as follows:

(A)The average values of Young's modulus, bending strength and density of the composites were 3.82GPa, 25.3MPa and 1.22g/cm^3, respectively. These bending strength values were little less than these of MDF in Japanese Industrial Standards (JIS-A5905).

(B) The C value of the composites exhibited excellent humidity conditioning property. This value was more than that of Japanese cedar and commercial porous ceramics.

(C) Fig.1 shows the ratio of non-oxidized DHA. Because the ratio of non-oxidized DHA in the desiccator containing the composites was larger than that of control (desiccator without composites), it was confirmed that the composites have antioxidant property.

Therefore, we would say that we could produce composites having enough strength without hindering the characteristics of artificial zeolite and condensed tannin when using cellulose nanofibers as a binder.

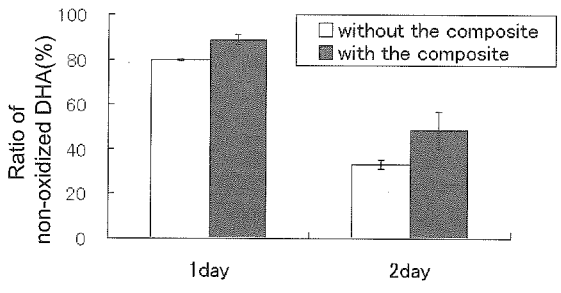

Fig.1 antioxidant property of the composite

Development of Environmental-Friendly Boards from Gramineous Plants

Keiji Kaiho

Laboratory of Sustainable Materials, RISH, Kyoto University

【Introduction】 In recent years, non-wood lignocellulosic plants have been of great interest from the viewpoint of effective utilization for natural resources. However, the only limited kinds of plants have been studied. In addition, fossil resources-based synthetic adhesives which have serious problem for human health and environment were usually used. The purpose of this study is to manufacture of boards from various Gramineous plants by using steam-injection press. First, various binderless boards (BB) utilizing self-bonding properties were investigated. To improve the board properties, the addition of chitosan was also investigated.

【Materials and Methods】 Bagasse-rind and -pith, straws (wheat, rice and reed) and bamboo were used as Gramineous materials. In each material, particle having the moisture content of about 10% were prepared. The steam-injection condition of BB was a steam pressure of 1MPa (180°C) for 6 min, and total pressing time was 7min. The dimension of each board was 230×230×7(mm) and the target density was varied from 0.6 to 1.0g/cm^3. In chitosan added board (CB), chitosan was dissolved in acetic acid solution (1wt%), and the solution was sprayed. The solid content of chitosan sprayed was 2 to 10%. As references, the board bonded with polymeric diphenylmethane diisocyanate resin (PMDI) was manufactured. In this case, solid content was 6%. The board properties were evaluated not only modulus of rupture (MOR) and internal bond strength (IB) by JIS A 5908, but also accelerated aging treatment.

【Result and Discussion】 Fig.1 shows the MOR and IB of various boards (density: 0.9 g/cm^3) from wheat, bamboo and bagasse-rind. In BB of wheat, bamboo and bagasse-rind, the strength of bagasse-rind was superior to those of other materials. When chitosan was added to the bagasse-rind board, the MOR and IB were 25 and 0.64 MPa, respectively. These values indicated about twice as strength as those of the bagasse-rind binderless board. Compared to the PMDI board, the strengths were slightly low. Fig.2 shows the thickness swelling of various bagasse-rind boards under accelerated aging treatments. The thickness swelling of BB increased with the treatment. The behavior of CB was similar to that of PMDI board. This indicated that chitosan-added board has good dimensional stability. This reason seemed to be that the chemical reaction between chitosan and sugar in bagasse-rind occurred.

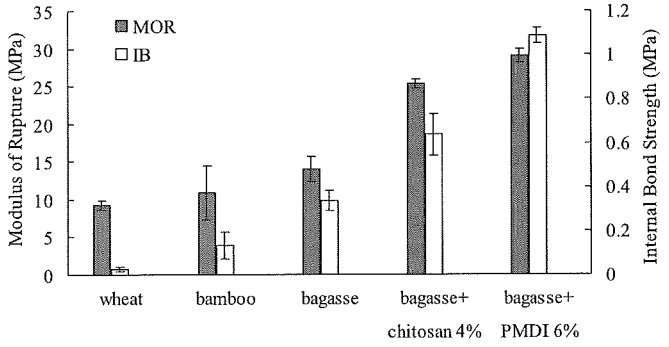

Fig. 1 MOR and IB of each board.

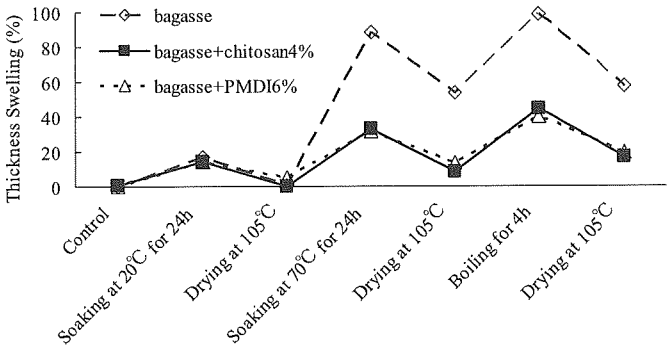

Fig. 2 Thickness swellings of each board under accelerated aging treatment.

Wooden Blocks' Shear Wall
- Utilization of hygro-mechanical properties of wood to improve the strength -

B. Ivón Hassel
Laboratory of Structural Function, RISH, Kyoto University

In forestry regions of Latin America, traditional houses are built of a reinforced concrete frame and masonry infill, non-autochthonous materials that require high transportation and energy production costs. Although masonry walls are deeply-rooted in this society as part of its traditional construction system, there can be a sustainable, cost effective alternative in the use of wooden blocks to build shear walls [1]. This construction method uses no steel elements as connectors, which is of interest at the time of disposal [2], and moreover, allows readjustments and recycling of materials after seismic impacts.

The objective of this research is to study the performance of a *Wooden Blocks' Shear Wall* that incorporates 63% compression ratio's sugi (*Cryptomeria japonica D. Don*) element without fixation treatment. These elements recover their radial dimension when absorbing humidity from the air, improving the stiffness of the wall by adding stress to the neighboring blocks when expanding [3][4][5]. Utilization of the *diamond key* allows the structure to be readjusted and reused after the occurrence of earthquakes.

The blocks are made of glued laminated timber (GLT) European red pine, with dimensions of 60cm length by 22cm height and 9cm width. Shaped with tongue and grooves on their sides with a 45 degree angle cut at each corner, enabling to fit the *diamond key* perpendicularly to the surface of the wall.

The study of the shear wall was done by performing both full scale cyclic shear tests and finite elements method analysis. The mechanical properties of the materials were obtained using Digital Image Correlation (DIC) [6] in combination with the single cube method, rosette strain gauges and the model of Guitard for resinous trees [7]. Two sample configurations (1P (91cm length x 273cm height) and 2P (182 x 273cm)) were tested with a full scale cyclic shear test, with and without keys. The strength of 2P was 1.71 times higher than that of 1P. The stiffness of 2P was 6 times higher than 1P. Comparing samples with and without keys, 1P+keys presented 1.5 times higher stiffness than 1P-keys, and 2P+keys presented 2.6 times higher stiffness than 2P-keys. The monotonic shear test showed a displacement difference of +1.13mm with respect to the FEM analysis, and +1.94mm with respect to the proposed mechanical model when applying the yielding load. The displacement difference between the FEM for the cyclic shear test and the experimental one was +0.24mm in the elastic zone. This study showed the interest of this innovative and sustainable shear wall. Its efficiency in terms of stiffness have has been successfully tested using experiments and numerical methods.

REFERENCES

[1] Eto Y., Inoue M., Kinoshita I., Kikuchi S., and Shimizu T. (1996). Fundamental study on development of wood brick structures IV: *Horizontal loading test of wall opening*. Proceedings of the Annual meeting of Architectural Institute of Japan, Kinki, Japan:83-84

[2] TANAKA K., Miyazaki H., et al. (2004). Development of new recycle system of used lumber from dismantled wooden house. Proceedings 8th World Conference on Timber Engineering WCTE, Lahti, Finland.

[3] Kitagawa M. and Komatsu K. (2005). Utilization of Compressed-Sugi Dowels as Joint Material in Timber Structures. Sustainable Humanosphere Bulletin of Research Institute for Sustainable Humanosphere. Kyoto, Kyoto University: No 1: 15.

[4] Dwianto W., Morooka T., et al. (1999). "Stress Relaxation of Sugi (*Cryptomeria japonica D.Don*) Wood in Radial Compression under High Temperature Steam. "Holzforschung Vol. 53 (No. 5): 541-546.

[5] Jung K., Hwang K. and Komatsu K.. (2006). "Effect of changes in the moisture content due to surrounding relative humidity on the contact stress in traditional mortise and tenon joints I. *Effects of komisen insertion and joint drying on the contact stress between end grain of column and sill.*" Mokuzai Gakkaishi Vol. 52 (No.1): 44-49.

[6] Berard Pierre (2006). Digital Image Correlation applied to strain measurement.

[7] Guitard D. (1987). Mécanique du matériau bois et composites. Toulouse, Cépaduès-Editions.

Study on development of analog integrated circuits for space electromagnetic environment monitor

Takashi Matsumoto
Laboratory of Space Radio Science, RISH, Kyoto University

Environments in space are strongly controlled by electromagnetic phenomena. Since space plasmas are collision less, we can recognize a status of electromagnetic environments by monitoring plasma/radio waves. Plasma wave receivers can be used to monitor space electromagnetic environments. For example, they can monitor the interaction between the huge structures such as space power station/satellite and space plasmas that might cause artificial disturbances around them. However, since the weight and size of typical plasma wave receivers are heavy and large, they are not suitable for the electromagnetic environment monitors, which are distributed around space structures in order to make it possible to monitor in multiple points. Therefore, we need to re-design plasma wave receivers and to realize a very light weight and compact monitor instrument.

To develop the compact monitoring system, we design a part of analog electric circuits for the monitoring system, based on the ASIC (Application Specific Integrated Circuit) technology. Using ASIC technology, we can realize small and light weight analog circuits, and reduce its electricity consumption.

We have designed several important components of the whole analog circuits for the space electromagnetic monitor instruments i.e., differential amplifiers and AD converters. The differential amplifiers are required low noise characteristics on their observation band frequency. In computer simulation, we have realized the noise level of them as 100nV/(Hz)1/2 at 100 Hz and as 30nV/(Hz)1/2 in the frequency range above 1kHz. This noise level is lower than the specification of space electromagnetic environment monitor. In its function and performance tests, its noise level reaches 300nV/(Hz)1/2 at 100 Hz and 100nV/(Hz)1/2 in the frequency range above 1kHz. In its performance, we need further improvement of the noise level by re-designing.

In the present paper, we introduced the results of our design and performance tests of the ASIC dedicated for the space electromagnetic environment monitor. Further, we propose the analog block diagram of the monitor system. In this diagram, we show the possibility of realization for a new type of instrument in space.

A study on the effect of solar and microwave radiation force on solar power satellite orbit

Teppei Oyama
Laboratory of computer simulation for humanospheric sciences, RISH, Kyoto University

Solar Power Satellite/Station (SPS) is a powerful solution for environmental problems such as exhaustion of fossil fuels. Because SPS has large solar panels, solar radiation pressure is one of key perturbations to SPS orbit. In addition to this, microwave power transmission exerts a reaction force on SPS. Our objective is qualitative and quantitative analysis of the effect of solar and microwave radiation force on SPS orbit.

At first, we give the physical interpretation of these two perturbations, a rough estimation of effects on SPS orbit, and the comparison with other perturbations such as J_2 perturbation. The averaged equation of eccentricity tells that solar radiation force gives rise to the secular change of the eccentricity. The 1-dimensional potential analysis tells that microwave radiation force brings a small broadening of the semi-major axis.

Then, we investigate the possibility of strict geosynchronization of SPS by steering the pitch angle of the solar panel. Two control methods are proposed. One of them is conducted by optimal control theory.
These methods demand extremely high reflectivity of the solar panel, about 94¥%. Therefore, these methods are considered not practical.

Finally, we derive averaged equations of motion about the eccentricity and the argument of the perigee to find appropriate orbits for the SPS, by considering that SPS can send a microwave to a rectenna cite even if the eccentricity shifts from zero to some extent. The derived equations have Hamiltonian, which enables us to compute the long-term behavior of SPS on the eccentricity-argument of perigee phase space. We can classify the SPS perturbed orbits into libration, rotation and unstable orbits, depending on the behavior of SPS on the phase space. There exists an equilibrium point in the libration region of phase space where the secular change of the eccentricity becomes zero and the apse-line is strictly synchronized to the earth-sun line.

We derive the same averaged equations by canonical perturbation theory, which enables us to calculate the simultaneous effects of solar and microwave radiation force in an elegant manner. We found that microwave radiation force shifts the equilibrium point.

In addition to the two-dimensional analysis, we investigate the out-of-plane effects of the solar radiation with respect to equatorial plane numerically. The orbit inclination and the eccentricity oscillate due to the solar radiation force normal to the orbit plane. A secular change in the right ascension of the ascending node also occurs, resulting in the precession of orbit plane. It was shown that three-dimensional equilibrium point exists in the ecliptic plane as same as that in the equatorial plane for the two-dimensional case.

From a long-term viewpoint, we propose a new and effective orbit for SPS at the nonzero equilibrium eccentricity, which can minimizes the deviation of microwave incidence angle at the rectenna cite. For the SPS operation, the out-of-plane radiation pressure effect is cancelled by tilting the attitude of the SPS.

Simulation study on dynamics of high-energy particles in the Earth's magnetosphere

Fengliang Tang
Laboratory of Space Radio Science, RISH, Kyoto University

With the development of the world, more and more countries have putting their eyes on the Space Exploration. Now, there are plenty of satellites and spacecrafts in the space near the Earth. But we have to face a serious problem made by high energy particles of Radiation Belt which are full of trapped energetic charged particles. Because they can reduce the life time of satellites, causing the wrong operations, understanding the high energy particle dynamics is quite important.

Especially, high energy particles can be injected from the magnetotail into the inner magnetosphere associated with the substorms. However, there are still many uncertainties about the mechanisms of producing ring current and accelerating the particles to the very high energy level of Mev.

We used a 3-dimensional model to perform the test particle simulations of the high energy particles' dynamics in the magnetosphere and tried to understand more clearly. Figure1 shows the model of the present computer experiment.

We performed test particle simulation code in the simple dipole magnetic field model and realistic magnetic field model by using the IGRF code and Tsyganenko 1996 code. In addition to the magnetic field, we also incorporated the Large-scaled convection electric field and found out the particles' dynamics was totally different from the cases which had magnetic field effect only. Figure2 shows the trajectory of electron which is injected from the magnetotail region into the inner magnetosphere under the actions of electric and magnetic field.

Using these models, we also performed the test particle simulation code to investigate the particle injection phenomenon under the conditions of different convection electric field and different geomagnetic activity levels. The particle injection happens more effectively during the more intense geomagnetic activities levels ($Kp > 4$). If the $Kp >$ (6, 6+, 7-), then the particle injection can be quite effective, we can see clearly the particles transfer from the tail region into the inner magnetosphere. The effective region of the Large-scaled convection electric field in x direction is from the tail region until the dipole field area about 3~5 radii on the night side of the Earth. If the electric field region extends longer in y and z directions, the particles can be accelerated much more.

Figure3 shows mirror points trajectories of 8 electrons' which had the same initial kinetic energy and different pitch angles under the intense condition.

REFERENCES

[1] Omura, Y., and D. Summers (2006), Dynamics of high energy electrons interacting with whistler-mode chorus emissions in the magnetosphere, *J. Geophys. Res., 111,* A09222, doi: 10.1029/2006 JA011600.

[2] Reeves, G.D. (1998), Relativistic Electrons and Magnetic Storms: 1992-1995, *Geophys. Res. Lett., 25,* 1817.

[3] Tsyganenko, N.A, (1995), Modeling the Earth's magnetospheric magnetic field confined within a realistic magnetopause, *J. Geophys. Res.,100,* (A4), 5599-5612.

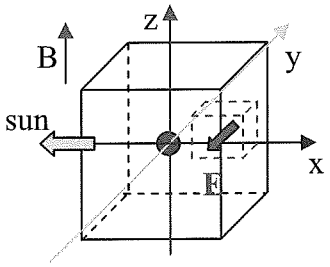

Figure1

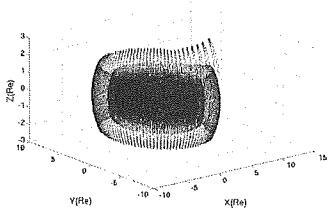

Figure2

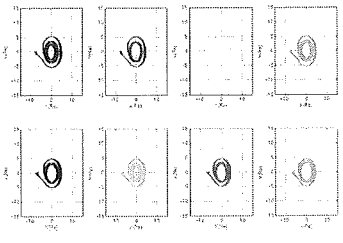

Figure3

Test Particle Simulations on Acceleration of Relativistic Electrons by Coherent Whistler-Mode Waves in the Earth's Radiation Belt

Naoki Furuya
Hashimoto Laboratory, RISH, Kyoto University

It is well known that in a recovery phase of geomagnetic storm, the flux of relativistic electrons (~MeV) in the Earth's outer radiation belt can increase to beyond pre-storm levels. They cause serious damage to electrical devices in satellites. Nowadays, space weather forecasting, in which predicting and preventing the damage from high energy particles, is increasing in importance as space activity becomes more developed.

By means of test particle simulations, we have found a very efficient acceleration process of relativistic electrons in the outer radiation belt. This is due to particular nonlinear resonant trapping by coherent whistler-mode waves in a dipole magnetic field. During the acceleration process, wave trapped electrons change the direction of motion to the same direction of wave propagation, and we call the process relativistic turning acceleration (RTA).

On the assumption that wave frequency is constant, with a sufficiently long whistler-mode chorus wave packet of the order of a few hundred milliseconds, electrons of a few hundred keV are accelerated to the range of a few MeV through a single resonant trapping process. The necessary wave amplitude is a few hundred pT. The minimum energy of electrons accelerated by RTA, and the maximum energy attained by it are derived analytically and verified by the test particle simulations.

In reality, however, chorus emission is a whistler-mode wave packet which has a finite length and has a frequency which increases in time. We found that electrons are also accelerated in a few hundred keV by RTA when two chorus emissions with time dependent frequency are generated at the equator and propagate to the north and south. We also studied the evolution of energy distribution functions by Green's function approach. We found that a delta function in energy space evolves into a distribution with high-energy tail, which can be the mechanism for the generation of relativistic electron fluxes in the outer radiation belt.

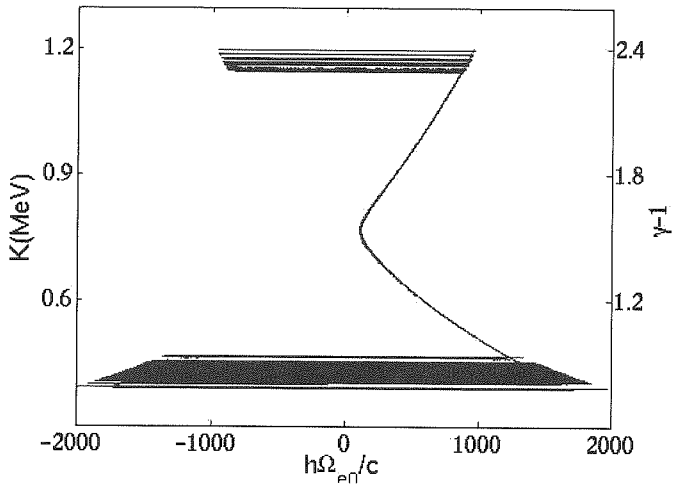

Fig1. Trajectory showing energy increase. Horizontal axis means the distance h Ω_{e0}/c and vertical axis is electron kinetic energy (MeV). 21 out of 90 electrons are trapped and accelerated.

Study on Space Plasma Perturbations Caused by a Spatial Gradient of Intense EM beam Intensity

Narihiro Nakamoto
Laboratory of Applied Radio Engineering for Humanosphere, RISH, Kyoto University

Before the realization of SPS (Space Solar Power System) and its prior experiments, we need to understand the mechanism and the extent of interactions between the microwave beam and the ionospheric plasma.
In this study, we particularly focus on the plasma perturbations by Ponderomotive force which is one of the nonlinear interactions caused by the spatial gradient of the electromagnetic (EM) beam intensity. To investigate the dynamics of plasma cavitation by Ponderomotive force and their characteristics, we performed computer experiments and theoretical considerations.

From simulation results, we found out the basic dynamics of a plasma cavitaion by Ponderomotive force. When the EM beam with a radial spatial gradient of its intensity propagates in the plasma, electrons and ions are moved out of the beam by the effects of Ponderomotive force. With this plasma perturbation, electro-static ion waves which propagate radially to the EM beam are enhanced.
In the existence of the external magnetic field, this plasma cavitation has an anisotropy by the effects of Ponderomotive force and the external magnetic field.

To understand the more detailed characteristics of this plasma cavitation, we performed theoretical considerations by the plasma fluid theory. From these considerations, we derived theoretical density variation by Ponderomotive force and revealed the detailed parameter dependencies and characteristics of the temporal and spatial variation of a plasma cavitation, which basically agree with the simulation results. In addition, we revealed the damping of the ion-acoustic waves by the plasma kinetic effects makes the differences between theoretical values and simulation results.

Finally we estimated the density variation by this plasma cavitation with the SPS parameters which are currently proposed. From this estimation, the density variation by the cavitation becomes about 10^{-3} % of the initial plasma density. Therefore the plasma cavitation isn't likely to be a problem in SPS.

Study on a software retrodirective system for microwave power transmission

Yoshiyuki Ohata
Laboratory of Space Radio Science, RISH, Kyoto University

A SPS (Solar Power Satellite) is one of the most important and clean power sources to solve global warming and energy problems. In a SPS model, the SPS transmits microwave by a phased array antenna of 1 to 2 km in diameter from the geostationary earth orbit to the ground rectenna of 2 to 5 km in diameter.It is necessary to measure the direction of the receiving point accurately and to achieve beam-forming to the direction in high accuracy.The required accuracy of the beam control is less than 0.001 degree.

A retrodirective antenna array has a property that it sends a power beam back to the direction of its originating source. We adopt a software retrodirective system that computationally calculates the direction-of-arrival of a pilot signal and the phase distribution of the transmitting phased array. A trial to make this system had been performed before [1]. The purpose of the present study is to make the software retrodirective system more highly accurate and evaluate the system experimentally.

First, we built up the basic software retrodirective system and measured its beam pattern and detected the main beam direction. As a result, the difference between the main beam direction obtained from the experiments and the direction of pilot signal transmitting antenna was 2.75 degrees. The difference was caused by estimation error of the direction of arrival.

Next, we added a beam direction correction system which measures the power distribution on the reception site to the software retrodirective system. As a result, the difference between the main beam direction obtained from the experiments and theory was improved to be 0.25 degrees by using this system.

Next, we propose that the method of calibrating the phase of each element. This is effective to solve the problem that the power transmission efficiency is decreased by the secular distortion etc. of the power transmission system.

Finally, we assembled these systems above and demonstrated that the accuracy of the beam direction was highly improved and the high beam collection efficiency was achieved.

REFERENCES

[1] Kozo Hashimoto, Hiroshi Matsumoto, and Miki Mayu, Software Retrodirective system for SPS (in Japanese), TECHNICAL REPORT OF IECE, SPS2003-15, 2004.

Study on Integration of Analog Circuits for Plasma Wave Instruments

Hiroshi Imakubo
Laboratory of Space Radio Science, RISH, Kyoto University

Recently, on space environment measurement missions, it has been the main stream to conduct multiple point observations at the same time by formation flight of satellites. In addition, the investigations of deep space environment have been needed. These streams in space missions lead to the increase of demands for Plasma Wave Instruments (PWI). Especially, the restriction for the size and the weight comes to be severer and severer, the downsizing and light-weighting of the analog parts that occupies quite large area on PWI are necessary. Therefore, we develop the one-chip analog parts of PWI using the Analog Specific Integrated Circuit (ASIC) technology.

Of the analog parts, we design and develop the integration of the Gm-C filter for the frequency band restriction low pass filter, the folded cascade op-amps for a main amplifier and the switched capacitor filter for an anti-aliasing filter. Using the 0.36 (m) process of Taiwan Semiconductor Company (TSMC). Finally, we also evaluate the performance of the developed chips. As a result, Gm-C filters on the developed chips showed lower cut-off frequency and higher noise level characteristics than we expected. These filters also displayed low Common Mode Rejection Ratio (CMRR) as 40dB. Those points, however, can be solved by the design based on thoughtful consideration of elements' fluctuation. The folded cascade op-amps showed the good gain characteristic. Although the noise level is higher than the specification, it can be improved by the modification, especially for MOSFET gate size. We apply the op-amps for a switched capacitor. We design and check the performance by the transient analysis. We confirm the output signals reflected the input as disintegration signals and the op-amps and the switch circuits act normally.

Finally, we estimate the size and the weight of the integration chip as PWI analog parts. Compared with A4 size and 400g of a conventional PWI printed circuit board, the size and the weight were only several square meters and several g. About those prospects, it is inevitably possible to answer the demands of missions in the future.

REFERENCES

[1] K. Hirotsugu, Study on the Plasma Waves in the Geomagnetic Tail Region Via Spacecraft Observations, Faculty of Engineering, Kyoto University Ph.D. thesis, 1998.

Development of a small-size and high-power rectenna for a wireless power distribution system in a building

Miyagawa Tetsuya
Laboratory of Space Radio Science, RISH, Kyoto University

As a new application of wireless power transmission technology, we propose a wireless power distribution system in a building. This system distributes electric power wirelessly through the closed space in the building. The closed space, which is composed of a deck plate and a flat plate, plays a role as a microwave transmission line[1)].

We described the necessity of a rectifier circuit that converts microwave power into 50W DC power. The size of the rectifier circuit is necessary to be smaller than 10^3. Next, we newly developed a small-sized and high-power rectifier circuit with a 16-way power divider. The experimental results showed that it had RF-DC conversion efficiency of 50% at an input microwave power of 18W. The size of the developed rectifier circuit was 112mm in length and 102mm in width. We also researched the relation between endurance and SPICE parameters of a diode, and derived requirement of the diode parameters for a high-power rectifier circuit. We described limitation of a small-sized high-power rectifier circuit, when a conventional rectifier circuit is expanded on a plane surface.

Next, we newly developed and examined a 3D rectifier circuit.
With respect to the 3D circuit composition, the loss of a vertically-connected-type circuit was small. When the interval between the adjacent substrates was 5mm or more, the characteristic impedance was not affected. Then, we developed a small-sized and high-power rectifier circuit with a 64-way power divider, composed of a 8-way wilkinson power divider and 8rectifier circuits with a 8-way power divider. The rectifier circuit with a 64-way power divider provided 55% RF-DC conversion efficiency at an input microwave power of 100W. The size of the rectifier circuit was 125mm in length, 110mm in width and 95mm in height.

Finally, we demonstrated practical examinations of a receiving adapter.
This adapter converted 100W input into about 40W DC output, even if the load of the adapter output was replaced. It could be operated for about three hours at 100W microwave input.

REFERENCES

[1] Adachi Tatsuhiko, Development of a wireless power distribution system in a building (in Japanese), Master thesis of Kyoto University, 2006

Publications in 2006
(Articles in English published in refereed journals)

Sasaki S, Baba K, Nishida T, Tsutsumi Y, Kondo R, The cationic cell-wall-peroxidase having oxidation ability for polymeric substrate participates in the late stage of lignification of *Populus alba* L., Plant Mol. Biol, 62, 797-802 (2006)

Nge Thi Thi, Sugiyama J, Surface functional groups dependent apatite formation on bacterial cellulose microfibrils network in a simulated body fluid, J Biomed Mater Res, 81A, 124-134 (2006)

Hirata, T, Fujimura F, Horikawa Y, Sugiyama J, Morita T, and Kimura S, Molecular assembly formation of cyclic hexa-β-peptide composed of acetylated clycosamino acids, Biopolymers (Peptide Sci), 88, 150-156 (2006)

Mueller M, Burghammer M, Sugiyama J, Direct investigation of the structural properties of tension wood cellulose microfibrils using microbeam x-ray fibre diffraction, Holzforschung, 60, 474-479 (2006)

Fukuda M, Sugiyama J, Morita T and Kimura S, Fully Hydrophobic Artificial Protein but Water Dispersible due to Large Dipole, Polymer J, 38, 381-386 (2006)

Fujimura F, Hirata T, Horikawa Y, Sugiyama J, Morita T and Kimura S, Columnar assembly of cyclic β-amino acid functionalized pyranose rings, Biomacromolecules, 7, 2394-2400 (2006)

Ding S-Y, Xu Q, Mursgeda K. Ali, Baker JO, Bayer EA, , Barak Y, Lamed R, Sugiyama J, Rumbles G, Himmel ME, Versatile derivatives of carbohydrate-binding modules for imaging of complex carbohydrates approaching the molecular level of resolution, BioTehcniques, 41, 435-442 (2006)

Fujimura F, Fukuda M, Sugiyama J, Morita T, Kimura S, Parallel assembling of dipolar columns composed of stacking cyclic tri-β-peptide, Org Biomol Chem, 4, 1896-1901 (2006)

Clair B, Almeras T, Yamamoto H, Okuyama T, Sugiyama J, Mechanical state of native cellulose microfibrils in tension wood, Biophys J, 91, 1128-1135 (2006)

Horikawa Y, Itoh T, Sugiyama J, Preferential uniplanar orientation of cellulose microfibrils re-investigated by FTIR technique, Cellulose, 13, 309-316 (2006)

Clair B, Almeras T, Sugiyama J, Compression stress in opposite wood of angiosperms: observations in chestnuts, mani and poplar, Annals of Forest Science, 63, 1-4 (2006)

Yoshioka Y, Takabe K, Sugiyama J, Nishio Y, Newly developed nanocomposites from cellulose acetate/poly-ε-caprolactone/layered silicate I: synthesis and morphological characterization, JWood Sci, 52, 121-127 (2006)

Ding S-Y, Smith S, Xu Q, Sugiyama J, Jones M, Rumbles G, Bayer EA, Himmel ME, Ordered arrays of quantum dots using cellulosomal proteins, Industrial biotechnol, 1, 198-206 (2006)

Kim N-H, Imai T, Wada M, Sugiyama J, Molecular directionality in cellulose polymorphs, Biomacromolecules, 7, 274-280 (2006)

Matthews JF, Skopec CE, Mason PE, Succato P, Torget RW, Sugiyama J, Himmel ME, Brady JW, Computer simulations of water structuring adjacent to microcrystalline cellulose Iβ structure, Carbohydr Res, 241, 138-152 (2006)

Amirta R, Tanabe T, Watanabe T, Honda Y, Kuwahara M Watanabe T, Methane fermentation of Japanese cedar wood pretreated with a white rot fungus, Ceriporiopsis subvermispora, J Biotechnol, 123, 71-77 (2006)

Tsukihara T, Honda Y, Watanabe T and Watanabe T, Molecular breeding of white rot fungus, Pleurotus ostreatus, by homologous expression of its versatile peroxidase MnP2, Appl Microbiol Biotechnol, J Biotechnol, 71, 114-120 (2006)

Tsukihara T, Honda Y, Sakai R, Watanabe T Watanabe T, Exclusive overproduction of recombinant versatile peroxidase MnP2 by genetically modified white rot fungus, Pleurotus ostreatus, J Biotechno, 126, 431-439 (2006)

Ohashi Y, Kan Y, Watanabe T, Honda Y Watanabe T, Redox silencing of the Fenton reaction system by an alkylitaconic acid, ceriporic acid B produced by a selective lignin-degrading fungus, Ceriporiopsis subvermispora, Or Biomol Chem, 5, 840-847 (2006)

Sakakibara N, Nakatsubo T, Suzuki S, Shibata D, Shimada M, Umezawa T, Metabolic Analysis of the Cinnamate/Monolignol Pathway in Carthamus tinctorius Seeds by a Stable-Isotope-Dilution Method, Org Biomol Chem, 5, 802-815 (2007)

Sakai S, Nishide T, Munir E, Baba K, Inui H, Nakano Y, Hattori T, Shimada M, Subcellular localization of glyoxylate cycle key enzymes involved in oxalate biosynthesis of wood-destroying basidiomycete Fomitopsis palustris grown on glucose, Microbiology, 152, 1609-1620 (2006)

Takano T, Tobimatsu Y, Hosoya T, Hattori T, Ohnishi J, Takano M, Kamitakahara H, Nakatsubo F, Studies on the dehydrogenative polymerizations of monolignol beta-glucosides. Part 1. Syntheses of monolignol beta-glucosides, (E)-isoconiferin, (E)-isosyringin, and (E-)-triandrin, Journal of wood chemistry and technology, 26, 215-229 (2006)

Sugiyama A, Shitan N, Sato S, Nakamura Y, Tabata S, Yazaki K, Genome-wide analysis of ATP-binding cassette (ABC) proteins in a model legume plant, Lotus japonicus: comparison with Arabidopsis ABC protein family, DNA Res, 13, 205-228 (2006)

Ohara K, Yamamoto K, Hamamoto M, Sasaki K, Yazaki K, Functional characterization of OsPPT1, which encodes p-hydroxybenzoate polyprenyltransferase involved in ubiquinone biosynthesis in Oryza sativa, Plant Cell Physiol, 47, 581-591 (2006)

Yazaki K, Yamanaka N, Masuno T, Konagai S, Shitan N, Kaneko S, Ueda K, Sato F, Heterologous expression of a mammalian ABC transporter in plant and its application to phytoremediation, Plant Mol Biol, 61, 491-503 (2006)

Yazaki K, ABC transporters involved in the transport of plant secondary metabolites, FEBS Lett, 580, 1183-1191 (2006)

Okumura S, Sawada M, Park Y-W, Hayashi T, Shimamura M, Takase H, Tomizawa K, Transformation of poplar (Populus alba) plastids and expression of foreign proteins in tree chloroplasts, Transgenic Res., 15, 637-646 (2006)

Okumura S, Sawada M, Shimamura M, Park Y-W, Hayashi T, Yamashita A, Hattori M, Kanamoto H, Takase H, Miyake C Tomizawa K, J Arid Land Stud, 15, 505-508 (2006)

Kato N, Dubouze, E, Kokabu Y, Yoshida S, Taniguchi Y, Dubouzet J G, Yazaki K, Sato F, Identification of a WRKY Protein as a Transcriptional Regulator of Benzylisoquinoline Alkaloid Biosynthesis in Coptis japonica, Plant Cell Physiol, 48, 8-17 (2007)

Shitan N, Horiuch, K, Sato F, Yazaki K, Bowman Birk proteinase inhibitor confers heavy metal and multiple drug tolerance in yeast, Plant Cell Physiol, 48, 193-197 (2007)

Shitan N, Tanaka M, Terai K, Ueda K, Yazaki K, Human MDR1 and MRP1 recognize berberine as their transport substrate, Biosci Biotech Biochem, 71, 242-2456 (2007)

Konishi T, Takeda T, Miyazaki Y, Ohnishi-Kameyama M, Hayashi T, O'Neill M A and Ishii T, A plant mutase that interconverts UDP-arabinofuranose and UDP-arabinopyranose, Glycobiology, 17, 345-354 (2007)

Garcia-Fernandez, Tsuda T, A global distribution of sporadic E events revealed by means of CHAMP-GPS occultations, Earth, Planets and Space, 58, 33-36 (2006)

Furumoto J, Tsuda T, Iwai S, and Kozu T, Continuous humidity monitoring in a tropical region with the equatorial atmosphere radar (EAR), J Atmos Oceanic Tec J Atmos Oceanic Tec, 23, 538-551 (2006)

Wrasse C M, Nakamura T, Tsuda T, Takahashi H, Medeiros A F, Taylor M J, Gobbi D, A. Salatun, Suratno, E. Achmad, and A. G. Admiranto, Reverse ray tracing of the mesospheric gravity waves observed at 23S (Brazil) and 7S (Indonesia) in airglow imagers, J Atmos Solar-Terr Phys, 68, 1163-181 (2006)

Alexander S, Tsuda T, Furumoto J, Shimomai T, Kozu T, Kawashima M, A Statistical Overview of Tropospheric Convection during CPEA Campaign, J Meteorol Soc Japan, 84, 57-93 (2006)

Ratnam M V, Tsuda T, Shibagaki Y, Kozu T, Mori S, Gravity Wave Characteristics over the Equator Observed during CPEA Campaign using Simultaneous Multiple Stations Data, J Meteorol Soc Japan, 84, 239-257 (2006)

Sridharan S, Tsuda T, Nakamura T, Kozu T, Mori S, Russell J M, Observations of the 7-day Kelvin Wave in the Tropical Atmosphere during the CPEA Campaign, J Meteorol Soc Japan, 84, 259-275 (2006)

Tsuda T, Ratnam M V, Kozu T, and Mori S, Characteristics of 10-day Kelvin Wave Observed with Radiosondes and CHAMP/GPS Occultation during the CPEA Campaign (April-May, 2004), J Meteorol Soc Japan, 84, 277-293 (2006)

Sridharan S, Tsuda T, Vincent R A, Nakamura T, and Achmad E, A Report on Radar Observations of 5-8-day Waves in the Equatorial MLT Region, J Meteorol Soc Japan, 84, 295-304 (2006)

Venkat Ratnam M, Tsuda T, Kozu T, Mori S, Long-term behavior of the Kelvin waves revealed by CHAMP/GPS RO measurements and their effects on the tropopause structure, Annales Geophysicae, 24, 1355-1366 (2006)

Mousa, A., Aoyama Y, and Tsuda T, A simulation analysis to optimize equatorial GPS radio occultation mission, Earth, Planets and Space, 58, 919-925 (2006)

M.V. Ratnam, T. Tsuda, S. Mori, Kozu T, Modulation of tropopause temperature structure reveal by simultaneous radiosonde and CHAMP GPS measurements, J Meteorol Soc Japan, 84, 989-1003 (2006)

PUBLICATIONS

Alexander S, Tsuda T, Measurements of vertical eddy diffusivity across the tropopause using radio acoustic sounding system(RASS), Geophys Res Lett, 34 (2006)

Wrasse C M, Nakamura T, Takahashi H, Medeiros A F, Taylor M J, Gobbi D, Denardini C M, Fechine J, Buriti R A, Salatun A, Suratno, Achmad E, Admiranto AG, Mesospheric gravity waves observed near equatorial and low-middle latitude stations: wave characteristics and reverse ray tracing results, ANNALES GEOPHYSICAE, 24, 3229-3240 (2006)

Shiokawa K, Suzuki S, Otsuka Y, Ogawa T, Nakamura T, Mlynczak MG, Russell JM, A multi-instrument measurement of a mesospheric front-like structure at the equator, J Meteorol Soc Japan, 84A, 295-304 (2006)

Shibata Y, Nagasawa C, Abo M, Maruyama T, Saito S, Nakamura T, Lidar observations of sporadic Fe and Na layers in the mesopause region over equator, J Meteorol Soc Japan, 84A, 317-325 (2006)

Shiokawa K, Suzuki S, Otsuka Y, Ogawa T, Nakamura T, Horinouchi T, An intense gravity wave near the mesopause region observed by a Fabry-Perot interferometer and an airglow imager, J Geophys Res, 112, D07106-8 (2007)

Balan N, Kawamura S, Nakamura T, Yamamoto M., Fukao S, Oliver W L, Hagan M E, Aylward A D, Alleyne H, Simultaneous mesosphere-lower thermosphere and thermospheric F region observations using middle and upper atmosphere radar, J Geophys Res, 111, A10S17 (2007)

Hashiguchi N O, Yamanaka M D, Ogino S -Y, Shiotani M, Sribimawati T, Seasonal and interannual variations of temperature in tropical tropopause layer (TTL) over Indonesia based on operational rawinsonde data during 1992-1999., J Geophys Res, 111, doi:10.1029/2005JD006501 (2006)

Shibata T, Voeme H, Hamdi S, Kaloka S, Hasebe F, Fujiwara M, and Shiotani M, Tropical cirrus clouds near cold point tropopause under ice supersaturated conditions observed by lidar and balloon-borne cryogenic frost point hygrometer, J Geophys Res, 112, doi:10.1029/2006JD007361 (2007)

Noriyuki N, Suzuki J, Hamada A and Shiotani M, Rapid Transitions in Zonal Wind Around the Tropical Tropopause and their Relation to the Amplified Equatorial Kelvin Waves., SOLA, Vol.3, 13-16 (2007)

Hasebe F, Fujiwara M, Nishi N, Shiotani M, Voemel H, Oltmans S, Takashima H, Saraspriya S, and Komala N, In situ observations of dehydrated air parcels advected horizontally in the Tropical Tropopause Layer of the western Pacific, Atmospheric Chemistry and Physics, accepted

Takashima H, Shiotani M, Ozone variation in the Tropical Tropopause Layer as seen from ozonesonde data., J Geophys Res, accepted

Yokoyama T, Fukao S, Upwelling Backscatter Plumes in Growth Phase of Equatorial Spread F Observed with the Equatorial Atmosphere Radar, Geophys Res Lett, 33, L08104, doi:10.1029/2006GL025680 (2006)

Maruyama T, Saito S, Yamamoto M, Fukao S, Simultaneous observation of sporadic E with a rapid-run ionosonde and VHF coherent backscatter radar, Ann Geophys, 24, 153-162 (2006)

Luce H, Hassenpflug G, Yamamoto M, Fukao S, High-resolution vertical imaging of the lower atmosphere using the new MU radar system, Ann Geophys, 24, 791-805 (2006)

Pavlov A V, Fukao S, Kawamura S, A Modeling study of Ionospheric F2-region storm effects at low geomagnetic latitudes during 17-22 March 1990, Ann Geophys, 24, 915-940 (2006)

Fukao S, Yokoyama T, Tayama T, Yamamoto M, Maruyama T, Saito S, Eastward traverse of equatorial plasma plumes observed with the Equatorial Atmosphere Radar in Indonesia, Ann Geophys, 24, 1411-1418 (2006)

Gavrilov N M, Fukao S, Hashiguchi H, Kita K, Sato K, Tomikawa Y, Fujiwara M, Combined MU radar and ozonesonde measurements of turbulence and ozone fluxes in the tropo-stratosphere over Shigaraki, Japan, Geophys Res Lett, 33, L09803, doi:10.1029/2005GL024002 (2006)

Fukao S, Coupling Processes in the Equatorial Atmosphere (CPEA): A Project Overview, J Meteor Soc Japan, 84A, 1-18 (2006)

Shibagaki Y, T. Kozu T, Shimomai T, Mori S, Murata F, Fujiyoshi Y, Hashiguchi H, Fukao S, Evolution of a Super Cloud Cluster and the Associated Wind Fields Observed over the Indonesian Maritime Continent during the First CPEA Campaign, J Meteor Soc Japan, 84A, 19-31 (2006)

Seto T H, Yamamoto M K, Hashiguchi H, Fukao S, Abo M, Kozu T, Mahally Kudsy, Observational Study on Westerly Wind Burst over Sumatra, Indonesia by the Equatorial Atmosphere Radar - A Case Study During the First CPEA Campaign -, J Meteor Soc Japan, 84A, 95-11 (2006)

Shibagaki Y, Shimomai T, Kozu T, Mori S, Fujiyoshi Y, Hashiguchi H, Yamamoto M K, Fukao S, Yamanaka M D, Multiscale Aspects of Convective Systems Associated with an Intraseasonal Oscillation over the Indonesian Maritime Continent, Mon Weather Rev, 134, 1682-1696 (2006)

PUBLICATIONS

Unnikrishnan K, Saito A, Fukao S, Differences in daytime and nighttime ionospheric deterministic chaotic behavior: GPS total electron content analyses, J Geophys Res, 111, A07310, doi:10.1029/2005JA011313 (2006)

Balan N, Kawamura S, Nakamura T, Yamamoto M, Fukao S, Oliver W L, Hagan M E, Aylward A D, Alleyne H, , Simultaneous mesosphere-lower thermosphere and thermospheric F region observations using middle and upper atmosphere radar, J Geophys Res, 111, A10S17, doi:10.1029/2005JA011487 (2006)

Dhaka S K, Yamamoto M K, Shibagaki Y, Hashiguchi H, Fukao S, Chun H -Y, Equatorial Atmosphere Radar observations of short vertical wavelength gravity waves in the upper troposphere and lower stratosphere region induced by localized convection, Geophys Res Lett, 33, L19805, doi:10.1029/2006GL027026 (2006)

Renggono F, Yamamoto M K, Hashiguchi H, Fukao S, Shimomai T, Kawashima M, and Kudsy M, Raindrop size distribution observed with the Equatorial Atmosphere Radar (EAR) during the CPEA-I observation campaign, Radio Sci, 41, RS5002, doi:1029/2005RS003333 (2006)

Murata F, Yamanaka M D, Hashiguchi H, Mori S, Kudsy M, Sribimawati T, Suhardi B, Emrizal, Dry intrusions following eastward-propagating synoptic-scale cloud systems over Sumatera Island, J Meteor Soc Japan, 84, 277-294 (2006)

Matsuda S, Hashiguchi H, Fukao S, A study on multibeam pulse chasing for bistatic radar, Electronics and Communications in Japan, 89, 11-21 (2006)

Kawashima M, Fujiyoshi Y, Ohi M, Honda T, Kozu T, Shimomai T, Hashiguchi H, Overview of Doppler radar observations of precipitating cloud systems in Sumatera island during the first CPEA campaign, J Meteor Soc Japan, 84A, 33-56 (2006)

Mori S, Hamada J, Yamanaka M D, Kodama Y, Kawashima M, Shimomai T, Shibagaki Y, Hashiguchi H, and Sribimawati T, Vertical Wind Characteristics in Precipitating Cloud Systems over West Sumatera, Indonesia, Observed with Equatorial Atmosphere Radar: Case Study on 23-24 April 2004 during the CPEA Campaign Period-1, J Meteor Soc Japan, 84A, 113-131 (2006)

Araki R, Yamanaka M D, Murata F, Hashiguchi H, Oku Y, Sribimawati T, Kudsy M, Renggono F, Seasonal and interannual variations of diurnal cycles of wind and cloud activity observed at Serpong, West Jawa, Indonesia, J Meteor Soc Japan, 84A, 171-194 (2006)

Maekawa Y, Fujiwara T, Shibagaki Y, Sato T, Yamamoto M, Hashiguchi H, and Fukao S, Effects of tropical rainfall on the Ku-band satellite communications links to the Equatorial Atmosphere Radar Observatory, J Meteor Soc Japan, 84A, 211-225 (2006)

Saito S, Yamamoto M, Hashiguchi H, and Maegawa A, Observation of three-dimensional structures of quasi-periodic echoes associated with mid-latitude sporadic-E layers by MU radar ultra-multi-channel system, Geophys Res Lett, 33, L14109,doi:10.1029/2005GL025526 (2006)

Shams M I, Kagemori K Yano H, Compressive deformation of wood impregnated with low molecular weight phenol formaldehyde (PF) resin IV Species dependency, J Wood Science, 52, 179-183 (2006)

Shams M I, Morooka T Yano H Compressive deformation of wood impregnated with low molecular weight phenol formaldehyde (PF) resin V Effects of steaming pretreatment, J Wood Science, 52, 389-304 (2006)

Nogi M, Ifuku S, Abe K, Handa K, Nakagaito A N, Yano H, Fiber-content dependency of the optical transparency and thermal expansion of bacterial nanofiber reinforced composites, Applied Physics Letters, 88, 133124 (2006)

Nogi M, Abe K, Handa K, Nakatsubo F, Ifuku S Yano H, Property enhancement of optically transparent bio-nanofiber compositesby acetylation, Applied Physics Letters, 89, 233123 (2006)

Ifuku S, Nogi M, Abe K, Handa K, Nakatsubo F, Yano H Surface Modification of Bacterial Cellulose Nanofibers for Property Enhancement of Optically Transparent Composites:Dependence on Acetyl-Group DS, Biomacromolecules, in press

Okahisa Y, Yoshimura T, Imamura Y, Seasonal and height-dependent fluctuation of starch and free glucose contents in moso bamboo (Phyllostachys pubescens) and its relation to attack by termites and decay fungi, J Wood Science, 52, 445-451 (2006)

Okahisa Y, Yoshimura T, Imamura Y, Changes of free glucose and starch contents in moso bamboo (Phyllostachys pubescens) during the transpiration drying method (hagarashi), Bamboo Journal, in press

Tanaka F, Iwata T, Estimation of the elastic modulus of cellulose crystal by molecular mechanics simulation, Cellulose, 13, 509-517 (2006)

Kawasaki T, Kawai S, Thermal insulation properties of wood-based sandwich panel for use as structural insulated walls and floors, J Wood Sci, 52, 75-83 (2006)

Kawasaki T, Zhang M, Wang Q, Komatsu K, Kawai S, Elastic moduli and stiffness optimization in four-point bending of wood-based sandwich panel for use as structural insulated walls and floors, J Wood Sci, 52, 302-310 (2006)

Umemura K, Kawai S, Modification of Chitosan by the Maillard Reaction using Cellulose Model Compounds., Carbohydrate Polymers, 68, 242-248 (2007)

Noguchi M, akino S, Komatsu K, Development of wooden portal frame structures with improved columns, J Wood Sci, DOI: 10.1007/s10086-005-0714-y (2006)

Chang W -S, Hsu M –F, Komatsu K, Rotational performance of traditional Nuki joints with gap I: theory and verification, J Wood Sci, DOI: 10.1007/s10086-005-0734-7 (2006)

Noguchi M, Komatsu K, Estimation of stiffness and strength in timber knee joints with adhesive and verification by experiment, J Wood Sci, DOI 10.1007/s10086-005-0802-z (2006)

Chang W -S, Komatsu K, Min-Fu Hsu M –F, Chen W -J, On mechanical behavior of traditional timber shear wall in Taiwan I: background and theory derivation, J Wood Sci, DOI 10.1007/s10086-006-0825-0 (2006)

Chang W -S, Komatsu K, Hsu M –F, Chen W -J, On mechanical behavior of traditional timber shear wall in Taiwan II: simplified calculation and experimental verification, J Wood Sci, DOI 10.1007/s10086-006-0826-z (2006)

Kartal S N, Hwang W J, Imamura Y, and Sekine Y, Effect of essential oil compounds and plant extracts on decay and termite resistance of wood, Holz als Roh und Werkstoff, 64, 455-461 (2006)

Kartal S N, Hwang W J, Yoshimura T, Imamura Y, Evaluation of leaching medium effect on the release of copper, chromium, and arsenic from treated wood, Build Env, 42, 1188-1193 (2007)

Kartal S N, Ayrilmis N, Imamura Y, Decay and termite resistance of plywood treated with various fire retardants, Build Env, 42, 1207-1211 (2007)

Nakai T, Kartal S N, Hata T, Imamura Y, Chemical characterization of pyrolysis liquids of wood-based composites and evaluation of their bio-efficiency, Build Env, 42, 1236-1241 (2007)

Okahisa Y, Yoshimura T, Imamura Y, Seasonal and height-dependent fluctuation of starch and free glucose contents in moso bamboo (Phyllostachys pubescens) and its relation to attack by termites and decay fungi, J Wood Sci, 52, 445-451 (2006)

Kartal S N, Katsumata N, Imamura Y, Removal of copper, chromium, and arsenic from CCA-treated wood by mold and staining fungi, For Prod J, 56, 33-37 (2006)

Kartal S N, Brischke C, ARapp A O, Imamura Y, Biological effectiveness of didecyl dimethyl ammonium tetrafluoroborate (DBF) against Basidiomycetes following preconditioning in soil bed tests, Wood Sci Tech, 40, 63-71 (2006)

Hwang W J, Kartal S N, Imamura Y, Evaluation of new quaternary ammonium compound, didecyldimethylammonium tetrafluoroborate (DBF) imcompsrison with DDAC: Leachability and termite resistance tests, Holz als Roh und Werkstoff, 64, 111-116 (2006)

Kartal S N, Hwang W J, Shinoda K, Imamura Y, Laboratory evaluation of boron-containing quaternary ammonia compound didecyl dimethyl ammonium tetrafluoroborate (DBF) for control of decay and termite attack and fungal staining of wood, Holz als Roh und Werkstoff, 64, 62-67 (2006)

Tsunoda K, Transfer of fipronil, a nonrepellent termiticides, from exposed workers of Coptotermes formosanus (Isoptera: Rhinotermitidae9 to unexposed workers, Sociobiology, 47, 563-575 (2006)

Kubota S, Shono Y, Matsunaga T, Tsunoda K, Laboratory evaluation of bistrifluron, a benzoylphenylurea compound, as a bait toxicant against Coptotermes formosanus (Isoptera: Rhinotermitidae), J Econ Entomol, 99, 1363-1368 (2006)

Yamaoka Y, Tsunoda K, Determination of the amount of fipronil recovered from freshly treated and treated/stored sandy loam, Sociobiology, 48, 621-626 (2006)

Tsunoda K, Effect of 18-months' storage of treated sandy loam on the transfer of fipronil from exposed workers to unexposed workers of Coptotermes fromosanus (Isoptera: Rhinotermidae), Sociobiology, 48, 627-634 (2006)

Hwang, W J., YoshimuraT, Tsunoda K, Imamura Y, Efficacy of two alkylammonium compounds in controlling the attack of wood by western drywood termite, Incisitermes minor (Isoptera: Kalotermitidae), Sociobiology, 48, 471-478 (2006)

Hwang W J, Kartal S N, Yoshimura T, Imamura Y, Synergistic effect of heartwood extractives and quaternary ammonium compounds on termite resistance of treated wood, Pest Manag Sci, 63, 90-95 (2006)

Indrayani Y, Yoshimura T, Imamura Y, Detection of the activities of the western dry-wood termite, Incisitermes minor (Hagen), in small infested logs by using a micriowave detector, Jpn J Environ Entomol Zool, 17, 29-32 (2006)

Indrayani Y, Matsumura K, Yoshimura T. Imamura Y, and Itakura S, Development of microsatellite markers for the drywood termite Incisitermes minor (Hagen), Mol Ecol Note, 6, 124-125 (2006)

Kurosaki F, Koyanaka H, Hata T Imamaura Y, Macroporous carbon prepared by flash heating of sawdust, Carbon, 45, 671-673 (2006)

Kakitani T, Hata T, Kajimoto T, Imamura Y, Designing a purification process for chromium-, copper- and arsenic-contaminated wood, Waste Management, 26, 453-458 (2006)

Kakitan T, Hata T, Kajimoto T, Imamura Y, A Novel Extractant for Removal of Hazardous Metals from Preservative-Treated Wood Waste, J Env Qual, 35, 912-917 (2006)

Indrayani Y, Yoshimura T, Yanase Y, Fujii Y, Matsuoka H, Imamura Y, Observation of feeding behavior of three termite (Isoptera) species: Incisitermes minor, Coptotermes formosanus and Reticulitermes speratus, Sociobiology, 49, 121-134 (2007)

Indrayani Y, Yoshimura T, Yanase Y, Fujii Y, Imamura Y, Evaluation of the temperature and relative humidity preferences of the western dry-wood termite Incisitermes minor (Hagen) using acoustic emission (AE) monitoring, J Wood Sci, 53, 76-79 (2007)

Katsumata N, Yoshimura T, Tsunoda K, Imamura Y, Difference in the termite feeding on gamma-irradiated wood specimens between three laboratory colonies of Coptotermes fromosanus (Isoptera: Rhinotermitidae), Sociobiology, 49, 143-150 (2007)

Katsumata N, Tsunoda K, Toyoumi A, Yoshimura T, Imamura Y, Comparative termite (Isoptera. Rhinotermitidae) feeding preference among gammma-irradiated and unirradiated wood, Sociobiology, 50, 155-162 (2007)

Katoh Y, Omura Y, Parametric study of resonant scattering process by narrow band whistler mode waves driven by temperature anisotropy, J Plasma Phys, 72, 935-939 (2006)

Umeda T, Omura Y, Miyake T, Matsumoto T, and Ashour-Abdalla M, Nonlinear evolution of the electron two-stream instability: Two-dimensional particle simulations, J Geophys Res, 111, A10206, doi:10.1029/2006JA011762 (2006)

Krasovsky V L, Matsumoto H, Omura Y, Condition for charged particle trapping in a three-dimensional electrostatic potential well in the presence of a magnetic field, Phys Scr, 74, 227-231 (2006)

Katoh Y, Omura Y, Simulatin study on nonlinear frequency shift of narrow band whistler mode waves in a homogeneous magnetic field, Earth, Planet and Space, 58, 1219-1225 (2006)

Omura Y and Summers D, Dynamics of high-energy electrons interacting with whistler mode chorus emissions in the magnetosphere, J Geophys Res, 111, A09222, doi:10.1029/2006JA011600 (2006)

Blomberg L G, Cumnock J A, Kasaba Y, Matsumoto H, Kojima H, Omura Y, Moncuque M, Wahlund J -E, Electric fields in the Hermean environment, Advances in Space Research, 38, 627-631 (2006)

Blomberg L G, Matsumoto H, JBougeret J -L, Kojima H, Yagitani S, Cumnock J A, Eriksson A I, Marklund G T, Wahlund J -E, Bylander L, A ° hle´n L, Holtet J A, Ishisaka K, Kallio E, Kasaba Y, Matsuoka A, Moncuquet M, Mursula K, Omura Y, Trotignon J G, MEFISTO – An electric field instrument for BepiColombo/MMO, Advances in Space Research, 38, 672-679 (2006)

Katoh Y, Omura Y, A study of generation mechanism of VLF triggered emission by self-consistent particle code, J Geophysl Res, 111, A12207, doi:10.1029/2006JA011704 (2006)

Usui H, Miyake Y, Okada M, Omura Y, Sugiyama T, Murata K T, Matsuoka D, Ueda H O, Development and Application of Geospace Environment Simulator for the Analysis of Spacecraft-Plasma Interactions, IEEE Transactions on plasma science, 34, 2094-2102 (2006)

Funaki I, Usui H, Nakayama Y, Kuninaka H, Experimental simulation of spacecraft charging by artificial ion-beam emission, IEEE Transactions on plasma science, 34, 2031-2037 (2006)

Katoh Y, Omura Y, Computer simulation of chorus wave generation in the Earth's inner magnetosphere, Geophys Res Letters, 34, L03102, doi:10.1029/2006GL028594 (2007)

Mitani T, Shinohara N, Matsumoto H, Aiga M, Kuwahara N, Ishii T, Noise-Reduction Effects of Oven Magnetron With Cathode Shield on High-Voltage Input Side, IEEE Transaction on Electron Devices, 53, 1929-1936 (2006)

Sasaki S, Tanaka K, Higuchi K, Okuizumi N, Kawasaki S, Shinohara N, Senda K, Ishimura K, A New Concept of Solar Power Satellite : Tethered-SPS, Acta Astronautica, 60, 153-165 (2006)

Morioka A, Miyoshi Y, Masuda S, Tsuchiya F, Misawa H, Matsumoto H, Hashimoto K, and Oya H, Micro-type III radio bursts, Astrophysical Journal, 657, 567-576 (2007)

Funaki I, Ueno K, Yamakawa H, Nakayama Y, Kimura T, and Horisawa H, Interaction between Plasma Flow and Magnetic Field in Scale Model Experiment of Magnetic Sail, Fusion Science and Technology, 51, 226-228 (2007)

Funaki I, Kojima H, Yamakawa H, Shimizu Y, Nakayama N, Laboratory Experiment of Plasma Flow around Magnetic Sail, Astrophysics and Space Science, 307, 63-68 (2007)

PUBLICATIONS

Morimoto M, Yamakawa Y, Uesugi K, Periodic Orbits with Low-thrust Propulsion in the Restricted Three-body Problem, Journal of Guidance, Control, and Dynamics, 29, 1131-1139 (2006)

Yamakawa H, Orbital Dynamics of Sun-Facing Solar Sails under the Constraint of Constant Sail Temperature, The Journal of the Astronautical Sciences, 54, 12-27 (2006)

Sustainable Humanosphere 第3号

発　行　日　平成19年8月31日
編集兼発行者　京都大学 生存圏研究所
京都府宇治市五ヶ庄
印　刷　所　ユニバース印刷
京都府長岡京市友岡 2-10-2